Grant Agreement: 768936

TEMPO

# D5.3: PERFORMANCE ASSESSMENT REPORT MONITORING SEASON 2021-2022

This project has received funding from the European Union's Horizon 2020 research and innovation programme under grant agreement No 768936.

| PROJECT DOCUMENTATION SHEET | |
|---|---|
| **Project Acronym** | **TEMPO** |
| **Project Full Title** | Temperature Optimisation for Low Temperature District Heating across Europe |
| **Grant Agreement** | **768936** |
| **Call Identifier** | H2020-EE-2017-RIA-IA |
| **Topic** | EE-04-2016-2017 – New heating and cooling solutions using low grade sources of thermal energy |
| **Type of action** | IA Innovation Action |
| **Project Duration** | 54 months (October 2017 – March 2022) |
| **Coordinator** | Vlaamse Instelling voor Technologisch Onderzoek NV (BE) – VITO |
| **Consortium partners** | Nodais AB (SE) – NODA<br>Austrian Institute of technology (AT) – AIT<br>Thermaflex international holding (NL) - THF<br>Steinbeis Innovation gmbH (DE) - Solites<br>Vattenfall Europe (DE) - Vattenfall<br>Enerpipe (DE) – Enerpipe<br>A2A Calore & servizi (IT) - A2A<br>Hogskolan i Halmstad (SE) – HU<br>Euroheat & Power (BE) – EHP |
| **Website** | www.tempo-dhc.eu |
| **Disclaimer** | The sole responsibility for the content of this document lies with the authors. It does not necessarily reflect the opinion of the funding authorities. The funding authorities are not responsible for any use that may be made of the information contained herein. |

| DELIVERABLE DOCUMENTATION SHEET | |
|---|---|
| **Number** | **Deliverable D5.3** |
| **Title** | Performance assessment report monitoring season 2021-2022 |
| **Related WP** | WP5 (Evaluation and Knowhow Transfer) |
| **Related Task** | Task 5.2 (Data analyses and performance assessment) |
| **Lead Beneficiary** | AIT |
| **Author(s)** | Ralf-Roman Schmidt (AIT) – ralf-roman.schmidt@ait.ac.at<br>Aurelien Bres (AIT) – aurelien.bres@ait.ac.at<br>Andreas Fiegl (ENERPIPE) – andreas.fiegl@enerpipe.de<br>Davy Geysen (VITO) – davy.geysen@vito.be<br>Ilaria Marini (A2A) – ilaria.marini@a2a.eu<br>Thomas Schmidt (Solites) – schmidt@solites.de<br>Tijs Van Oevelen (VITO) – tijs.vanoevelen@vito.be |
| **Contributor(s)** | Luca Scapino (VITO)<br>Thomas Neven (VITO) – thomas.neven@vito.be |
| **Reviewer(s)** | Dirk Vanhoudt (VITO) – dirk.vanhoudt@vito.be<br>Johan Desmedt (VITO) – johan.desmedt@vito.be |
| **Nature** | R (Report) |
| **Dissemination level** | PU (Public) |
| **Due Date** | March 2022 (M54) |
| **Submission date** | 31/03/2022 (M54) |
| **Status** | Final |

| QUALITY CONTROL ASSESSMENT SHEET | | | |
|---|---|---|---|
| **Issue** | **Date** | **Comment** | **Author** |
| **V0.1** | 12/02/2022 | Draft structure | Ralf-Roman Schmidt (AIT) |
| **V0.2** | 16/02/2022 | First draft | Aurelien Bres (AIT) |
| **V0.3** | 18/03/2022 | Updated data | Aurelien Bres (AIT) |
| **V0.4** | 28/03/2022 | Second draft for review | Ralf-Roman Schmidt (AIT) |
| **V0.5** | 29/03/2022 | Peer review | Dirk Vanhoudt (VITO) |
| **V0.6** | 31/03/2022 | Quality check | Johan Desmedt (VITO) |
| **V0.7** | 31/03/2022 | Submitted to EC | Johan Desmedt (VITO) |

# EXECUTIVE SUMMARY

The TEMPO – Temperature Optimisation for Low Temperature District Heating across Europe – project develops technical innovations that enable district heating networks to operate at lower temperatures. The developed innovations were demonstrated and implemented in the following district heating networks:

- **Brescia** (Italy): The Brescia district heating network is heated by a waste-to-energy plant (~70% coverage), residual heat from industry and a cogeneration unit, and peak-load gas boilers. The A2A network currently operates at temperature levels around 120/60°C. The A2A pilot project involves two locations: The Fornaci site corresponds to a part of the district heating network in Brescia. Additional analyses have been performed on thirty other multi-family houses served by the DH network in Brescia (the "city demo").
- **Windsbach**, region of Nuremberg (Germany): The ENERPIPE demonstration site consists of a new network which supplies heat to a low-density rural area of new buildings. Heat is provided by residual heat of a biogas plant, biogas CHPs and a peak gas boiler.

This report describes the monitoring results and the calculation of key performance indicators. Further details on the innovations and their implementation can be found in [1] and [2].

For the **A2A demo,** the results can be summarized as follows:

**1. Mixing station installation**: By mixing return water of this branch with hot water from the main network, the supply temperature to the Fornaci branch can be reduced. During the low-temperature operation phase the supply temperature after the mixing station was on average 17 K lower than during default high-temperature operation. It has been observed that reducing the supply temperature in the network branch reduces the heat distribution losses with 4% on average. Furthermore, one of the main benefits of the mixing station within TEMPO was the possibility to use advanced control algorithms for supply temperature control. Thus, the mixing station was an important enabler for using the local branch of the district heating network as a storage since control of the overall supply temperature in the full Brescia district heating network was not possible.

**2. Smart district heating controller for return temperature reduction:** Control of the apartment building supply temperature (test A) resulted in an average reduction of the primary return temperature of 0.7 K, up to 2 K for some days depending on the outdoor temperature. At the same time, the peak energy was reduced by 330 kWh per day on average and up to 700 kWh per day, representing 60% to 70% of the baseline peak energy. Unfortunately, the capacity limits of the apartment building substation led to deteriorated performance during very cold weather.

**3. Smart district heating controller for peak load reduction:** Control of the mixing station supply temperature (test B) has been able to reduce the peak energy by 200 to 500 kWh per day, depending on outdoor temperature. These numbers represent a reduction by about 30% to 50% of the baseline peak energy, evaluated with respect to a notional peak power threshold. However, during very cold weather (below 7 °C outdoor

temperature), the peak energy unfortunately increased due to capacity limits of the apartment building substation.

**4. Fault detection and building optimization:** The approach to optimization of the building installations developed in TEMPO has been applied to two sets of buildings (single-family houses of the Fornaci demo, multi-family houses of the city demo). While the accuracy of automated fault detection and diagnosis was limited (as shown by cross-validation on the simulation training data) because of monitoring data limited to the primary side (except for two buildings), combining automated predictions with performance metrics made identification of poorly performing buildings very efficient. Remediating the identified faults would imply important communication effort but could result in a significant reduction of return temperatures. i.e. fixing the faults leading to temperatures above 55 °C (which may be assumed to be the "low-hanging fruits") would yield an average (flowrate-weighted) reduction in return temperature of 1.4 K.

**5. Visualization in the city demo (non-expert users):** Particular care was taken to simplify the complex results of the TEMPO project by using clear indicators and diagrams and avoid any confusing information. It was important to clearly distinguish the performance of the individual building, the baseline as well as the performance of the best performing buildings. Further on, the communication process towards the building managers and their technicians needed to be carefully designed and aligned within different departments within A2A, since those building managers are key customers of A2A. The involvement of the local technicians is important, since the building managers often have non or very little technical background or knowledge on the building heating system. The feedback from one building technician shows, that the communication process was partly successful and leads to clear statements on the building performance and the reasons causing high return temperatures, also the discussion with A2A technicians is a positive result, leading to an improved performance of the heating system in terms of reduced return temperatures. However, even more time and resources would be required to intensify the communication to the building managers and involve their local technicians.

**6. Visualization in the Fornaci demo (expert users):** The feedback from expert users were gathered through a questionnaire. It shows that the visualisation tool can provide relevant decision-support for expert users. Most are positive to the concept as such, although a significant segment of the users provided relevant suggestions for further improvements. The main theme in among the suggestions was to simplify the practical usage of the system. One conclusion related to this is to remember the fact that the expert users are experts on district heating systems, not experts on IT-systems. Furthermore, many suggested to more clearly clarify the performance metrics involved. The conclusion relating to this is that additional documentation is important when used in a commercial setting. This would provide the requested clarification, without cluttering the visualisation tool itself. Additional requirements were added for future implementation in a post-TEMPO development iteration

For the **ENERPIPE demo**, the results can be summarized as follows:

**1. Decentralized buffer tanks:** DH network substations with buffer tanks offer the potential for a reduction of the connection capacity to the individual buildings as peak load from consumption can be covered from the buffer tanks. As a consequence, also the design heat load for the DH network can be reduced. A simulation study was conducted to

elaborate the technical and economical optimisation potential of the decentralised buffer tank concept. Investigations show a reduction potential of design house connection capacity rates for new standard single-family houses from today's 30 kW down to theoretically 7.5 kW. Further on, smaller DH pipe dimensions enable cost savings for the DH network, but larger buffer tank volumes generate higher cost in the house stations. In sum the variation in total yearly cost for the investigated configurations with double pipes in standard insulation was calculated to 11%. However, an increased risk of reduced comfort for the consumers has to be taken into account, if heat demands differ too much from design conditions. Presented analysis allow an assessment of these effects based on maximum load coverage periods for two excess demand scenarios and different technical configurations.

**2. Fault detection and building optimization:** While it was originally expected that the recent installations would not be subject to many faults, the impact of faults turned out to be significant. This was due to a recurring issue with return lances, a number of which were too short. This issue demonstrated the value of being able to detect anomalous behaviour quickly (but was addressed by the TEMPO innovation) but also the importance of being able to remedy the corresponding faults quickly, which turned out to be more challenging than expected. The latest version of the buffer tank will be equipped with direct return outlets instead of return lances, which will avoid the issue in new installations.

**3. Smart district heating controller for smart buffer charging:** The possibility was investigated to reduce the peak load in the DH network by pre-charging the decentralized buffer tanks. However, even though simulations showed that a theoretical peak reduction of 35% was feasible, the following challenges were faced in the field. First, the smart controller had to be deployed on top on the already existing automatic buffer charging controller. This controller was designed to implement the conventional charging behaviour of the buffer, i.e., if the top temperature drops below 50 °C, the cycle starts automatically, limiting the flexibility to shift the charging process. Another complexity in the solution is the fact that four different systems are involved to get a control signal to the decentralized buffers. This is leading to two main disadvantages: Problems surface slowly as there is no single system having an overview of the complete workflow and it takes multiple persons to debug in case problems are detected, making problem solving very time consuming. Further on, the buffer size is impacting the available flexibility (i.e. they have to charge 8 to 10 times a day). In future, increasing incentives for extra demand-side flexibility can lead to larger decentralized buffer storages.

**4. Smart district heating controller for CHP optimization:** The optimization of the operation of the CHP is done based on forecasts of the electricity price and the forecast of the total heat load, leading to a theoretical improvement of the electricity revenues by 8%. Unfortunately, in the field several unforeseen events happen which made the forecasting of the heat load difficult: Unplanned maintenance can have an impact on heat input/output or data communication; an additional heat input from a "satellite site" was difficult to forecast; new houses were connected to the network during the project runtime. However, a feasible optimal plan was calculated. Further on, the electricity prices used were not up to date when running the optimization in the afternoon. Apparently, the DH owner had access to updated prices every hour. Luckily these price updates differed only slightly from the initial ones but they still resulted in the calculation of a sub-optimal plan. In the future, the MPC has to have direct access to the price updates that the DH owner receives. Finally,

the optimal plan sent to the DH owner was an advice. The DH owner was responsible for choosing the timeslots for operating the CHP, thus the CHP operation was not identical. To move from an advised plan to a fully automated plan in which no intervention from the DH owner is needed, it is important to adapt the MPC taking into account as much as possible the unforeseen events for forecasting and the latest price updates. Only this will give the DH owner the necessary trust to move to a fully automated CHP operation.

**Overall conclusions and lessons learned:**

The focus of the TEMPO project was to develop technical innovations that enable district heating networks to operate at lower temperatures. The evaluation of the test for the different TEMPO innovations showed following successes:

**First: The TEMPO innovations allowed to increase the performance of the DH networks in the two demo sides:**

- **A2A demo:**
  - The mixing station allows to locally reduce the supply temperature by on average 17 K and therefore reduced the heat distribution losses by 4% on average. However, the main functionality of the mixing station was to enable the full smart district heating controller implementation.
  - The smart district heating controller enabled a reduction of the primary return temperature of 0.7 K and up to 2 K by controlling the secondary supply temperature. At the same time, the peak energy was reduced by 60% to 70%. By controlling the mixing station supply temperature, the peak energy could be reduced by 30% to 50%.
  - The automated prediction of secondary side faults in combination with an evaluation of performance metrics allowed to identify poorly performing buildings very efficient. Remediating the "low-hanging fruits" of the identified faults would yield in a reduction of return temperature by 1.4K
  - The visualization for non-expert users resulted in productive feedback from technician, leading to clear statements on the building performance and the reasons causing high return temperatures, as well as the bilateral discussion of improvement options.
  - Visualization for expert users was rated positive by the involved experts.

- **ENERPIPE demo**
  - The decentralized buffer tanks allowed to reduce the connection capacity rates for new standard single-family houses from today's 30 kW down to theoretically 7.5 kW. Further on, smaller DH pipe dimensions enable cost savings for the DH network of around 11% of the yearly total costs
  - The smart district heating controller for smart buffer charging allowed a theoretical peak reduction of 35%.
  - The smart district heating controller for CHP optimization based on forecasts of the electricity price and the forecast of the total heat load allowed a theoretical improvement of the electricity revenues by 8%.
  - After some anomalous behaviour was detected, faults were corrected and the average return temperatures were reduced by 7.8 K.

**Second: Following technical barriers for the implementation of the TEMPO innovations have been identified, analysed and partly tackled:**

- **A2A demo:**
  - The implementation of ICT and monitoring equipment need to be carefully planned to ensure full connectivity and interoperability.
  - Capacity limits of the apartment building substation led to deteriorated performance during very cold weather.
  - The accuracy of automated fault detection and diagnosis was limited because of monitoring data was mostly available on the primary side.

- **ENERPIPE demo**
  - The existing inflexible rule-based controllers/backup controllers on the buildings side posed difficulties for the integration of innovative control concepts.
  - Four different ICT systems are involved to get a control signal to the decentralized buffers, leading to two main disadvantages: no single system having an overview of the complete workflow and it takes multiple persons to debug.
  - The rather small buffer size was reducing the available flexibility.
  - The forecasting of the heat load was difficult due to unplanned maintenance, additional heat input from a "satellite" and the connection of new houses during the project runtime.
  - The electricity prices used for CHP optimization were not up to date when running the optimization.
  - The optimal plan sent to the DH owner was an advice, but the DH owner was responsible for operating the CHP, thus the real CHP operation was not identical to the optimization.

**Third: The implementation of the innovations showed important lessons learned in terms of processes for the future deployment and scaling of the TEMPO innovations**

- Innovations developed in TEMPO made it easier to detect and diagnose suboptimal behaviour in specific buildings. However, legal and organisational hurdles meant that in most cases it was not possible to share the information with the end consumers and carry out audits of the building installations to ascertain the cause of suboptimal behaviour, let alone to remediate the issues rapidly.
- Every involvement and communication towards the customer is sensitive and needs to be planned carefully. The contractual terms as well as responsibilities and the ownership of the buildings and/or the DH substations must be carefully evaluated when proposing activities on customers side. Therefore, sufficient time and resources needs to be taken into account.

# TABLE OF CONTENTS

# GLOSSARY / LIST OF ACRONYMS

| ACRONYM | DEFINITION |
|---|---|
| **CHP** | Combined heat and power plant |
| **CSV** | Comma-separated values |
| **DH** | District Heating |
| **DHN** | District Heating Network |
| **HDD** | Heating degree days |
| **HT** | High-temperature (operation) |
| **KPI** | Key performance indicator |
| **LT** | Low-temperature (operation) |
| **MFH** | Multi-family house |
| **MILP** | Mixed-Integer Linear Programming |
| **MPC** | Model Predictive Control |
| **PLC** | Programmable logic controller |
| **RL** | Reinforcement Learning |
| **SFH** | Single-family house |
| **SoC** | State of Charge |
| **TEMPO** | Temperature Optimisation for Low Temperature District Heating across Europe |
| **WP** | Work package |

# 1.INTRODUCTION

The TEMPO – Temperature Optimisation for Low Temperature District Heating across Europe – project develops technical innovations that enable district heating networks to operate at lower temperatures. By decreasing the temperature in the systems, it reduces heat losses and allows a higher share of renewable and excess heat to be used as heat sources. The use of these heat sources will be crucial to adapt current district heating systems and create new ones suitable for a sustainable energy system.

The developed innovations are demonstrated and implemented in 2 district heating networks which cover 90% of the district heating market types. The two demonstration sites of TEMPO are located in the regions of Nuremberg (Germany) and Brescia (Italy).

- **Windsbach, region of Nuremberg (Germany):** The ENERPIPE demonstration site consists of a new district heating network which supplies heat to a less dense area of new buildings. Heat is provided by residual heat of a biogas plant, biogas CHPs and a peak gas boiler.
- **Brescia (Italy):** The A2A pilot project involves part of the Brescia district heating network in a low building density area consisting mainly of terraced houses and some apartment blocks. The existing network is heated by a waste-to-energy plant (~70% coverage), residual heat from industry and CHP, and peak-load gas boilers. The A2A network in Brescia started operating in the '70s, and currently operates at temperature levels around 120/60°C.

The description of the functionality of the different innovations, the improvements to the state-of-the-art, the costs and the impact of the results on the overall proposed solution can be found in [1].

This report describes the monitoring results and the calculation of key performance indicators for the demonstration sites and their results after the final monitoring season 2021-2022. For the ENERPIPE demonstration site, where monitoring started in March 2019, this is the fourth monitoring season. For the A2A demonstration site, where monitoring started in November 2019 after the installation of a mixing station, this is the third monitoring season.

For each demonstration site, the results presented in this report have been derived by aggregating several sources of monitoring data. Daily averages have been calculated for the relevant monitored parameters, and days with missing or clear outlier values have been screened out. The comparison of baseline and test performance was based on linear correlations between daily average values of the outdoor temperature and daily average values of parameters of interest as calculated for each period. Comparable values were then calculated by applying the resulting linear regression models (which are also illustrated as trendlines in scatter plots) to the same test period outdoor temperatures. More information on the performance assessment methodology is provided in the annexes.

# 2.A2A DEMONSTRATION SITE

## 2.1 INTRODUCTION

The Brescia district heating network of A2A has a supply temperature up to 130 °C in winter and 90 °C in summer, while the return temperature is around 60 °C and almost constant all the year; the maximum operating pressure of the network is 16 bar.

The first demonstration site[1] (**Fornaci**) corresponds to a part of the DH network in Brescia, connecting buildings are from the 1990s in a low-density area. Additional analyses have been performed on thirty other multi-family houses served by the DH network in Brescia. These additional buildings are referred to as "**city demo**"[2].

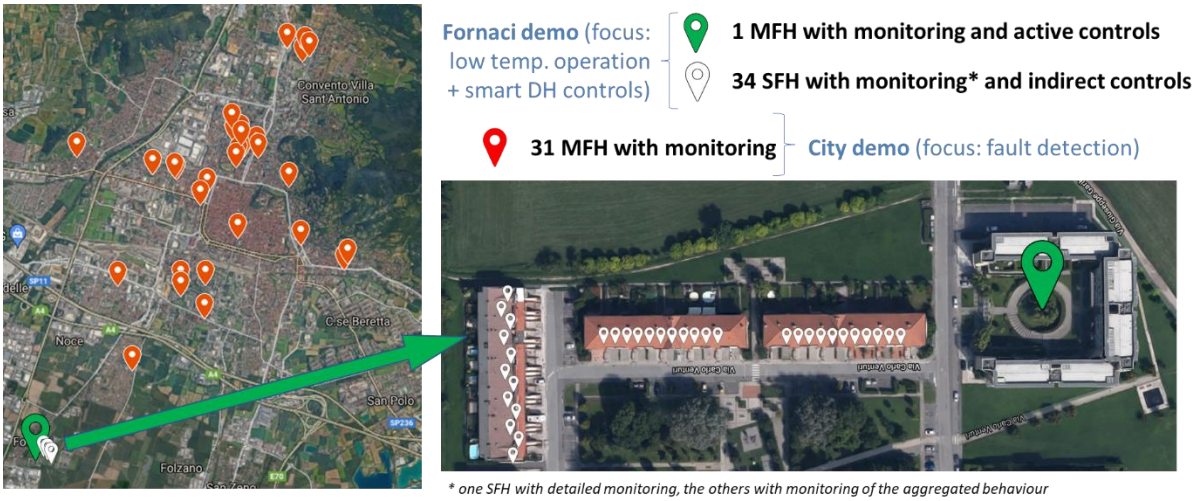


*Figure 1: the demo sites of A2A in the Brescia district heating network*

The following sections present results for each innovation applied in the demonstrator and its relevant key performance indicators (KPIs):

- **Mixing station** at the Fornaci demo: Comparing high temperature and low temperature operation for the time range January 2021 to February 2022 in terms of supply and return temperatures and heat distribution losses.
- **Smart controller** at the Fornaci demo (time range August 2021 to February 2022):
  - Smart control for peak load reduction
  - Smart control for return temperature reduction
- **Building installation optimization/fault detection** at the Fornaci demo and for the city demo buildings
- **Visualization** at the Fornaci demo (expert users) and for city demo (non-expert users)

[1] A more detailed overview of the A2A demonstration site and its innovations is provided in TEMPO deliverable D4.2 (see [8]).
[2] Formerly also referred to "mitigation site" buildings

## 2.2 MIXING STATION INSTALLATION

The first innovation tested in the A2A demonstration site is the mixing station. The primary side of the mixing station is connected to the main DH network. The secondary side of the mixing station supplies heat to the demonstration site network branch. By mixing return water of this branch with hot water from the main network, the supply temperature to this branch can be reduced. The mixing station was installed in November 2019 and mixing operation began in January 2020. These tests started in mid-January 2020, and the supply temperature of the demo site was progressively lowered from the value of the main network (around 120 °C) to around 90-100 °C.

### 2.2.1 SUPPLY AND RETURN TEMPERATURES

Supply temperatures (after mixing) and return temperatures were compared in so called "high-temperature" and "low-temperature" operation for the period from January 1st, 2021, to February 28th, 2022, excluding days with smart controller tests and days with problems.

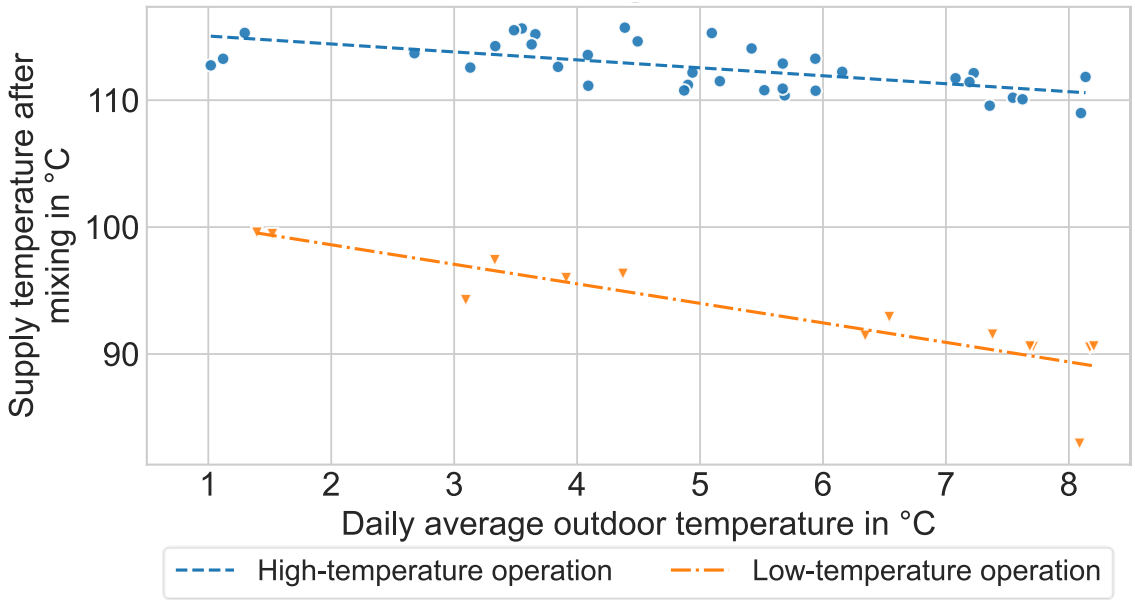


*Figure 2: Daily averages of supply temperature after mixing vs outdoor temperature, for high-temperature and low-temperature operation.*

Over this time range, the supply temperature after mixing, as shown in Figure 2, was in average 17 K lower during low temperature operation than during high temperature operation. As can be seen in Figure 3, the effect of low-temperature operation on return temperatures at the mixing station was very limited. On average, return temperatures increased by 0.2 K with low-temperature operation in comparison to high-temperature operation.

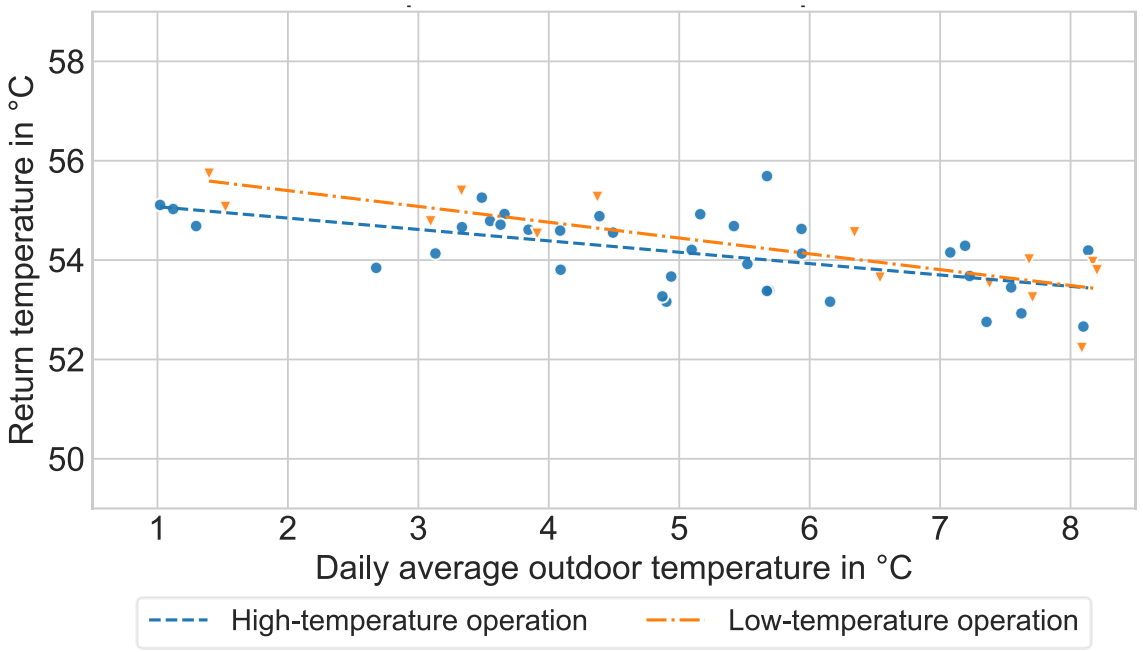


*Figure 3: Daily averages of return temperature at the mixing station vs outdoor temperature, for high-temperature and low-temperature operation.*

### 2.2.2 HEAT DISTRIBUTION LOSSES

Heat distribution losses were calculated as the difference in thermal powers measured at the mixing station and at the consumers, for periods when consumer data from both single-family houses and the apartment building are available (see Figure 37 in Annex 3). The considered periods range from February 10th, 2021, to February 28th, 2022. Over these periods, the distribution losses account for 17% of the overall heat supply.

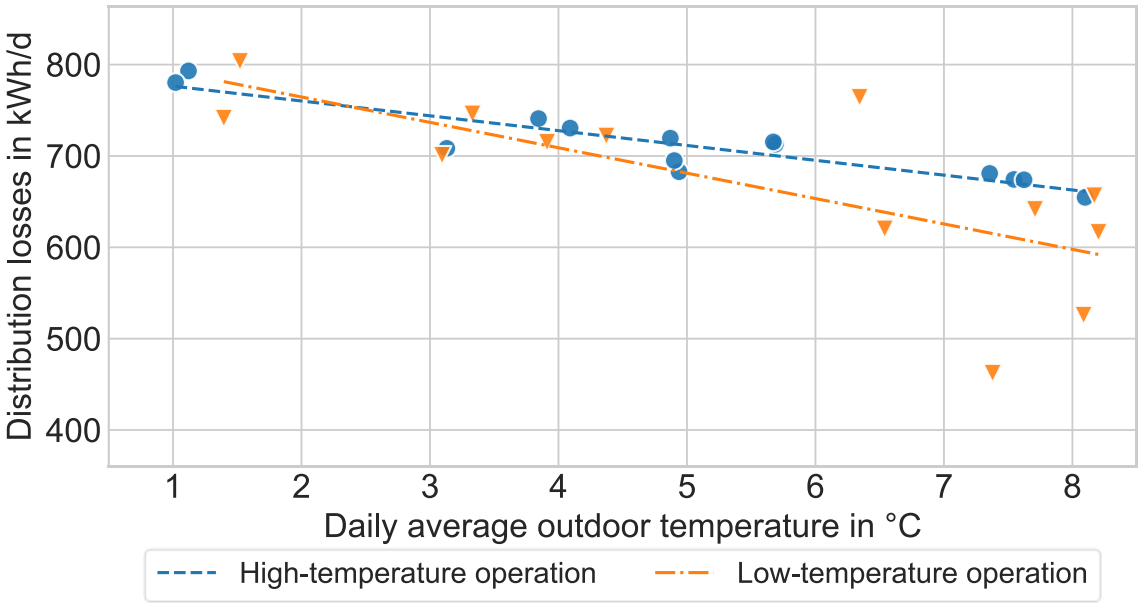


*Figure 4: Daily averaged distribution losses vs outdoor temperature at the A2A demonstration site in high-temperature operation vs low-temperature operation.*

In average, heat distribution losses were found to be 29 kWh/d lower during low-temperature operation (713 kWh/d in average) than during high-temperature operation (684 kWh/d in average), which amounts to a **4% reduction in heat distribution losses**. It can be seen, that in the range of 1-5°C outdoor temperatures, there is hardly a reduction of the heat distribution losses.

### 2.2.3 CONCLUSIONS

The installation of the mixing station in the demo site district heating network branch has enabled the possibility to test low-temperature operation as well as to modify the local supply temperatures.

During the monitoring phase, the supply temperature after the mixing station was on average 17 K lower during low-temperature operation, than during default high-temperature operation. It has been observed that reducing the supply temperature in the network branch reduces the heat distribution losses with 4% on average. The reduction of the heat distribution losses can be attributed to the supply pipes, because the temperature in the return pipes has been largely unaffected. Furthermore, lower supply temperatures would make it possible to make direct use of local alternative low-temperature heat sources (for instance waste heat and heat pumps) with lower greenhouse gas emissions. These heat sources would be impossible or considerably less efficient with high supply temperatures. The mixing station can be considered as an important preparatory step in this regard.

Moreover, one of the main benefits of the mixing station within TEMPO was the possibility to use advanced control algorithms for supply temperature control, as considered in the next paragraph. Thus, the mixing station was an important enabler for using the local branch of the DH network as a storage since control of the overall supply temperature in the full Brescia DH was not possible.

## 2.3 SMART DISTRICT HEATING CONTROLLER

The description of the functionality and the improvements to the state-of-the-art can be found in [2].

In the heating season 2021-2022, several different tests with the smart district heating controller have taken place:

- Control of the apartment building for return temperature reduction (Test A)
- Control of the mixing station for peak load reduction (Test B)
- Integrated control of the mixing station and apartment building for peak load reduction (Test C)

Besides these three different smart control regimes, the demo site was also regularly operated without smart control to monitor the baseline behaviour. In these baseline periods, the mixing station and apartment building were not actively controlled. Only baseline periods with the mixing station operating in low-temperature mode are used below for evaluation of the smart district heating controller. Table 1 gives an overview of the different test periods and the outdoor temperature ranges that were encountered during these tests.

*Table 1: Overview of test periods and outdoor temperature ranges for the different test types.*

| | **Test period(s)** | | **Range of daily average outdoor temperatures** |
|---|---|---|---|
| | **From** | **To** | |
| **Test A** | 25/10/2021 | 07/11/2021 | 8 °C – 14 °C |
| | 10/01/2022 | 16/01/2022 | 1 °C – 6 °C |
| **Test B** | 15/11/2021 | 28/11/2021 | 6 °C – 12 °C |
| | 24/01/2022 | 30/01/2022 | 2 °C – 6 °C |
| **Test C** | 06/12/2021 | 23/12/2021 | 1 °C – 5 °C |

The integrated smart control test (Test C) is not evaluated in this report, because the behaviour and performance of the controller in this test were not satisfactory. Further analysis of the results of this test is needed to better understand and resolve these issues.

### 2.3.1 MIXING STATION CONTROL FOR PEAK LOAD REDUCTION

In Test B, the smart controller determined the supply temperature of the mixing station to reduce the heat load peaks. Test B has taken place during two different periods: Test B1 from 15/11/2021 to 28/11/2021 and Test B2 from 24/01/2022 to 30/01/2022. An important difference between these two periods is the different weather. Test B1 took place in the fall with daily average outdoor temperatures in the range 6 °C – 12 °C, whereas Test B2 happened in the middle of winter with colder weather (2 °C – 6 °C).

Note that further in the text, peak load reduction is quantitatively assessed based on the amount of the thermal energy load that would be covered by expensive and/or fossil-based peak units. It is therefore assumed that the heat load above a certain thermal power threshold is coming from peak units. This notional threshold is based on heat generation data from 2020, when about 20% of the energy to the Brescia DH network was provided by a coal-fired peak unit. It is considered that the demo site covers only a small part of the Brescia district heating system. However, the reduction of peak-load boiler operation in the overall district heating network is assumed to be proportional. Correspondingly, the notional "peak load energy" is the energy that would have to be supplied by a peak load generation unit whenever a threshold of 169 kW (corresponding to the capacity of a notional base load generation unit) is exceeded. With this threshold, the peak load energy amounted to 20% of the total energy supplied by the mixing station in 2020 (see load-duration curve in Figure 5).

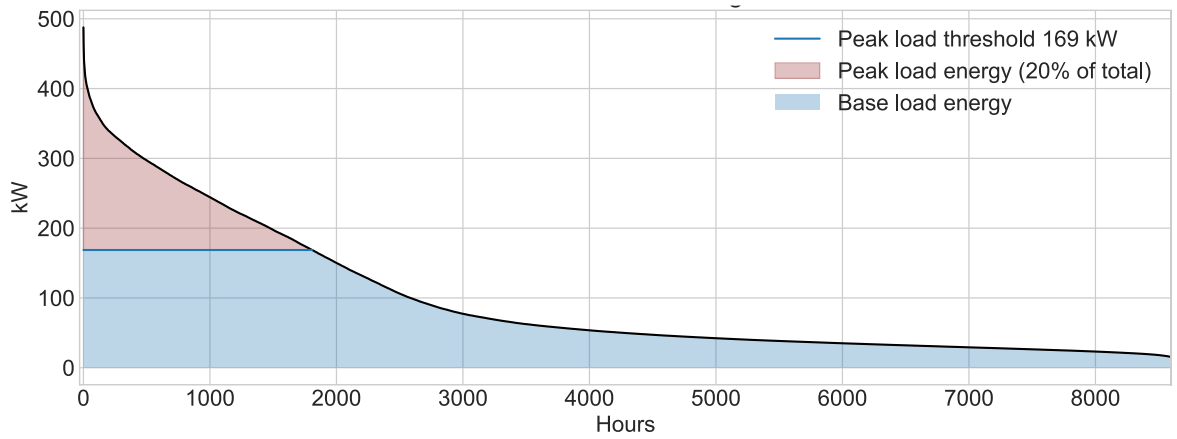


*Figure 5: Load-duration curve at the mixing station (in kW) for the year 2020, with notional "peak load energy" corresponding to loads above a threshold of 169 kW, accounting for 20% of the total supplied energy, represented in red.*

**Results:** Typical daily profiles for supply temperature and thermal power are displayed in Figure 6 (Test B1) and Figure 7 (Test B2). During the baseline low-temperature operation, the mixing station supply temperature profile is correlated to the outdoor temperature and therefore typically rather flat.

During Test B1 the control algorithm mostly kept the supply temperature as close to the lower limit as possible. Except for during the early morning (2am-5am) and afternoon (2pm-4pm), when the supply temperature was typically increased to charge the district heating network with thermal energy. These charging actions happened in anticipation of subsequent peak power demands. The magnitude of the supply temperature increase during charging actions balances the thermal power demand of the mixing station but is also sometimes limited by the available temperature level of the main district heating grid. Directly following these charging actions, the stored thermal energy is released – by reducing the supply temperature again – to reduce the thermal power that the mixing station needs to deliver. In this way, the daily thermal power profile is flattened, and the amount of energy that needs to be generated at peak powers is reduced.

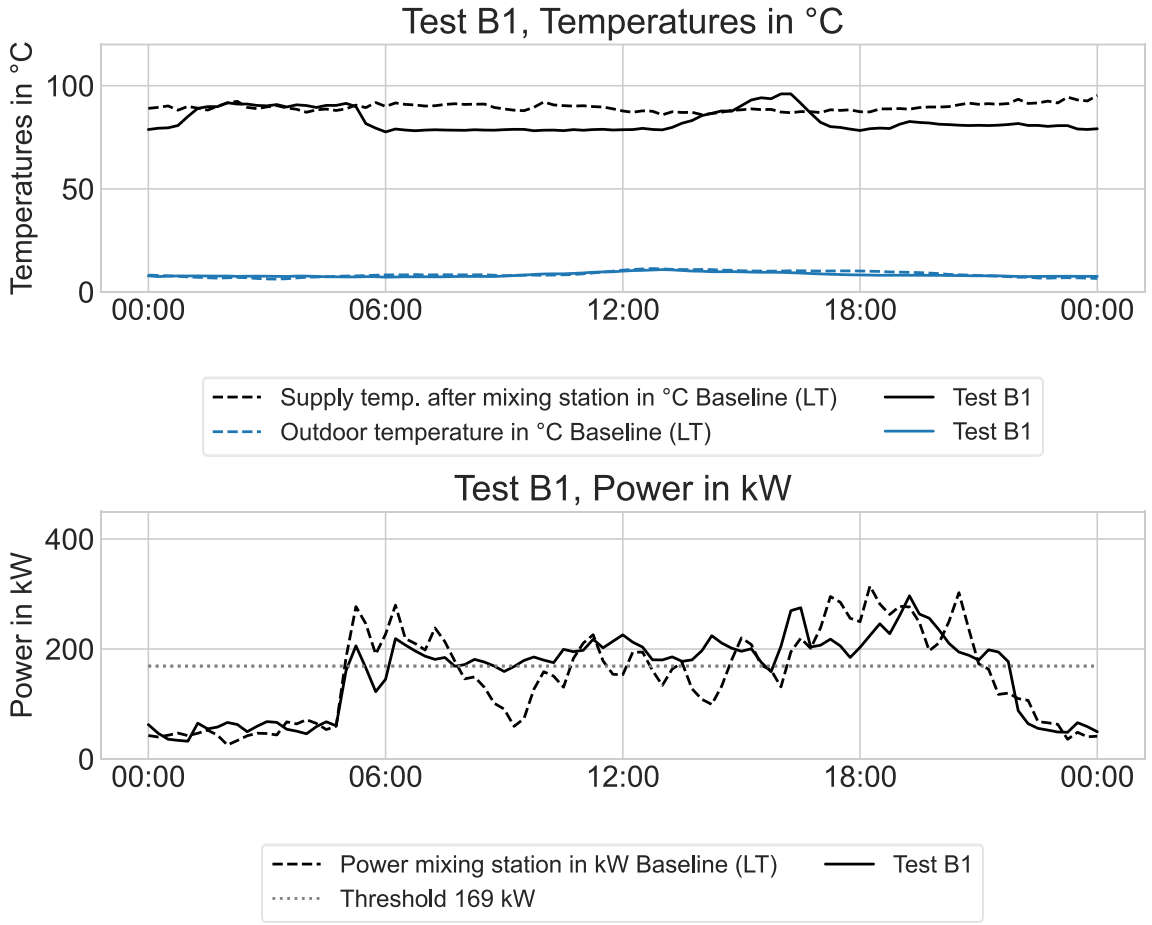


*Figure 6: Temperature and power profiles for two days representative of test B1 (November 21st, 2021) and of the baseline (low-temperature operation, November 8th, 2021) at comparable outdoor temperatures (8-9 °C in average).*

During **Test B2** (Figure 7), the typical behaviour of the smart controller was different than in Test B1. The supply temperature was now raised above the minimal value during a larger portion of the day. This is especially the case in the middle of the day, in between the morning and afternoon charging actions. This behaviour indicates that the controller expects the need for elevated supply temperatures to transfer sufficient heat to the customers to satisfy their thermal comfort. This also happened during times of high heat demand. Note that the outdoor temperature was substantially lower during Test B2 than during Test B1 which is accompanied by a higher heat demand. The magnitude of the daily supply temperature variations in test B2 is typically higher than those in Test B1. In Test B2, the mixing station supply temperature rose to 115 °C, made possible by the higher main grid temperature due to the colder weather.

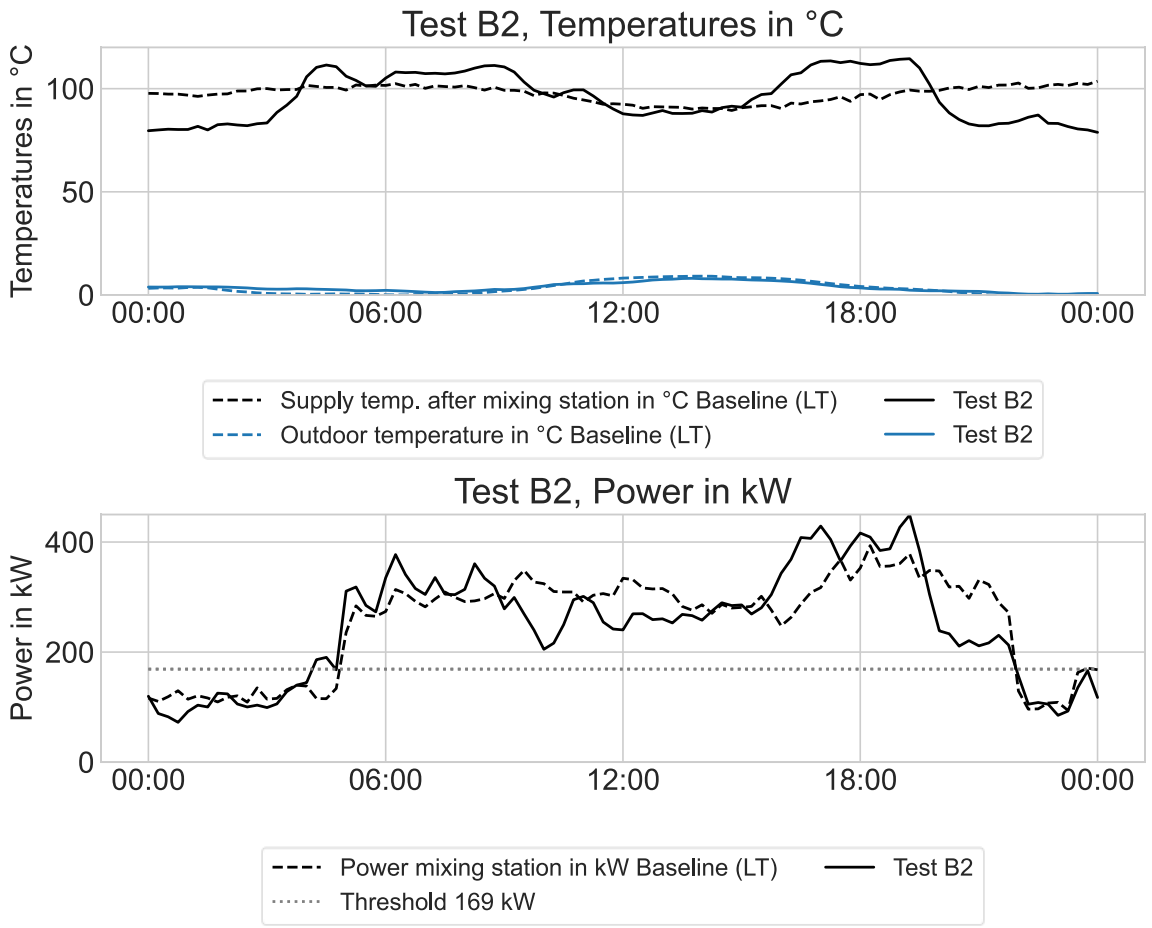


*Figure 7: Temperature and power profiles for two days representative of test B2 (January 28th, 2022) and of the baseline (low-temperature operation, January 23rd, 2022) at comparable outdoor temperatures (3 to 4 °C in average).*

In contrast to the expected behaviour, the thermal power profile of the mixing station clearly has higher peaks than the reference. Investigation of this issue has shown that the substation of the apartment building in the demo site operates at its capacity limits when the outdoor temperature is lower than about 7 °C. This means that the apartment building substation is operating at its maximum primary flow rate, trying but failing to achieve the secondary supply temperature setpoint. The reason for hitting this operational limit cannot be fully clarified with the available data and information. Possible explanations are: undersizing or wrong installation of the apartment building substation heat exchanger, incorrect settings of the substation controller, insufficient available differential pressure.

When the substation is operating at maximum flow rate, it is no longer capable of effectively controlling the building heat load. As a result, the assumption that the heat load is independent of the primary supply temperature no longer holds. Instead, an increase in the primary supply temperature leads to an increase of the thermal power. This can be seen in Figure 7. Consequently, because of the capacity limits of the apartment building substation, load shifting by mixing station control is not possible during cold weather. Note that similar substation capacity limits could have played a role in other buildings in the demo site also. However, the necessary data for verification is not available.

**Evaluation:** Figure 8 presents a graph of the daily amount of peak energy as a function of daily average outdoor temperature. Test B1 performed well in terms of reducing peak heat demand. On average, the peak energy consumption was reduced by between 200 kWh and 500 kWh per day (in average 317 kWh per day), depending on the outdoor temperature. In relative terms, this corresponds with 30% to 50% (38% in average) less peak energy than in the baseline operation without smart controller. Test B2 on the other hand shows a higher amount of peak load energy than in the baseline, about 400 kWh to 700 kWh per day (588 kWh per day in average), depending on the outdoor temperature. This is contrary to the desired behaviour. As explained before, this is due to the apartment building substation facing capacity limits when the weather is very cold. Indeed, Figure 9 shows that below around 7 °C outdoor temperature, this substation is not capable of reaching the secondary supply temperature setpoint anymore.

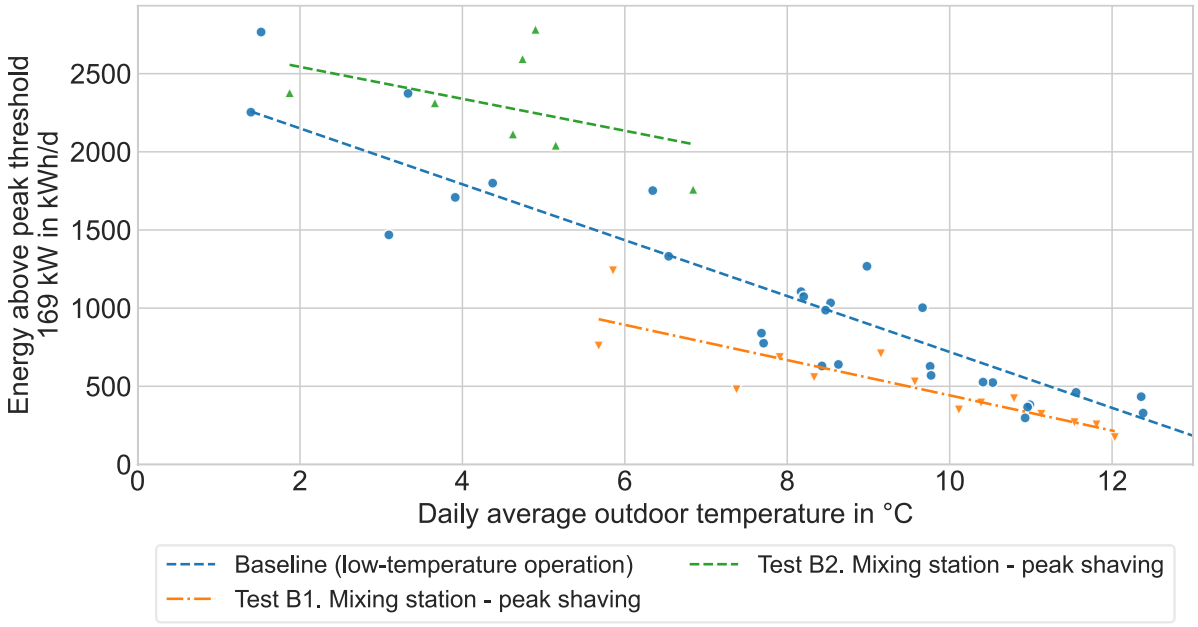


*Figure 8: Daily values of energy above peak power threshold of 169 kW vs outdoor temperature, for the peak load reduction tests vs baseline (low-temperature operation)*

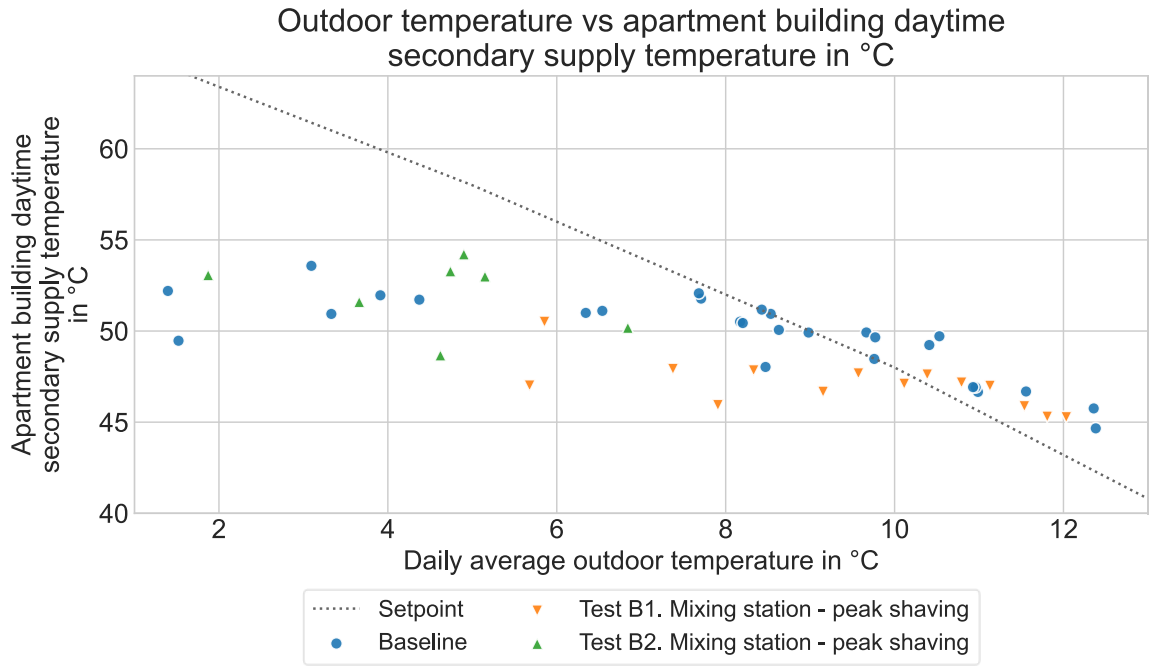


*Figure 9: Secondary supply temperature in the apartment building (daily averages, considering only daytime values for supply temperature), during low-temperature operation, Test B1 and Test B2, as well as setpoint value vs. outdoor temperature.*

### 2.3.2 APARTMENT BUILDING CONTROL FOR RETURN TEMPERATURE REDUCTION

In Test A, the smart controller determined the secondary supply temperature of the apartment building substation to reduce the primary return temperature. Test A has taken place during two different periods: Test A1 from 25/10/2021 to 07/11/2021 and Test A2 from 10/01/2022 to 16/01/2022. As with Test B, the weather conditions were very different between the two test periods. The outdoor temperature during Test A1 varied between 8 °C and 14 °C, whereas the weather during Test A2 was colder (between 1 °C and 6 °C).

**Results:** Figure 10 and Figure 11 respectively show the typical daily profiles of the key temperatures of the apartment building substation and the mixing station thermal power for Test A1 and Test A2. These days with typical test behaviour are compared with days in baseline operation, taking care that the outdoor temperature is very similar. Note that also the indoor temperature profiles in the test and in the baseline are almost the same. In the baseline operation of the apartment building, the secondary supply temperature profile is determined by the outdoor temperature profile through the substation controller heating curve. As a result, the supply temperature peaks during the morning and evening, and is lower in the middle of the day when outdoor temperatures are higher. However, the behaviour is different when the outdoor temperature is very low (< 7 °C). As discussed in the previous section, the apartment substation is then not capable of reaching the secondary supply temperature setpoint. For example, this happened on 21/01/2022 (Figure 11). Note that the apartment building space heating system is only active during the daytime (5am-10pm).

During the return temperature reduction **Test A1**, the secondary supply temperature profile has been flattened by the smart controller (05/11/2021) in comparison with the reference behaviour (09/11/2021). This has led to lower primary return temperatures during the peak times (5am-10am and 5pm-10pm), by up to 10–15 °C lower during some times. Furthermore, in these periods the mixing station thermal power is also reduced significantly.

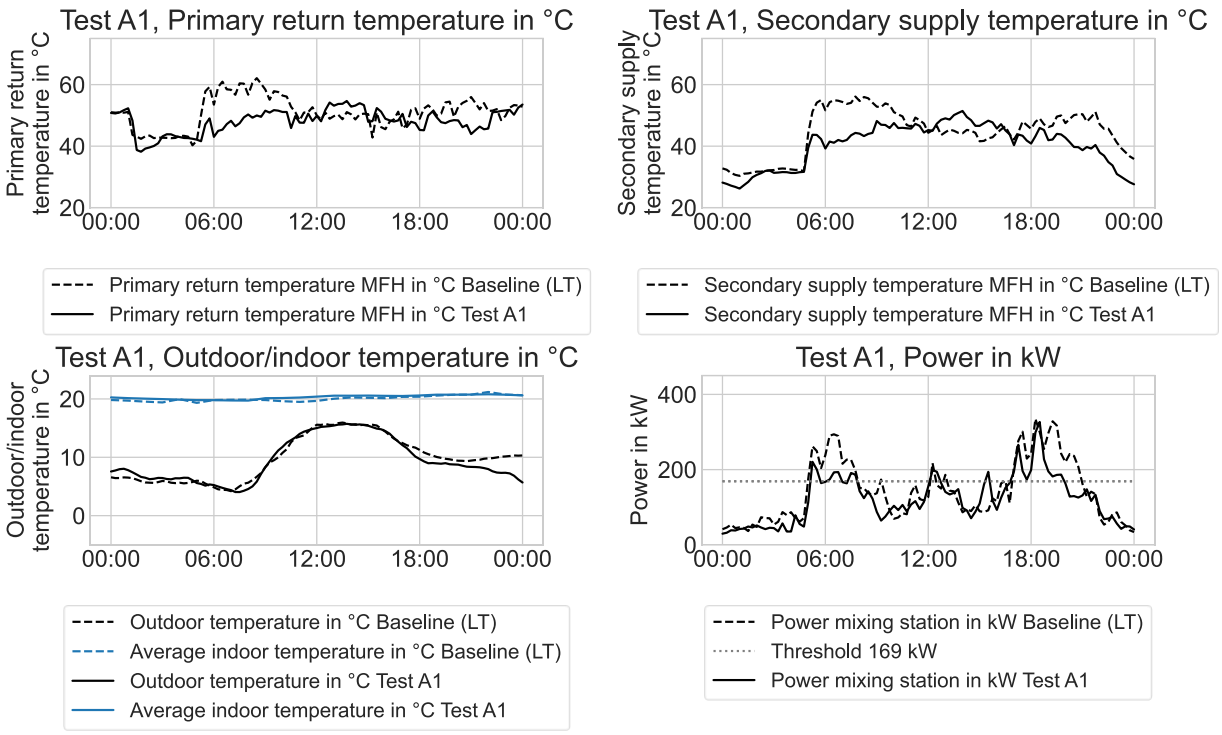


*Figure 10: Representative profiles for Test A1 (November 5th, 2021) vs baseline (November 9th, 2021) for similar conditions (outdoor temperatures in average between 9 and 10 °C)*

In **Test A2** (Figure 11), the smart controller could not significantly affect the secondary supply temperature profile of the apartment building. This is because the secondary supply temperature then was limited by the capacity of the substation, which happened to be insufficient during the cold weather. As a direct consequence, the apartment building return temperature and mixing station thermal power profiles are not affected either.

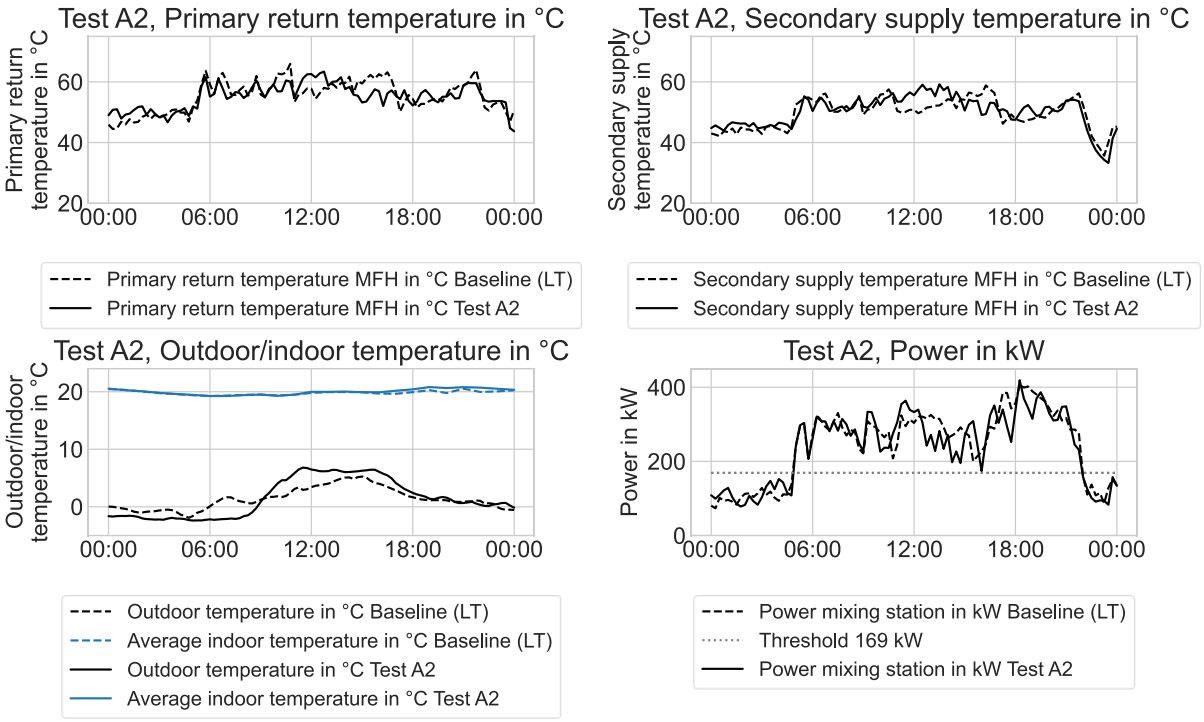


*Figure 11: Representative profiles for Test A2 (January 10th, 2022) vs baseline (January 21st, 2022) for similar conditions (outdoor temperatures in average 1-2 °C)*

**Evaluation:** The flowrate-weighted daily average primary return temperature of the apartment building substation is depicted as a function of the daily average outdoor temperature in Figure 12. It shows that the return temperature during Test A1 was reduced on average by 0.7 K with respect to the baseline. Also Test A2 shows a return temperature reduction with respect to the baseline trend (0.9 K on average). However, we do not want to claim this as a result of the smart controller due to the aforementioned capacity limits of the apartment building substation. It is shown in Figure 13 that indeed the secondary supply temperature in the apartment building could not be reduced with respect to the baseline, because in both situations the setpoint value could not be reached when the outdoor temperature is below 7 °C.

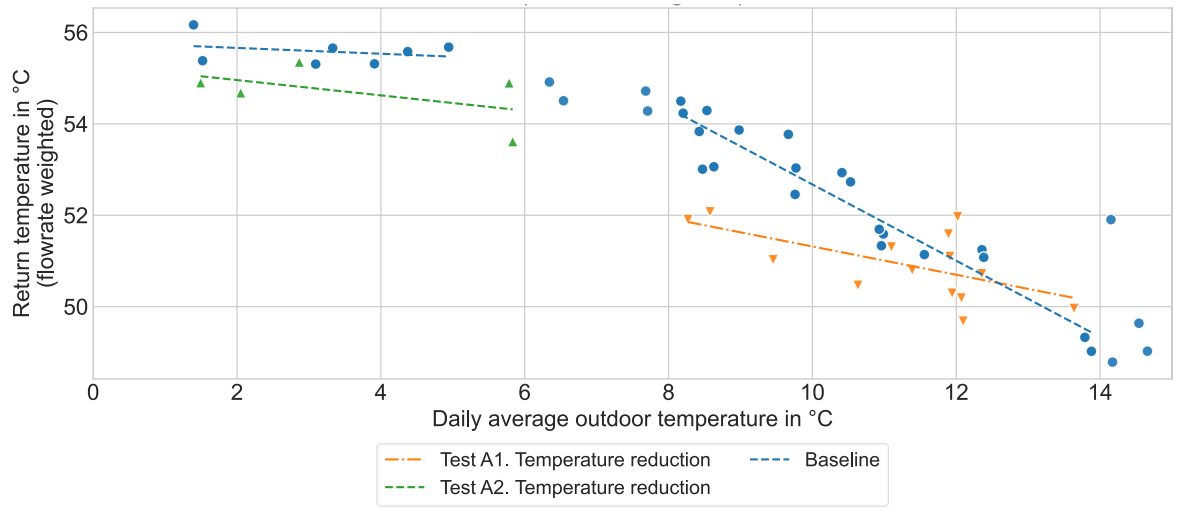


*Figure 12: Outdoor temperature vs flowrate weighted return temperature at the mixing station, for tests A1, A2 and the corresponding baseline (low-temperature operation)*

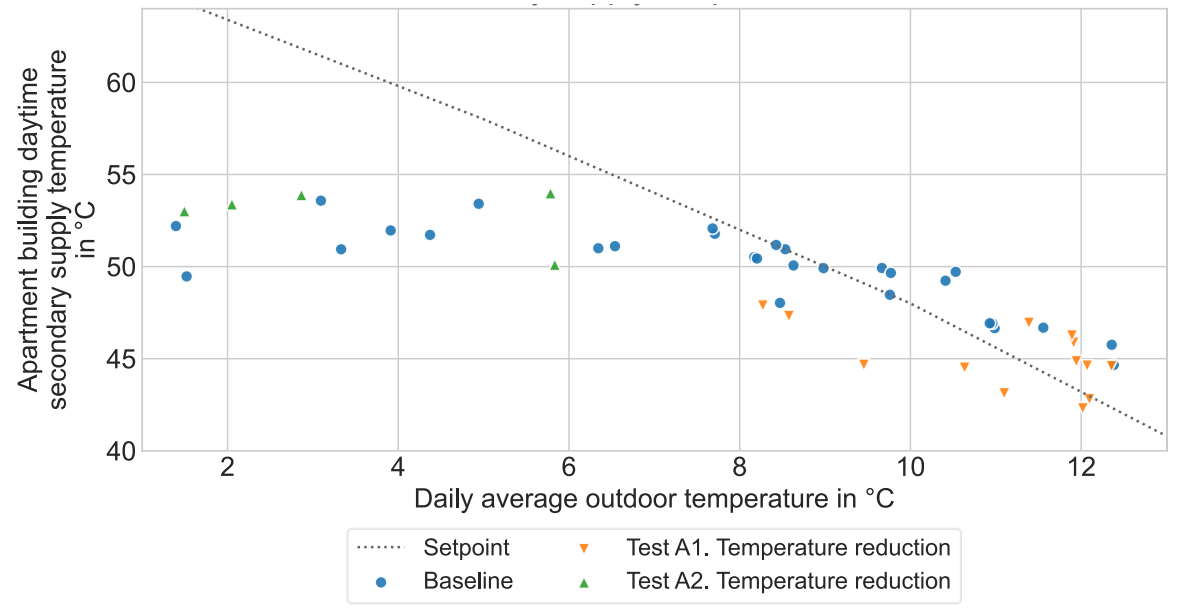


*Figure 13: Secondary supply temperature in the apartment building (daily averages, considering only daytime values for supply temperature), during low-temperature operation, Test A1 and Test A2, as well as setpoint value vs. outdoor temperature.*

Besides return temperature reduction, the control of the secondary supply temperature has as a "side effect" also a reduction of the peak demand. Figure 14 shows the daily peak energy provided by the mixing station as a function of outdoor temperature. It can be seen that in Test A1 – in addition to return temperature reduction – a reduction in the peak energy load by 330 kWh per day on average and up to almost 700 kWh per day was achieved, compared to the regular low-temperature operation of the mixing station. The reductions correspond with about 60% to 70% of the baseline peak energy load. Test A2 however did not result in peak load reduction, for the same reasons described above for return temperature reduction.

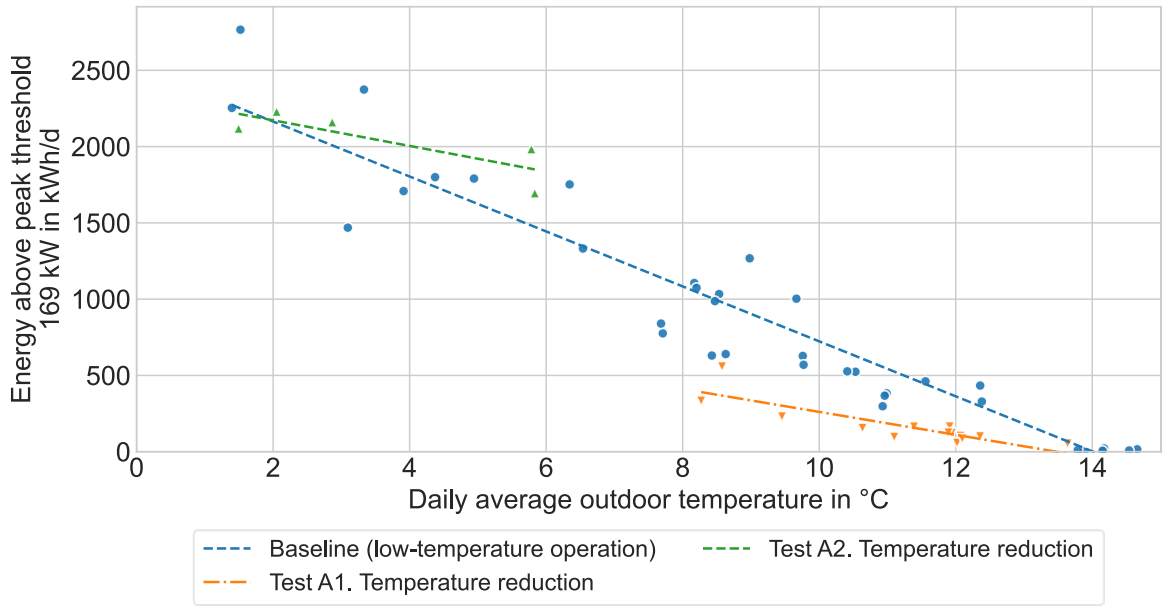


*Figure 14: Daily values of energy above peak power threshold of 169 kW vs outdoor temperature, for the return temperature reduction tests vs baseline (low-temperature operation)*

### 2.3.3 CONCLUSIONS

Tests with the smart district heating controller in the A2A demonstration site have led to the following results.

Control of the mixing station supply temperature (test B) has been able to reduce the peak energy by 200 to 500 kWh per day, depending on outdoor temperature. These numbers represent a reduction by about 30% to 50% of the baseline peak energy, evaluated with respect to a notional peak power threshold. However, during very cold weather (below 7 °C outdoor temperature), the peak energy unfortunately increased due to capacity limits of the apartment building substation.

Control of the apartment building supply temperature (test A1) resulted in an average reduction of the primary return temperature of 0.7 K, up to 2 K for some days depending on the outdoor temperature. At the same time, the peak energy was reduced by 330 kWh per day in average and up to 700 kWh per day, representing 60% to 70% of the baseline peak energy. Unfortunately, the capacity limits of the apartment building substation also led to deteriorated performance during very cold weather for this test. The primary return temperature reductions in Test A2 of 0.9 K on average are therefore considered coincidental.

## 2.4 FAULT DETECTION AND BUILDING OPTIMIZATION

The description of the functionality and the improvements to the state-of-the-art can be found in [2].

### 2.4.1 FAULT DETECTION IN THE FORNACI DEMO

A simulation-based approach to fault detection for optimization of the building installations has been applied to the multi-family house and to the single-family houses of the Fornaci demonstration site, for the later primary-side monitoring data with 10-minute frequency was available. As shown in Figure 15, the return temperatures of the individual buildings range from below 50 °C to more than 75 °C, and the fault detection algorithm tends to predict faulty operation in most of the buildings with high return temperatures.

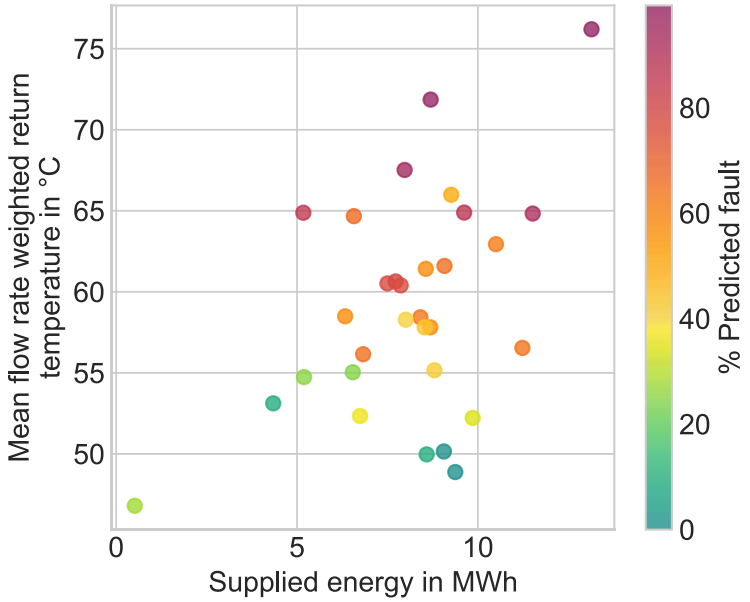


*Figure 15: Individual building performance for the single-family houses of the Fornaci demo from September 2021 to February 2022, in terms of supplied energy, mean (flowrate-weighted) return temperature and percent of predicted faulty behaviour (confidence score averaged over all days)*

Fixing the faults leading to temperatures above 60 °C (which may be assumed to be the "low hanging fruits") would yield an average (flowrate-weighted) reduction in return temperature of at least 2.7 K for all the single-family houses.

However, the substations of the SFH are owned by the individual house owners and managed by a variety of maintenance companies, and cannot be legally accessed by A2A. As a consequence, it was not possible to investigate further nor to remediate these faults.

### 2.4.2 FAULT DETECTION IN THE CITY DEMO

Primary-side data for 31 additional multi-family houses in Brescia ("city demo") were available. The simulation-based fault detection and diagnosis methodology was applied to these buildings.

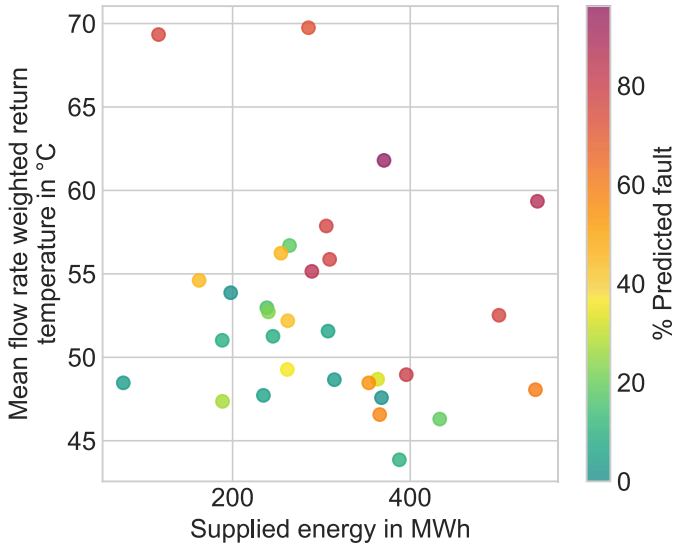


*Figure 16: Individual building performance for the city demo from September 2021 to February 2022, in terms of supplied energy, mean (flowrate-weighted) return temperature and percent of predicted faulty behaviour*

As shown in Figure 16, there was also a significant variability in building performance in this case, with two outliers reaching mean return temperatures of almost 70 °C and 13 buildings with mean return temperatures below 50 °C for the period September 2021 to February 2022.

However, flowrate-weighted return temperatures only correlate with fault predictions to a certain extent. A deeper look at the data reveals that the fault detection algorithm seems more prone to predict faults in cases where return temperatures are low in average but exhibit higher values either at times of low heat demand, or at times of very high heat demand (which do not occur frequently). Also, it might be biased to predict more faults in buildings with higher energy demand. Moreover, the algorithm has limited accuracy when only primary data are available: the classification accuracy calculated by cross-validation with simulated data is 79%, and taking into account differences between simulated and real data it can be expected that the accuracy with real data is lower. Remarks and indicators for the individual buildings can be found in the appendix (Table 10).

Fixing the faults leading to temperatures above 55 °C (which may be assumed to be the "low hanging fruits") would yield an average (flowrate-weighted) reduction in return temperature of 1.4 K.

### 2.4.3 CONCLUSIONS

The approach to optimization of the building installations developed in TEMPO has been applied to two sets of buildings (single-family houses of the Fornaci demo, multi-family houses of the city demo) in the A2A demonstrator. While the accuracy of automated fault detection and diagnosis was limited (as shown by cross-validation on the simulation training data) because of monitoring data limited to the primary side (except for two buildings), combining automated predictions with performance metrics made identification of poorly performing buildings efficient. Remediating the identified faults would imply important communication effort but could result in a significant reduction of return temperatures.

## 2.5 VISUALIZATION IN THE CITY DEMO (NON-EXPERT USERS)

The description of the functionality and the improvements to the state-of-the-art can be found in [2].

### 2.5.1 OVERALL PROCESS

For the visualization for non-expert users, the results of the fault detection activities described in 2.4 have been selected. Focus was on the buildings within city demo, since they have a relatively large impact compared to the SFH of the Fornaci demo. Further on, the SFH have private owners that often take care on their substations individually and the visualization would have been required more resources than available; also the substations of the SFH are directly inside the building with limited access.

The 31 MFH of the city demo are not operated by A2A but by an external company and A2A has no access to the substation of the MFH. Consequently, the demonstration has to be done via the responsible building managers and their technicians. Thus, one priority within TEMPO was to set-up a clear communication process, see Figure 17.

1. the monitoring data of the 31 MFH were extracted by A2A
2. the data has been analysed (see section 2.4.2), resulting in ranking of worst performing buildings in terms of high return temperatures. The 10 worst performing buildings have been selected, the test results are visualized and easy to understand and short reports for the buildings are created
3. Those reports are communicated to the building managers of the worst performing buildings
4. The building managers are asked to involve their technicians. The technicians are encouraged to get in discussion with A2A on possible improvements.

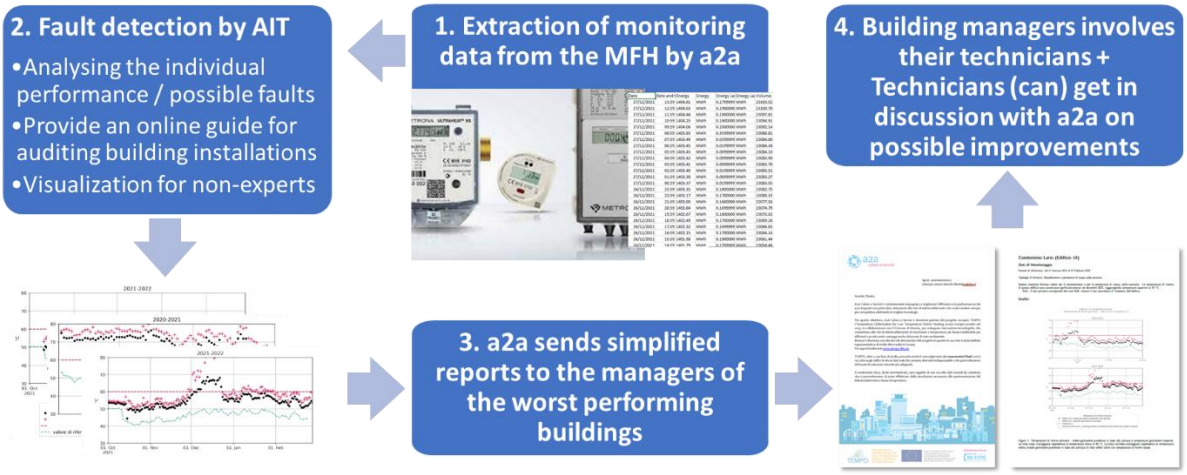


*Figure 17: Implemented activities and process for the visualization towards non-expert users in the city demo*

### 2.5.2 FEEDBACK

Following these evaluations, feedback was obtained. Figure 18 shows the example of one building, where high return temperatures have been identified by the algorithm between beginning of December 2021 and until around 20th December.

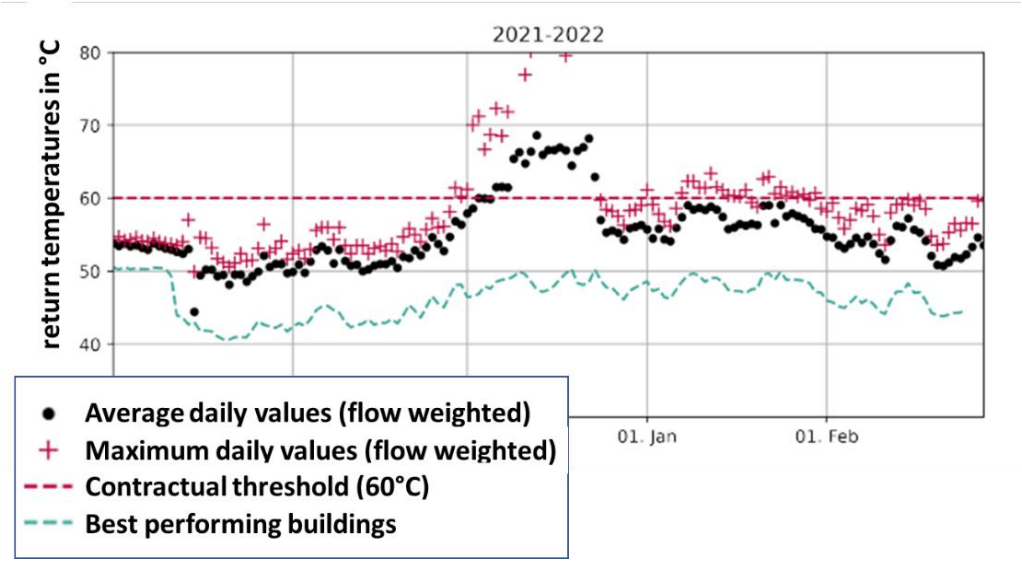


*Figure 18: Example results for the visualization towards non-expert users in the city demo (figure is translated back to English, but the reports were sent in Italian)*

This information has been sent to the responsible building manager and they are asked to forwarded the reports to their local technician. The communication between A2A technical personal and the local technicians revealed the reason for this behaviour: every winter, the heat exchanger for the domestic hot water preparation starting to foul, resulting in high return temperatures and a sub-optimal performance of the domestic hot water preparation. As a results, the building technicians are regularly cleaning the heat exchanger, resulting in decreasing return temperatures. In the communication, counter measures were suggested by A2A personal to avoid fouling in the future.

### 2.5.3 CONCLUSIONS

The main innovations for the visualization towards non-expert users developed within TEMPO are related to

- **Fist**: the visualization of the results. Here, particular care was taken to simplify the complex results of the TEMPO project by using clear indicators and diagrams and avoid any confusing information. It was important to clearly distinguish the performance of the individual building, the baseline as well as the performance of the best performing buildings.
- **Second**: The communication process towards the building managers and their technicians. Since those building managers are key customers of A2A, the communication processes need to be carefully designed and aligned within different departments within A2A. The involvement of the local technicians is important, since the building managers often have non or very little technical background or knowledge on the building heating system.

One of the main conclusions is, that every involvement and communication towards the customer is sensitive and needs to be planned carefully. The contractual terms as well as responsibilities and the ownership of the buildings and/ or the DH substations must be carefully evaluated when proposing activities on customers side. Therefore, sufficient time and resources needs to be taken into account.

The feedback from one building technician shows, that the communication process was partly successful and leads to clear statements on the building performance and the reasons causing high return temperatures, also the discussion with A2A technicians is a positive result, leading to an improved performance of the heating system in terms of reduced return temperatures. However, even more time and resources would be required to intensify the communication to the building managers and involve their local technicians.

## 2.6 VISUALIZATION IN THE FORNACI DEMO (EXPERT USERS)

The description of the functionality and the improvements to the state-of-the-art can be found in [2].

### 2.6.1 REVIEW STUDY

In order to evaluate the system performance of the expert-user visualisation system a review study was performed with the expert users. A set of seventeen energy system experts at A2A were introduced to the visualisation system and were asked to review the system for a period of time. After this period, a questionnaire was created, translated into Italian, issued to all the participant and they were asked to complete. The questionnaire was segmented in a primary section with twelve predefined questions with multi-answers and a secondary section where they could provide any input they wanted. The questions in the first part of the questionnaire were constructed in such a way that they could all be answers in one of five ways:

- Strongly disagree
- Disagree
- Neutral
- Agree
- Strongly agree

Therefore, it was possible to study the overall response to the system usage. Figure 19 shows the average distribution of the answers to the twelve questions. Interestingly enough, the results show a distinct segmentation between those who agree and those who disagree, while relatively few were neutral. A major part of the responders agreed and viewed the system in a positive way, although a significant group do not agree. However, based on the secondary part of the questionnaire, it seems as though several of the responders who answer with heavy disagreement do not do this because they do not like the system, but rather since they would like it to do more.

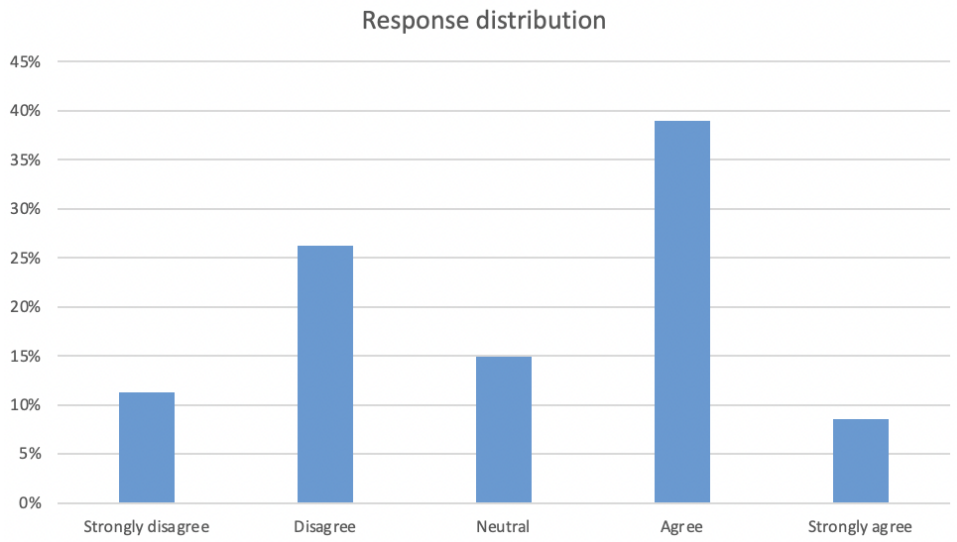


*Figure 19: Distribution of answers for the expert-user questionnaire*

The open-ended question for the secondary part provided several good inputs to the continued development of the system. Out of seventeen responders, as many as fifteen contributed additional input, which indicates a significant interest in the system. The most general comments related to making things easier to understand and to clarify the specific content. Furthermore, comments regarding design and layout of the different tabs of the Data Studio dashboard were relatively common among the responders.

Further development was performed based on the input from the questionnaire and it provided valuable feedback from potential users. Basically, the feedback was sectioned into three segments:

- Possible to address in TEMPO
- Possible to address in general, but not within the TEMPO project
- Not possible to address

The second bullet relates to things that might require significant software development efforts and that are clearly out-of-scope for TEMPO, although they are relevant for post-TEMPO commercial development. The last bullet relates to things that simply not possible to solve from a technical perspective, or things that are disregarded for other reasons.

### 2.6.2 CONCLUSIONS

Feedback from expert users were gathered through a questionnaire including multi-answer questions as well as an open input section. This provided a mix of input that could be both objectively and subjectively studied.

At first glance, the multi-answer question input seems to indicate a division among the expert users as to whether they are positive to the system or not, albeit with a clear predominance for being positive. However, the open input section indicates that most, if not all, of the experts are positive to the system as such. Rather, the ones who indicate negative answers in the multi-answer input, primarily what to improve it and found some functionality lacking.

A clear conclusion is that the visualisation tool can provide relevant decision-support for expert users. Most are positive to the concept as such, although a significant segment of the users provided relevant suggestions for further improvements. The main theme in among the suggestions was to simplify the practical usage of the system. One conclusion related to this is to remember the fact that the expert users are experts on district heating systems, not experts on IT-systems. Furthermore, many suggested to more clearly clarify the performance metrics involved. The conclusion relating to this is that additional documentation is important when used in a commercial setting. This would provide the requested clarification, without cluttering the visualisation tool itself.

Several inputs from the open input section resulted in further development of the visualisation tool. Furthermore, additional requirements were added for future implementation in a post-TEMPO development iteration.

# 3. ENERPIPE DEMONSTRATION SITE

## 3.1 INTRODUCTION

The ENERPIPE demonstration site[3] is located in Windsbach (6000 inhabitants, located 35 km south west of Nuremberg, Germany), where the municipality planned a new residential housing project supplied with district heating (DH) in a rural area. The constructions are planned in three phases, of which the first two are relevant for the project. Numbers of connected substations in each phase are summarized in Table .

The following sections present results for each innovation applied in the ENERPIPE demonstrator:

- The decentralized buffer concept, which aims at reducing the peak load, thus allowing pipe dimensions to be reduced. Since this innovation was implemented physically from the start, it can only be compared to hypothetical or simulated baselines.
- The smart district heating controller, which was applied both at the heat generation level (CHP optimization) and at the level of individual units, attempting to realize peak shaving by coordinated buffer charging
- Fault detection and building optimization

[3] A more detailed overview of the ENERPIPE demonstration site in Windsbach and its innovations is provided in D3.2 (see [10]).

## 3.2 DECENTRALIZED BUFFER TANKS

The description of the functionality, the improvements to the state-of-the-art, the costs and the impact of the results on the overall proposed solution can be found in [1].

### 3.2.1 SIMULATION STUDY FOR THE TECHNICAL AND ECONOMICAL OPTIMIZATION OF THE DECENTRALIZED BUFFER TANK CONCEPT

A simulation study was conducted to elaborate the technical and economical optimisation potential of the decentralised buffer tank concept. It comprises the decentralised buffer tank approach in the consumer buildings and the district heating (DH) network supplying the consumer buildings. Aim of the simulation study is a supply concept optimisation, which allows improvements in the design of future projects.

This section gives a summary of the main results and findings of the simulation study. The full documentation can be found in Annex 4.

Buffer tanks installed in the consumer buildings reduce the peak load demand of the consumers and thus also the peak load demand of the entire DH network. This effect is exemplarily shown in Figure 20. The illustrated buffer tank charging profile is the relevant profile for the house connection from the DH network point of view. The reduction in peak load demand allows for smaller DH network pipe dimensions, which can lead to lower investment costs for the piping as well as reduced thermal losses in the DH network. On the other hand, the concept leads to increased investment costs and thermal losses in the house stations compared to standard heat transfer substations. The simulation study looks into details of the relationship of consumer peak load reduction by various buffer tank volumes and the potential reduction of DH network pipe dimensions.

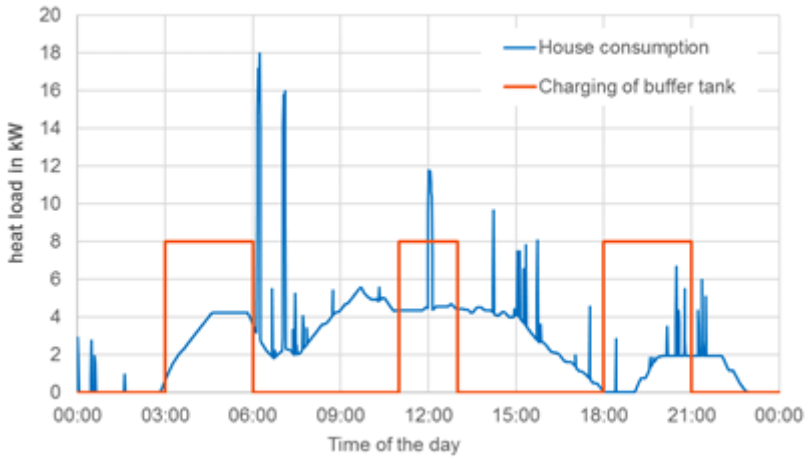


*Figure 20: Exemplary comparison of house consumption profile and buffer tank charging profile*

A first simulation model for the Enerpipe CaldoTHERM house station is developed and verified with measurement data. It allows a detailed investigation of the effects of different buffer tank sizes and house connection capacity rates in one-minute time steps taking into account the fast dynamics and inertia. Due to the high complexity of a DH network with a large number of consumers the combined DH network simulation model is simplified while

preserving all the essential effects described above. This simplification focuses on a representative DH network branch with only a limited number of consumers. In this branch, the mutual dependency of buffer tank volumes and DH network pipe dimensions is investigated in detail. Both the consumer substation part of the simulation model as well as the DH network branch model are verified with monitoring data to ensure high quality simulation results. The results of the detailed branch simulations are transferred into specific and generalised results that allow for an extrapolation of the findings for the full Windsbach DH network size and for general conclusions.

Figure 21 shows the maximum house connection heat capacity rate which increases with the applied volume flow. A deviation from linear behaviour can be observed for the range of 250 l/h to 500 l/h that is caused by differing return temperatures from the house stations because of a possible parallel operation of buffer tank charging and direct supply of the fresh water station.

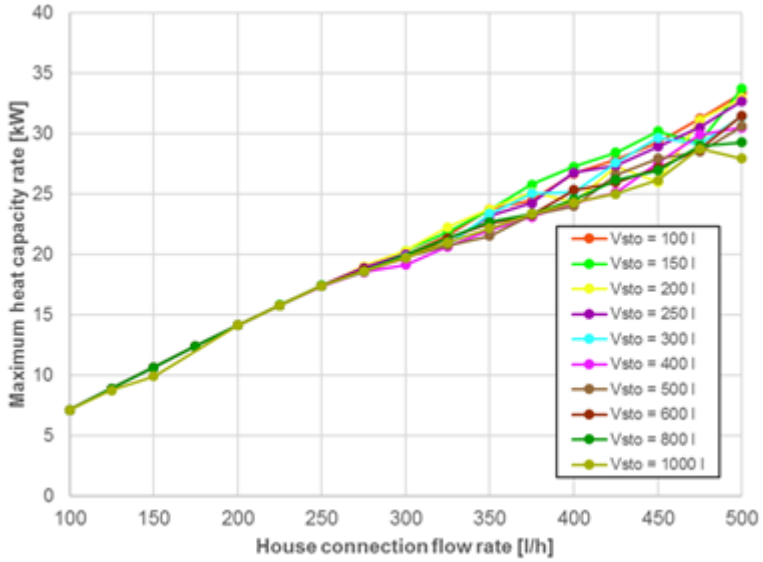


*Figure 21: Simulated maximum house connection heat capacity rate for different buffer tank volumes and house connection flow rates*

Simultaneity factors are an important aspect for the design of DH network pipe dimensions as they are applied to determine the design heat loads for single DH network sections and entire DH networks. From the simulations simultaneity factors for DH networks with decentralised buffer tanks are calculated, see Figure 22. No relevant correlation of the simultaneity factors with the buffer tank volume is identified. For comparison, selected literature values are also shown in Figure 22. Simultaneity according to [3] is valid for DH networks with existing single-family houses and traditional heat transfer substations for both DHW preparation and space heating demand. Simultaneity factors according to TUD [4] and DIN 4708 [4] are valid for DHW preparation only.

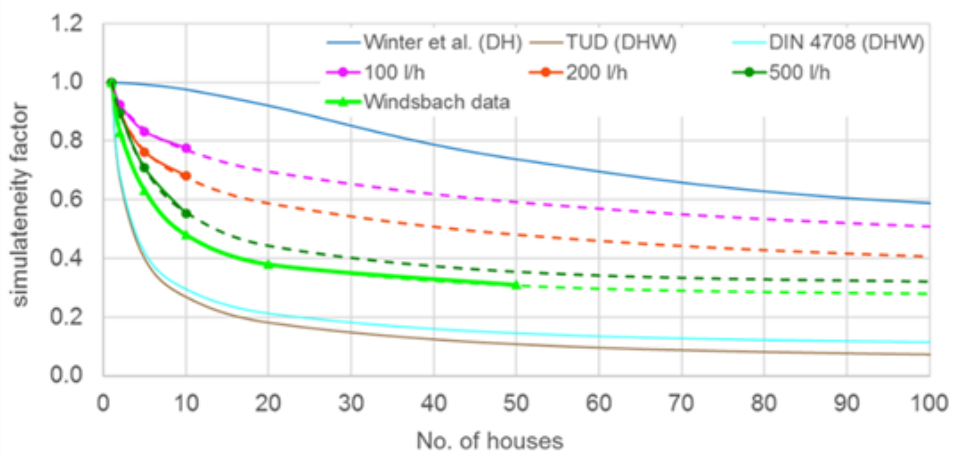


*Figure 22: Identified simultaneity factors for decentralised buffers and different house connection flow rates in comparison to selected literature values.*

The simultaneity factors for DH networks with decentralised buffer tanks are partly calculated from the simulations and Windsbach monitoring data (solid lines) and partly extrapolated from the calculated values (dashed lines). For the extrapolations an approach according to [3] is applied:

$$GLF(n) = a + \frac{b}{1+\left(\frac{n}{c}\right)^{d}}$$

n: number of consumers

GLF: simultaneity factor

For the three considered house connection flow rates and the Windsbach monitoring data the following sets of coefficients are identified:

| | 100 l/h | 200 l/h | 500 l/h | Windsbach data (425 l/h) |
|---|---|---|---|---|
| a | -88.236710 | -0.343790 | 0.285503 | 0.2487 |
| b | 90.375886 | 3.981482 | 0.855871 | 0.9960 |
| c | $4.32555*10^{24}$ | 0.018732 | 4.757875 | 3.0117 |
| d | 0.076685 | 0.170180 | 1.042957 | 0.9917 |

The results of the detailed branch simulations are transferred into specific and generalised results that allow for an extrapolation of the findings for the full Windsbach DH network size and for general conclusions.

For further investigations for Windsbach, a full-size DH network with the total heat load of the Windsbach DH network (phases 1 to 3) is considered. For the up-scaling of simulation results to the full-size DH network it is assumed that all consumers are single-family houses with the characteristics assumed for the simulations.

The design heat load for all pipe sections in the DH network is calculated for each of the considered design house connection flow rates based on the respective consumer nominal heat load according to Figure 21 and the simultaneity factors given in Figure 22. The design values given in Table 2 are determined for the three considered design house connection flow rates.

*Table 2: Design heat loads and simultaneity factors for the full-size DH network*

| Design house connection flow rate [l/h] | Resulting design heat load for DH network [kW] | Simultaneity factor for DH network [-] |
|---|---|---|
| 100 | 470 | 0.47 |
| 200 | 750 | 0.37 |
| 500 | 1450 | 0.31 |
| Windsbach design (425) | 1050 | - |

Annual heat losses for the buffer tanks are assumed equal to the average heat loss per buffer tank determined by the simulations for each parameter constellation. Annual heat losses from pipes per meter are assumed equal to the average heat losses determined by simulations for each parameter constellation with differentiation between house connection and main pipes.

With the new design, heat loads from Table 2 the Windsbach DH network is re-designed for the considered design house connection flow rates and a design flow speed in the DH pipes of 1.25 m/s. Figure 23 shows the distribution of the pipe dimensions for the re-designed DH network configurations in comparison to the Windsbach design. Smaller house connection flow rates mean smaller design heat loads and thus allow the installation of smaller pipe diameters in wider areas of the DH network.

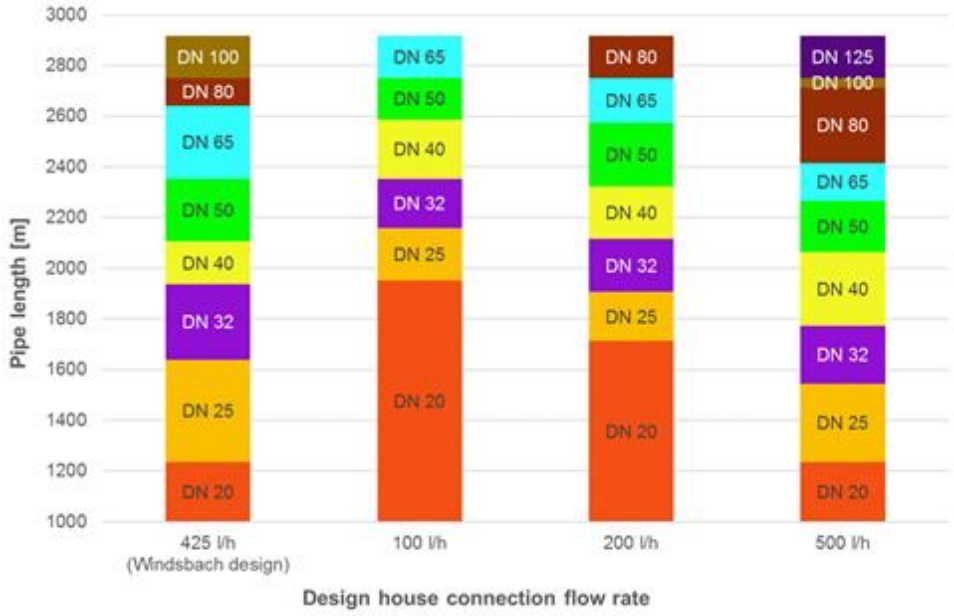


Figure 23: Distribution of pipe dimensions for the Windsbach DH network for different house connection flow rates

A consideration of thermal losses is shown in Figure 24 for different types of pipes. The buffer tank thermal losses are independent from the house connection flow rate and the type of DH pipes and increase with increasing buffer tank volumes. DH pipe thermal losses depend on the pipe type and decrease with increasing buffer tank volumes for house connection flow rates. In total the thermal losses stay rather constant for buffer tank volumes above 250 l for house connection flow rates of 500 and 200 l/h. They however increase for a small house connection flow rate of 100 l/h (see Annex 4). The reasons for the differences in the development of DH pipe thermal losses, which also strongly influences the total thermal losses, is a decrease of the DH pipe usage with an increasing buffer tank volume.

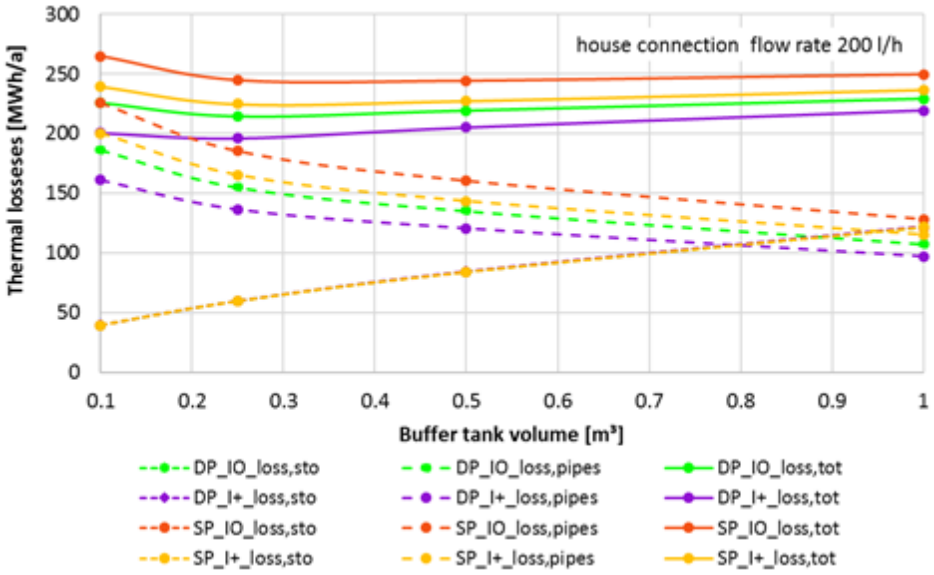


*Figure 24: Thermal losses as a function of buffer tank volume for different pipe types and a house connection flow rate of 200 l/h (DP: single pipe, DP: double pipe, I0: standard insulation, I+: improved insulation, sto: storage, tot: total)*

For cost estimations investment cost for the DH network and the house stations are considered. Corresponding unit cost is provided by Enerpipe. For the DH network, separate cost for materials (pipes, joints), installation and ground works is taken into account, separately for each nominal pipe diameter. Furthermore, unit prices for house stations with different buffer tank sizes and installation cost are considered.

For the economic calculation, a period of 20 years is assumed with a service life of the DH piping of 40 years and an interest rate of 4%. Maintenance cost of 1% per year for the DH network piping and 2% per year for the house stations is applied. For the consideration of thermal losses, a mean heat price of 7 ct/kWh is assumed.

Figure 25 exemplarily shows the results of the economic calculation for the investigated configurations and double pipes in standard insulation. For comparison, also a cost estimation of the latest Windsbach design is included. To be able to consider also the cost of thermal losses from DH pipes and buffer tanks yearly annuities are presented.

Total yearly annuities vary by 11% for the configurations with double pipes and 6% for the configurations with single pipes (see Annex 4). Single pipe configurations are between 11% and 17% more expensive than the corresponding double pipe configurations. According to Figure 25 a reduction of the house connection flow rate from 500 l/h to 200 l/h reduces the yearly cost between 5% and 7%, a reduction from 200 l/h to 100 l/h reduces the yearly cost by another 1.5% to 3.5%. For house connection flow rates of 200 l/h and 500 l/h, annuities for configurations with larger buffer tanks but the same house connection flow rate only slightly increase, as part of the extra cost for the larger buffer tanks can be compensated by reduced thermal losses.

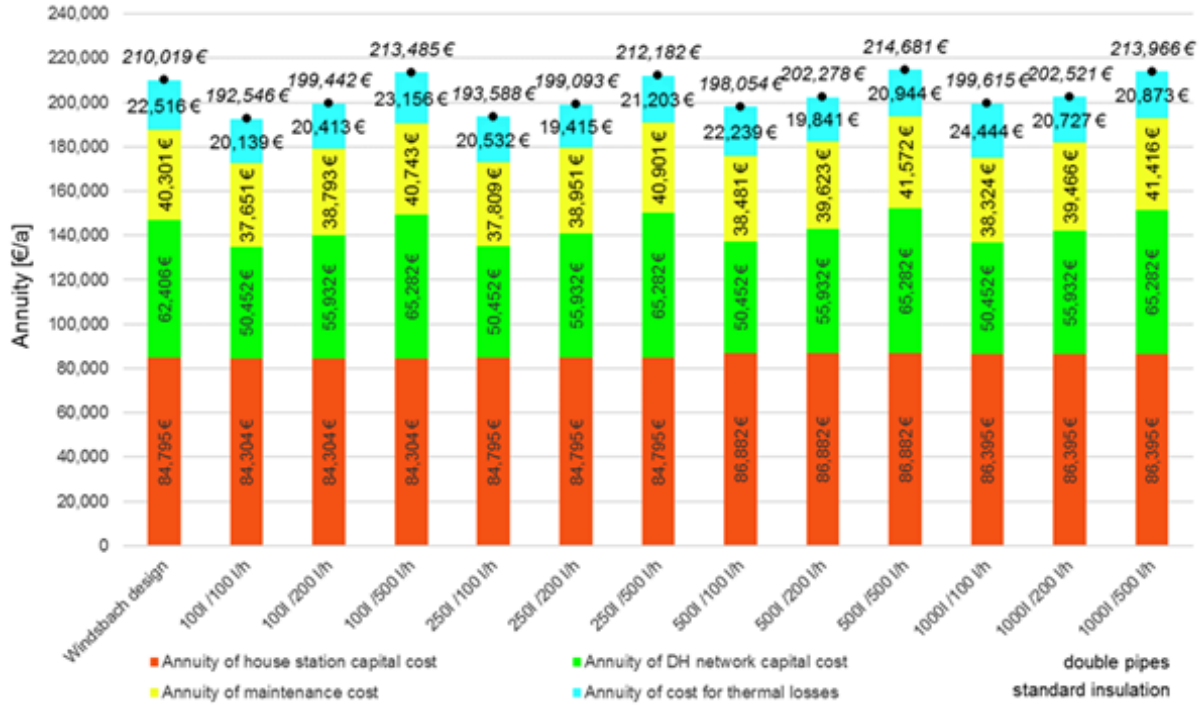


*Figure 25: Yearly cost for different configurations (double pipes with standard insulation)*

As demonstrated here, a reduction of the design house connection flow rate shows technical and economical optimisation potential for the overall system consisting of DH network and house stations with buffer tanks. On the other hand, a reduction of design values for the house connection flow rate also reduces the technical capability of the system to overcome exceptional larger heat demands of single or multiple consumers. In Annex 4, two figures are presented that allow for an assessment of some kinds of extra loads compared to the assumed standard demand.

### 3.2.2 CONCLUSIONS

DH network house stations with buffer tanks offer the technical potential for a reduction of house connection capacity rates as peak load from consumption can be covered from the buffer tanks and do not directly affect the DH network. If all or most of the consumers connected to a DH network are equipped with decentralised buffer tanks, this can be considered in the design of the DH piping network. Because of reduced peak heat demand from consumers also the design heat load for the DH network can be reduced. Two main effects can be distinguished in this respect. At first, the design house connection capacity rate of the single consumer buildings can be lower compared to standard substations without buffer tanks, if not designed for covering peak loads from consumption. Secondly, also the consumption profile of a house station with decentralised buffer tank changes compared to standard substations. This has an influence also on the simultaneity behaviour of multiple consumers.

Investigations conducted here are based on the Windsbach demonstrator with almost exclusively new single-family houses. For this application case, detailed simulation models were created for house stations with buffer tanks and for one selected DH network branch with, at the time of consideration, ten connected single family houses. Investigations show a reduction potential of design house connection capacity rates for new standard single family houses from todays 30 kW down to theoretically 7.5 kW.

New simultaneity factors could be derived for DH networks with single family houses and house stations equipped with buffer tanks and for different design house connection capacity rates or house connection flow rates, respectively. The new simultaneity factors allow DH network pipe designs taking into account the decentral buffer tank approach and reduced house connection capacity rates compared to standard designs.

Larger buffer tank volumes in house stations enable lower house connection capacity rates, smaller DH network pipe dimensions and reduced DH network thermal losses. At the same time on the other hand the reduction of DH network thermal losses is compensated to a nameable extend by increased thermal losses of the larger buffer tanks in the houses. In total, a variation of 26% of yearly heat demand necessary to cover total thermal losses was found for the investigated configurations with double pipes in standard insulation.

A similar development as for the thermal losses can be observed for the investment cost. Smaller DH pipe dimensions enable cost savings for the DH network, but larger buffer tank volumes generate higher cost in the house stations. Besides, yearly total cost figures are influenced by the varying thermal losses for different configurations. In sum, the variation in total yearly cost for the investigated configurations with double pipes in standard insulation was calculated to 11%.

As demonstrated, a reduction of design house connection capacity rates offers technical and economical optimisation potential. On the other hand, it goes along with an increased risk of reduced comfort for the consumers or temporal shortages in heat supply, if heat demands differ too much from design conditions. Presented analysis allow an assessment of these effects based on maximum load coverage periods for two excess demand scenarios and different technical configurations.

## 3.3 FAULT DETECTION AND BUILDING OPTIMIZATION

The description of the functionality, the improvements to the state-of-the-art, the costs and the impact of the results on the overall proposed solution can be found in [1].

### 3.3.1 RETURN TEMPERATURES

The simulation-based fault detection and diagnosis methodology was applied to the buildings in the Windsbach demonstration site. Faults turned out to be dominated by a recurring issue with short return lances in earlier versions of the buffer tank. Short return lances meant that the bottom of the buffer remained cold and the buffers kept charging, resulting in exceedingly high return temperatures.

Experiments with the automated fault detection algorithms showed that algorithms trained with the appropriate simulation data could detect this issue with good recall, but that the same accuracy could be achieved and even outperformed by the use of a hand-engineered metric for this issue: the flowrate-weighted average of the difference primary return temperature and buffer bottom temperature (above 10 K in critical cases of short return lances, mostly below 5 K otherwise).

The issue of short return lances was successfully solved in some buffers, with a strong impact on return temperatures, as shown in Figure 26. However, supply bottlenecks delayed the replacement of some return lances, some of which (for newly connected units) had not yet been replaced at the time of writing.

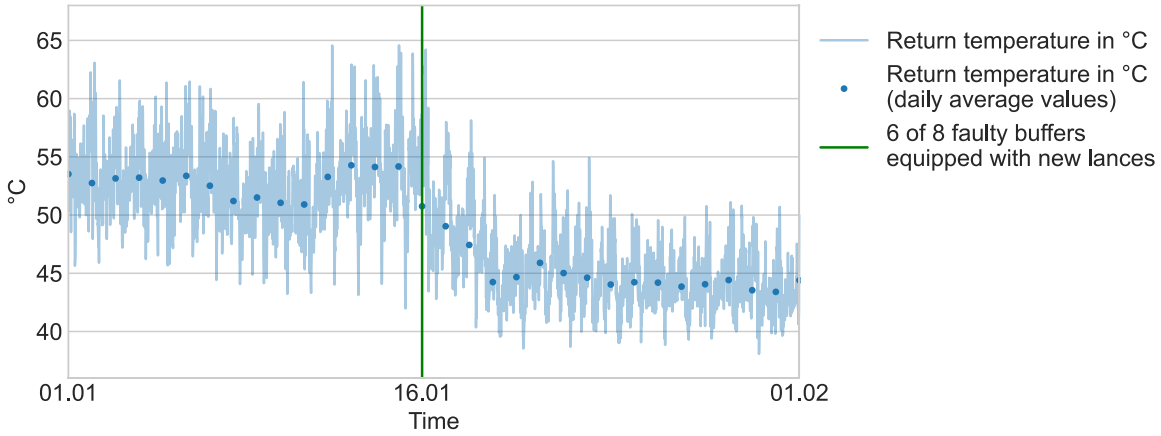


*Figure 26: Main return temperatures before and after replacing short lances in 6 of 8 faulty buffers on January 16th, 2021. The average return temperatures in the two weeks after vs before the intervention were reduced by 7.8 K.*

The impact of faulty buffers on the overall return temperature was again investigated empirically on February 3rd, 2022. On this day, four of the remaining poorly performing buffers were shut off for a duration of 2.5 hours after making sure they were sufficiently loaded. The resulting impact on the main return temperature is shown in Figure 27. Comparing to the hours just before and just after, the period with faulty buffers withdrawn showed a reduction in return temperatures of 3.0 K.

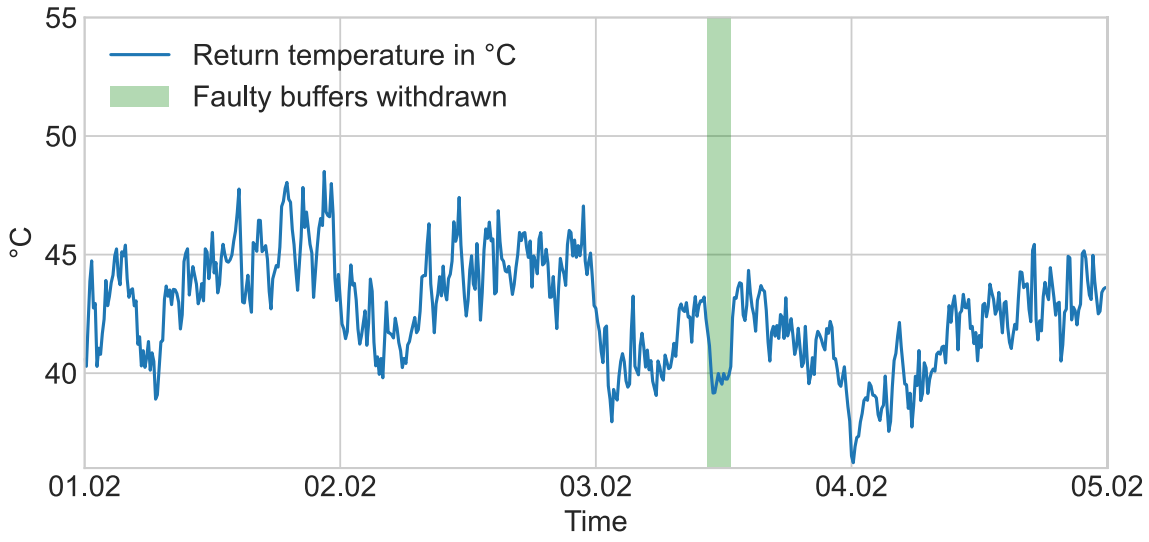


*Figure 27: Impact on main return temperature of temporarily withdrawing four faulty buffers on February 3rd, 2022*

As shown in Figure 28, the average return temperatures of the individual buildings in the last heating season range from 35 °C to 65 °C, with only three outliers above 60 °C and all other buildings below 55 °C. Flowrate-weighted return temperatures only correlate with fault predictions to a certain extent: the four rightmost dots below 50 °C have a high degree of predicted faults despite low to moderate return temperatures. A deeper look at the data (see detailed results in Table 11) shows that the corresponding units stand out not only in terms of energy consumption higher than average, but also because they exhibit behaviour differing from most other units, either in terms of charging times or in terms of weak correlation between valve position and flowrate. Thus, the automated fault detection algorithm did seem to bring attention to somehow irregular behaviour. Predictions of the automated fault detection algorithm were presented in web-based reports, together with metrics calculated from monitoring data, manual annotations and links to the guide for auditing building installations to reduce high return temperatures developed in the TEMPO project[4].

[4] https://tempo-dhc.ait.ac.at/building-guide

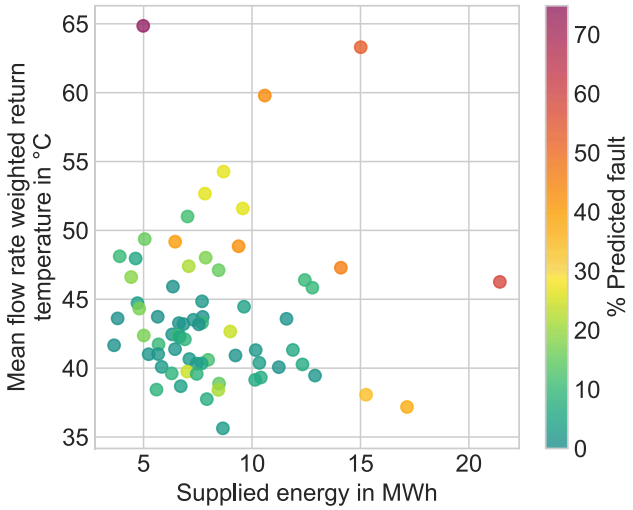


*Figure 28: Individual building performance for the substations of the Enerpipe demo from September 2021 to February 2022, in terms of supplied energy, mean (flowrate-weighted) return temperature and percent of predicted faulty behaviour*

### 3.3.2 CONCLUSIONS

The approach to optimization of the building installations developed in TEMPO has been applied to the single-family houses of the ENERPIPE demonstrator. While it was originally expected that the recent installations would not be subject to many faults, the impact of faults turned out to be significant. This was due to a recurring issue with return lances, a number of which were too short. This issue demonstrated the value of being able to detect anomalous behaviour quickly (but was addressed by the TEMPO innovation) but also the importance of being able to remedy the corresponding faults quickly, which turned out to be more challenging than expected. The latest version of the buffer tank will be equipped with direct return outlets instead of return lances, which will avoid the issue in new installations.

## 3.4 SMART DISTRICT HEATING CONTROLLER

The description of the functionality, the improvements to the state-of-the-art, the costs and the impact of the results on the overall proposed solution can be found in [1].

### 3.4.1 OPTIMIZED CHARGING

In order to reduce the pump costs and heat losses in the network, smart charging was applied on the decentralized buffers to reduce the peak load in the network even more. The initial smart control approach, consisting of the decentralized buffers following a predefined power profile, is discussed in [5]. Due to possible comfort violations, a new control concept was developed which only decides on the start of the charging cycle and not on the charging power, for more details see [6].

The limiting factor for integrating the smart charging of the buffers is that it has to be deployed on top of the Schneid GesmbH controller that is already present in the network. This controller charges the buffers automatically based on the measured temperature at the top and bottom of the buffer, taking into account a predefined hysteresis curve as explained in [1]. In short, this automatic buffer charging limits the available flexibility for the smart controller because the charging process can only be shifted for about 1h before the automatic charging takes over. In order to increase this flexibility, response tests were executed in which the hysteresis behaviour was switched off. This resulted in a small increase of flexibility as it took 30 minutes more before the automatic charging kicked in. Unfortunately, a side effect of switching off this hysteresis behaviour is the fact that the buffer will not load thoroughly because the charging process stops too early. Therefore it was decided to keep the hysteresis charging in place during the smart charging tests in the winter season of 2021 – 2022.

In addition to this limited flexibility, the increasing number of connections in the network also meant that the learning data was not always representative for the current behaviour of the DHN. In the end challenge solved itself as the number of connections in the network stabilized. During the testing period it was also observed that not all control signals were followed by the buffers, even at times when all requirements for starting a forced charging cycle were met. Two main reasons why the buffers would not follow a control signal, even when they were supposed to, were identified. The MPC, running on a VITO/EnergyVille server, sends the control signal to EnergyView where they are picked up by a monitoring script which will forward these control signals to the Schneid system. First, if communication between the systems is lost, the signals will not be applied. Secondly, if the monitoring script is not running, the signals will not be picked and therefore cannot be forwarded.

Due to the above limitations and unpredictable buffer responses, it was not possible to interpret the results of the smart buffer charging properly to formulate good and reliable conclusions. However, based on simulations we were able to come up with some expected results in an ideal world. Figure 29 shows an overview of a simulation with only two buffers and no smart control, the top two graphs show the buffer behaviour. The grey lines represent the top, middle and bottom temperature whereas the green line represents the smart activation signal and the red line shows the expected power demand. The bottom graph shows the aggregated heat load in the network. It can be seen from the peaks in the cumulative power demand that simultaneous loading of the two buffers happens

regularly. The next to last graph depicts the penalty calculated by the smart control algorithm, it shows a high penalty when simultaneous charging is happening (undesired behaviour) and a low penalty at other times (desired behaviour).

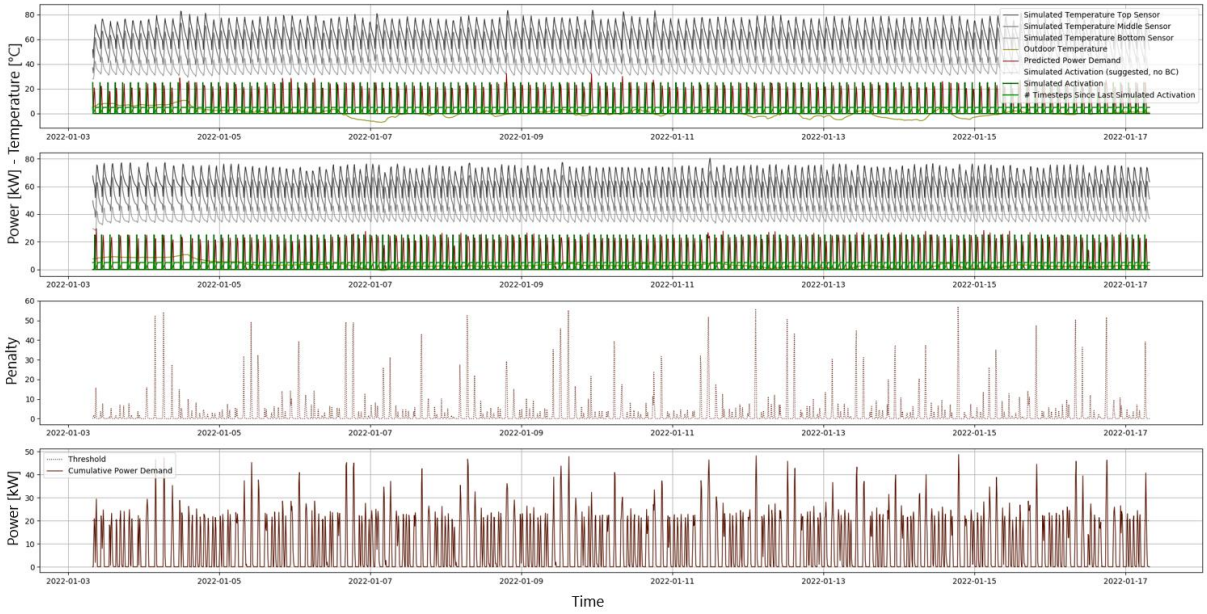


*Figure 29: Simulated buffer charging results for 2 buffers, together with the penalty and peak load in the network when no smart control was activated*

Figure 30 is similar to Figure 29 except that the smart controller was activated at 10 January 2022. It is clear that from that point onwards, the controller makes sure that the two buffers will never load simultaneously. This can be observed from the bottom two graphs as there are no peaks or high penalties anymore. These results are achieved by pre-charging one of the two buffers, based on its expected charging behaviour in the near future, which is learned from historical data.

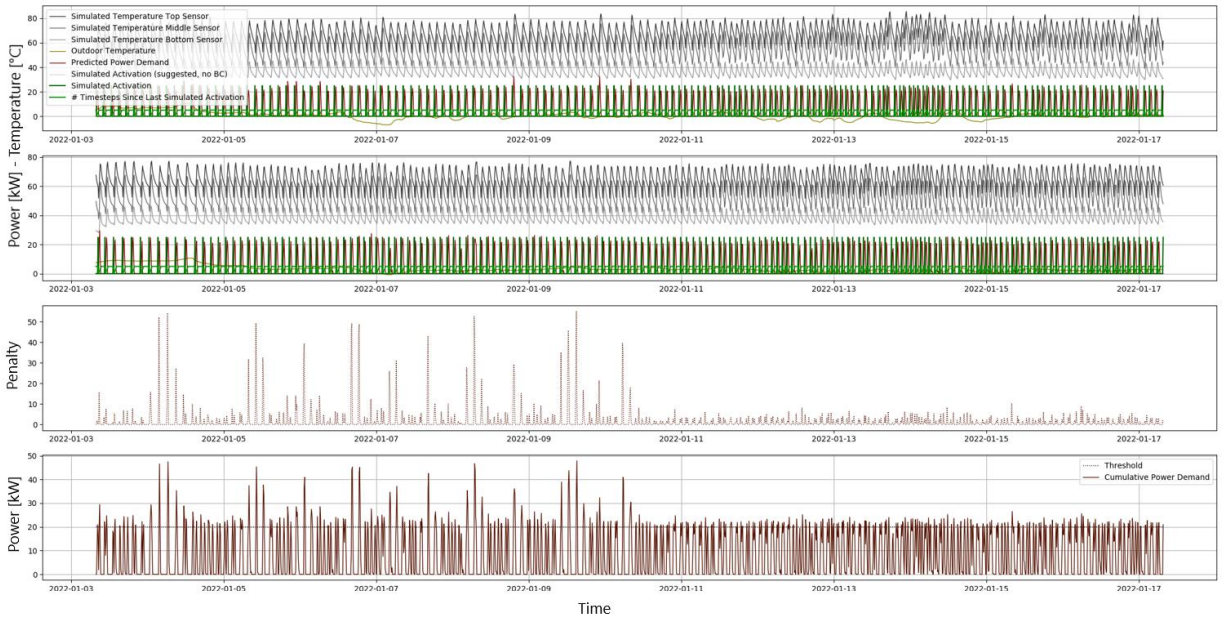


*Figure 30: Simulated buffer charging results for 2 buffers, together with the penalty and peak load in the network when smart control was activated at 10 January 2022*

This simulation was executed for 2 and 9 buffers in the system, leading to the following results:

- 2 buffers
  - Peak during training: 47.8 kW
  - Peak during smart control: 30.4 kW
  - **Peak reduction: 36 %**
- 9 buffers
  - Peak during training: 107.8 kW
  - Peak during smart control: 67.3 kW
  - **Peak reduction: 37 %**

As described above, these results are obtained in an ideal world in which all buffers would follow every control signal given by the smart controller. On top of that the hysteresis charging was switched off in these simulations, leading to an extra 30 minutes of flexibility. With some adaptations to the automatic control/hysteresis charging, it will also be possible to use this extra flexibility in the field. However, we know that these theoretical results will not be achieved in a real world deployment, from experience in other building applications we see that the performance in practice will be around 10% less than seen in the simulations. Our educated guess is that the smart charging of the buffers will therefore be able to **reduce the peak load with 25 % on average**.

The actual monitoring results presented in Section 2 show that this peak load reduction was not achieved during the real tests.

In section 3.4.3 we will go more in detail on how to tackle the practical hurdles to enable the full deployment of the smart charging algorithm in the Windsbach demo.

### 3.4.2 CHP OPTIMIZATION

For the winter season of 2021-2022 the CHP optimization algorithm discussed in [6] was updated to enable the optimization of the newly commissioned CHP with an electrical output of 400 kW, as described in [1].

In summary, the baseline control of a CHP in a district heating network is mostly based on a simple rule system taking into account the heat load of the network and the SoC of the central buffers, if available. In the Windsbach demo however the baseline control is different as the network owner already implements a type of manual smart control in which he checks the day-ahead price tariff and, based on his experience, defines a plan for the CHP to operate during high electricity prices (taking into account the expected heat load of the DHN). The owner executes this task twice a day updating the plan for the next 24 hours. A mixed-integer linear programming (MILP) approach was used to automate this cost optimized operation of the CHP, sending a mail twice a day to advice the network owner with the optimal plan. Version 1 calculated an optimal plan for the smaller CHP (135 $kW_e$) because the large CHP (400 $kW_e$) was not yet commissioned. In version 2, the algorithm was adapted to integrate the newly commissioned large CHP and advised optimal plans were sent from 15 October 2021 up to 28 February 2022.

As we are only sending an advice to the network owner, he can decide whether the CHP will follow the optimal plan completely, partially or not at all. The following graphs show some insights in how this advice is applied in practice.

The first graph in Figure 31 shows the comparison between the advised optimal operation (green) and the real measured operation (blue) of the CHP for 24 hours starting from 9 January 2022 11:00 CET. The dotted green and blue lines represent the estimated SoCs based on temperature estimations and measurements in the central buffer tank. The bold grey line depicts the received day-ahead price on which the operation is optimized. During these 24 hours the plan was followed quite well, except in the evening and early morning the CHP was started two hours later as advised but this had only a minor impact on the selling price of the electricity, in the advised plan the electricity was sold at 168.57 €/MWh as opposed to 167.01 €/MWh in practice. At certain times, the estimated SoC of the measured temperatures exceeds the boundaries of 0 % and 100 %. This is due to the fact that the SoC is estimated using a simplified buffer model in which we put the boundaries a bit more conservative as the real boundaries in order to make sure that we will never deplete or overcharge the central buffer tanks. This implies that, in reality, there is even more flexibility available to optimize the CHP operation.

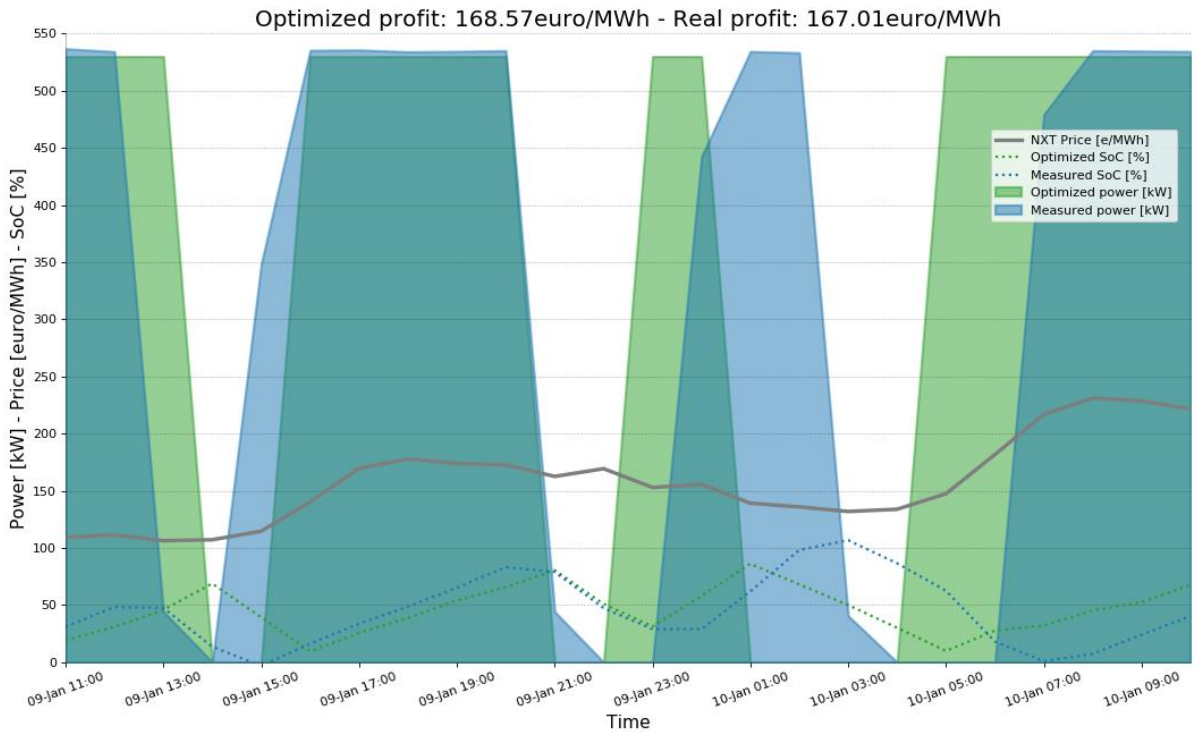


*Figure 31: Comparison between advised optimal operation (green) and the real operation (blue) of the CHP (09/01/2022 – 10/01/2022)*

Figure 32 shows a similar comparison for 11 January 2022 in which the measured output is more or less similar to the advised plan. At 15h00 the measured plan shows a modulated output of the CHP of around 100 kW, this is not allowed by the constraints in place on the optimal plan, as it was defined that it is a non-modulating CHP. Another difference is the fact the DH owner opted to start the CHP only three times during the day instead of four times by the optimal plan. In this case, limiting the cold starts of the CHP was more advantageous than the small difference (0.13 €/MWh) between the followed plan and the optimal plan. Currently, the cold starts of the CHP are limited to 4 in the MPC and there is no incentive to limit these starts in favour of a sub-optimal plan. However, such constraints could be added in the future.

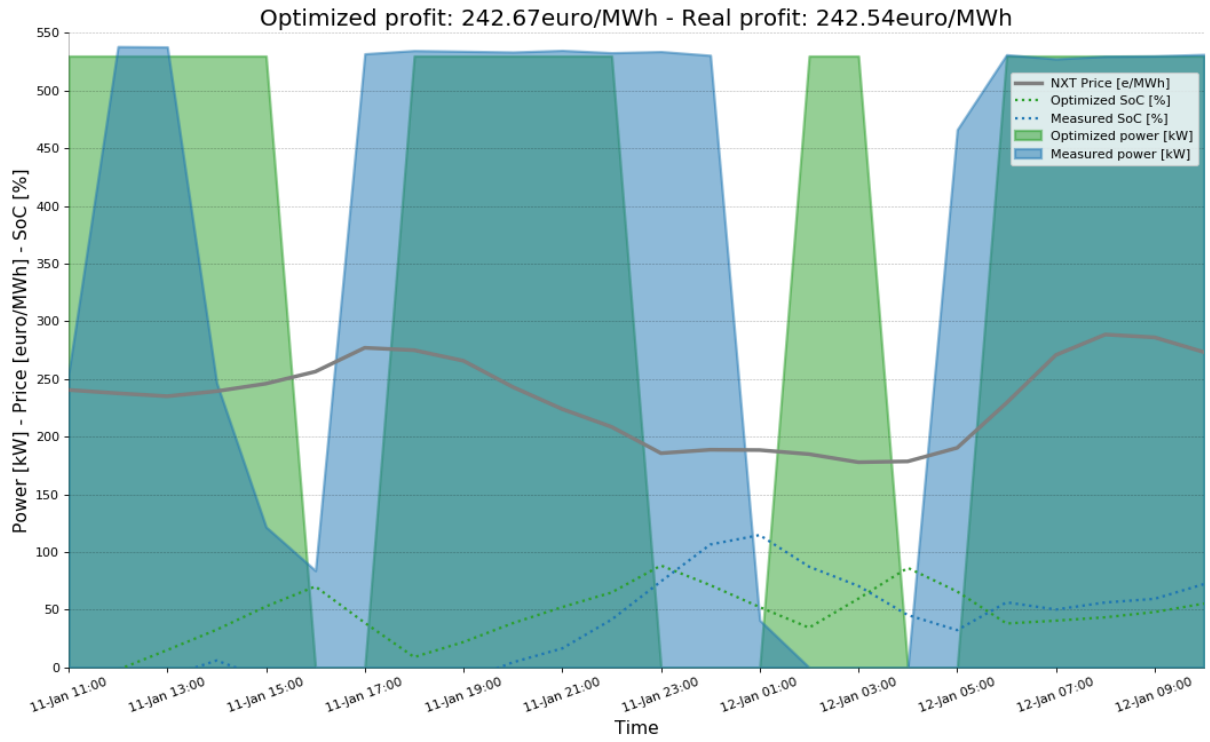


*Figure 32: Comparison between advised optimal operation (green) and the real operation (blue) of the CHP (11/01/2022 – 12/01/2022)*

If we compare the average price of the sold electricity by the optimal plan with the average day-ahead price, we get the following results for the period of 15 October 2021 until 28 February 2022:

- Average price of selling electricity : 164.03 €/MWh
- Average selling price optimal plan : 177.13 €/MWh
- Total electricity sold : 590 MWh
  - Revenues conventional control: : 96777.77 €
  - Revenues optimal control : 104506.7 €
  - **Increased revenue** : **7728.93 €**
  - **Percentual increased revenue** : **8 %**

Besides the increased revenues, integrating the calculation of an optimal plan also unburdens the DH owner who now has to calculate a plan manually twice a day. Furthermore, it can also decrease maintenance costs by limiting the cold starts of the CHP. In the end the goal is to deploy the smart control of the CHP in a fully automated way and moving from sending an advised plan via mail, to a submitted plan through an API, making any manual intervention unnecessary.

#### 3.4.2.1 EVALUATION OF THE PRIMARY ENERGY FACTORS FOR THE OPTIMIZED CHP OPERATION

Every time the biogas CHP in the ENERPIPE demo operates, the produced electricity is displaced electricity in the main grid. Thus a theoretical reduction of the fossil primary energy in the system would be possible, assuming that high electricity price correlate with high fossil primary energy in the grid and also with the operation of the CHP This relationship has been investigated, see Annex 5. As a result, it can be seen, that on some days, between 5 and 20% more fossil primary energy can be displaced in the optimized operation compared to the non-optimized operation. However, there are other days, where the performance of the non-optimized operation is better than in the optimized operation, see Figure 33.

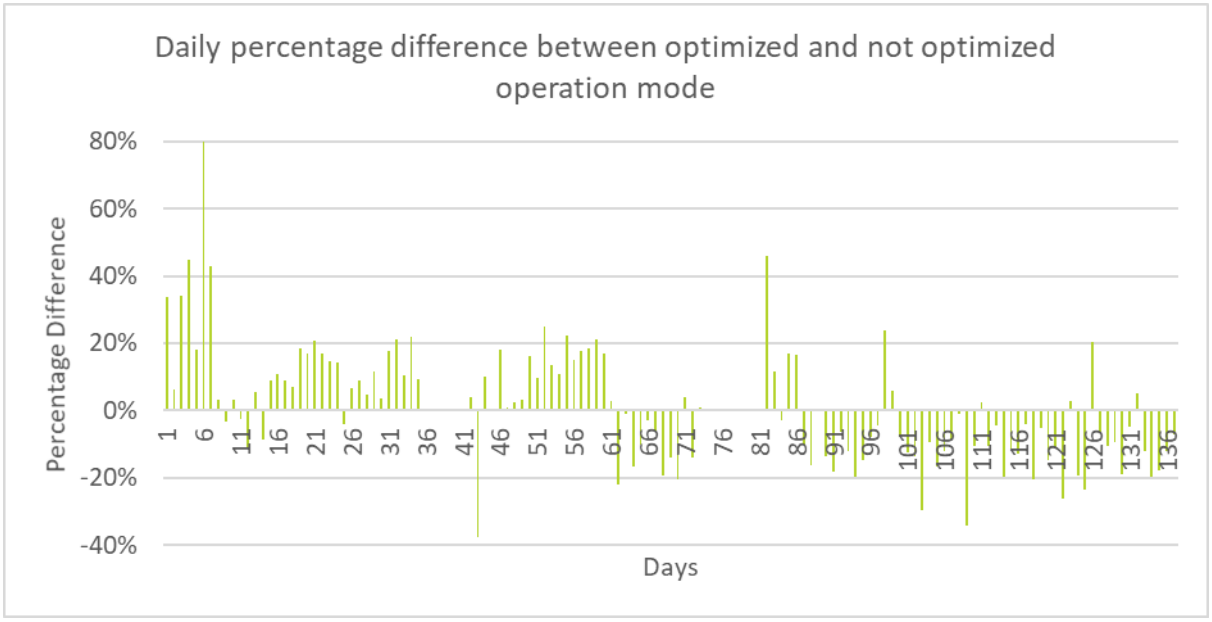


*Figure 33: Daily percentage difference between optimized and not optimized operation mode (displaced fossil power from the electricity grid)*

However, there are many occasions, where the CHP is turned off in the optimized mode, so no fossil primary energy is displaced. This is an advantage for the non-optimized mode, since it is running more often, and this is displacing fossil primary energy. This behavior needs a deeper investigation, especially if an optimization with regards to displaced fossil primary energy in the grid would be possible.

## 3.4.3 CONCLUSIONS

### 3.4.3.1 SMART BUFFER CHARGING

As discussed in section 3.4.1 it is possible to reduce the peak load in the network by pre-charging the buffers in order the decrease the simultaneity factor in the DHN. However, the results obtained by deploying the smart charging in Windsbach were not satisfactory, even though simulations showed that a theoretical peak reduction of 35 % was feasible. Here we will elaborate on the challenges that we faced in the field and how they can be addressed.

The most important challenge of the smart controller was the fact that it had to be deployed on top on the already existing automatic buffer charging applied by the Schneid DHN controller. This automatic charging had to stay in place serving as a backup controller in case the smart controller would violate the comfort boundaries. As this automatic controller was designed to implement the conventional charging behaviour of the buffer and not as a backup controller, this led to important limitations as explained in section 1.4 of [1]. For example, at an outdoor temperature of 5 °C, the smart controller can only start a charging cycle when the bottom temperature is below 40 °C and the top temperature is above 50 °C. If the top temperature drops below 50 °C, the cycle starts automatically. Therefore, limited flexibility (+- 1h) is available to shift the charging process of a buffer. To increase this flexibility, it should be possible to already start a charging process when the bottom temperature in the buffer is 45 °C. This can be achieved by reconfiguring the hysteresis setpoint from 5 °C to 0 °C. Unfortunately, because the stopping criteria for the charging process is based solely on the bottom temperature, an oscillation effect can occur in which the buffer is only charged for a couple of minutes as it starts charging when the bottom temperature is below 45 °C and it stops right after when the bottom temperature is above 45 °C. Due to this, it was decided to keep the hysteresis setpoint to 5 °C in the 2021-2022 winter tests. We are confident that this non-optimal cooperation between automatic charging and smart charging can be overcome by switching to a custom implemented back-up controller when smart charging is active. This back-up controller will take over from the automatic controller in order to ensure the comfort of the occupants. It would have to allow for a broader time window to start a charging cycle and it would have to take into account multiple temperature sensors in the buffer, instead of only the bottom one, in order to stop the charging cycle. To develop this back-up controller properly, consultation is needed between different stakeholders, e.g. VITO/EnergyVille for the smart charging, Enerpipe as the DHN controller and Schneid GesmbH as the developer of the automatic control system. This issue then shows how important it is to align between all the different stakeholders in the system starting from the design of the network. Unfortunately, this does not happen in most of the DHN projects because smart control is not yet common in this field. Moreover, in TEMPO the developer of the automatic control system, Schneid GesmbH, was not a direct partner in the project and because the task of creating a custom backup controller for the buffers is difficult and time consuming, we were not able to solve this drawback within the life of the project.

Another complexity in the solution is the fact that four different systems are involved to get a control signal to the decentralized buffers:

1. The control signal is calculated on a VITO/EnergyVille server
2. The signal is sent to the EnergyView platform hosted by NODA

3. Glue-code picks up the signal from EnergyView and sends it to the Schneid controller
4. The Schneid controller applies the signal onto the buffer

The above sequence shows that sending a signal can go wrong in several places, e.g. at VITO/EnergyVille side, at NODA side, in the glue-code or in the Schneid system. This scattered system has two main disadvantages:

- Problem awareness
  - Problems surface slowly as there is no single system having an overview of the complete workflow
- Problem solving
  - It takes multiple persons to debug in case problems are detected, making problem solving very time consuming

One solution would be to send the control signals directly to the Schneid system together with responses indicating if the control signal was correctly applied. In TEMPO this was not possible as all the signals and measurements had to be logged into EnergyView, which was the visualisation tool for the expert users.

Besides the hurdles on the software front, there is also a practical limitation impacting the available flexibility, namely the buffer size. The majority of the connected buildings have a 250 l buffer installed, which serves both for space heating and hot water. On a cold winter day a building consumes around 75 kWh of heat while only around 7.5 kWh of usable heat is stored inside the buffer. Taking into account that most of this heat is used between 5 a.m. and 10 p.m. it is clear that the flexibility to shift the charging cycles of the buffer is limited as they have to charge 8 to 10 times a day. However, the advantage of the limited space needed to install a small buffer is currently more important for the end-user than the added flexibility of installing a larger buffer. In future, increasing incentives for extra demand-side flexibility can lead to larger decentralized buffer storages.

Taking into account all the practical hurdles discussed above, we were not able to achieve the results that we expected. Related to peak shaving, differences between no control and smart control were not substantial. It was difficult to compare the different cases because it was not 100 % sure that the buffers were receiving the control signals properly at times the smart control was active. Despite this, we estimate that with the above described actions, the peak in the Windsbach DHN could be further reduced with 20 to 25 % (based on the theoretical maximum of 35 % peak reduction achieved in the simulations).

#### 3.4.3.2 CHP OPTIMIZATION

In this paragraph we discuss the findings and practical hurdles that we encountered when deploying the CHP optimization in the field. As we want to optimize the operation of the CHP, it is important to have a good forecast on what the total heat load will be in the DHN. In winter operation, this heat load is highly correlated with the outdoor temperature and a good forecast can be calculated using an outdoor temperature forecast. Unfortunately, in the field several unforeseen events happen which makes this forecasting more difficult:

- Unplanned maintenance
  - Can have an impact on heat input/output or data communication which is not taken into account by our heat load forecaster

- Heat input from satellite site
    - There is heat input from a satellite site, however this input is not correlated to the outside temperature nor to the time of the day and therefore difficult to forecast
- New connections in the network
    - New houses were connected regularly tot the network, these houses first have to heat up the screed which consumes a lot of heat. This heat cannot be taken into account by the heat load forecaster

As seen from the results in the previous section, we were still able to calculate a feasible optimal plan. Being able to take into account one or more of the above events will lead to higher revenues.

Besides forecasts of the heat load, it is also important to have access to the latest updates on electricity prices. In our setup, the prices containing information on the next 48 hours were sent automatically each morning from Enerpipe to NODA where they were added to EnergyView. The MPC then collected these prices through the EnergyView API and performed the optimization. However, at the end of the project it became clear that these prices were not the up to date when running the optimization at 17 h in the afternoon. Apparently the DH owner had access to updated prices every hour. Luckily these price updates differed only slightly from the initial ones but they still resulted in the calculation of a sub-optimal plan. In the future, the MPC has to have direct access to the price updates that the DH owner receives.

The optimal plan sent to the DH owner was an advice and therefore not equal to the measured plan as in the end, the DH owner was responsible for choosing the timeslots for operating the CHP. In order to move from an advised plan to a fully automated plan in which no intervention from the DH owner is needed, it is important to adapt the MPC taking into account as much as possible the unforeseen events for forecasting and the latest price updates. Only this will give the DH owner the necessary trust to move to a fully automated CHP operation.

# REFERENCES

[1] M. Abt, D. Geysen, A. Fiegl, T. Schmidt and A. Bres, "D3.3 Report integrated improved innovations in Enerpipe network," TEMPO, Brussels, 2021.

[2] R.-R. Schmidt, I. Marini, A. Bres, C. Johansson, D. Vanhoudt and T. V. Oevelen, "D4.3: Report – Integrated improved innovations in a2a network," TEMPO, Brussels, 2022.

[3] W. H. T. O. I. Winter, "Untersuchung der Gleichzeitigkeit in kleinen und mittleren Nahwärmenetzen," *Euroheat & Power,* pp. Part I 09/2001 p.53-57, Part II 10/2001 p. 42-47, 09 & 10 2001.

[4] AGFW, "FW 520 Part 2, Information sheet on basic design of apartment stations for heating water networks," AGFW, Frankfurt, 2004.

[5] D. Vanhoudt, A. Soares, G. Suryanarayana, D. Geysen and Van Oevelen Tijs, "D1.1 Report innovation installation guidelines 1st version," TEMPO, 2019.

[6] D. Vanhoudt , C. Johansson, R.-R. Schmidt, M. Abt, D. Geysen, C. Hermans, L. Scapino and T. Van Oevelen, "Report innovation installation guidelines 2nd version," VITO, 2021.

[7] Efficiency Valuation Organization, International Performance Measurement and Verification Protocol—Core concepts, Efficiency Valuation Organization, 2016.

[8] P. Leoni, I. Marini, A. Bres and C. Johansson, "Deliverable 4.2: Integrated innovations in A2A network," TEMPO, 2020.

[9] B. Windholz, D. Basciotti and C. Marguerite, "Deliverable 5.1: Generic monitoring principle and equipment for TEMPO," TEMPO, 2018.

[10] R. Baeten, D. Geysen, A. Fiegl, J. Brage and A. Bres, "Deliverable 3.2: Integrated innovations in ENERPIPE network," TEMPO, 2020.

[11] T. Ommen, W. B. Markussen and B. Elmegaard, "Heat pumps in combined heat and power systems," pp. 989-1000, 2014.

[12] A. Gubina, T. Medved, J. Zupančič, R. Guarde, G. García, C. Sarobe, A. Tuerk, J. Pucker and C. Neumann, "Use cases and Key Performance Indicators (KPIs) of the STORY project," 2018.

[13] TESS – Thermal Energy Systems Specialists, "TESSLibs 17 – Component Libraries for the TRNSYS Simulation Environment," TESS, Madison, 2018.

[14] SEL - Solar Energy Laboratory, University of Wisconsin, "TRNSYS - A TRaNsient SYstems Simulation Programme, Version 18," SEL, Madison, 2020.

[15] VDI – The Association of German Engineers, "VDI 4655:2021-07. Reference load profiles of residential buildings for power, heat and domestic hot water as well as reference generation profiles for photovoltaic plants," VDI, Düsseldorf, 2021.

# ANNEX 1: PERFORMANCE ASSESSMENT METHODOLOGY

## 1. GENERAL METHODOLOGY

This chapter describes the general methodology that was used to calculate the key performance indicators.

Most of the key performance indicators of interest in the project relate to savings (in energy, greenhouse gas emissions and so on). Savings cannot be measured directly, rather they must be determined by comparing consumption before and after implementation of measures. Since conditions are bound to change between periods, this requires a methodology to consistently adjust for changes in conditions [7]. Changes in conditions relate especially to outdoor temperatures (in both demonstrators) and, in the case of the Enerpipe demonstrator, to the number of connected units, which increased significantly from 2019 to 2022.

Daily averages are calculated for the relevant monitored parameters. Days without values and days with clear outlier values are screened out and not considered in further calculations. For the normalized comparison of baseline and test period, linear correlations between daily average values of the outdoor temperature $T_{amb}$ and daily average values of parameters of interest are calculated for each period, whereby this is only done for days with average outdoor temperature under a threshold of 18 °C. For warmer outdoor temperatures, values (e. g. of energy use) are assumed to depend on domestic hot water only and thus to be roughly constant. For this latter temperature range, the average value of the parameter of interest is calculated. In other words, the relationship between outdoor temperature and other quantities of interest is fit into a broken line with a breaking point at 18 °C – or, in cases where only the heating season is considered, into a simple line. Following this, one calculates the difference between actual (measured) values in the test period and baseline values recalculated from linear correlation for the test period. This yields the difference or savings for the test period. The obtained correlations are not perfect, as is evident from the results displaying scatter plots along with trend lines. Still, given the limited amount of data, a higher goodness of fit as could be obtained with more refined regression models (e.g. polynomial regression) and/or additional dependent variables would probably result in overfitting and thus not result in a more accurate assessment of savings.

In cases where the ranges of outdoor temperatures spanned by the baseline and test periods differ significantly, the considered periods have been restricted to contain only the range of outdoor temperatures which is covered in both baseline and test periods, so that the measured behaviour is interpolated but not extrapolated.

# 2. CALCULATION METHOD AND ASSUMPTIONS FOR THE A2A DEMONSTRATOR

The calculation of key performance indicators for the A2A demonstration site follows the general methodology described in the previous section. The monitoring periods summarized in Section 3 are considered. First tests of supply and return temperature optimization were performed in alternating periods of one or several weeks in the winter season 2020 - 2021. The tests reported in this deliverable were performed in alternating periods of one or several weeks in the winter season 2021 – 2022.

# 3. CALCULATION METHOD AND ASSUMPTIONS FOR THE ENERPIPE DEMONSTRATION SITE

In this chapter the calculation method and the assumptions for the Enerpipe demonstrator are described.

The calculation of key performance indicators for the ENERPIPE demonstration site follows the general methodology described in Section 1. A challenge for the use of key performance indicators in the ENERPIPE demonstration site is that the number of houses connected to the network increases over time, and with it the total heat demand and energy use. Thus, quantities of interest should be normalized. The outdoor temperature is derived from the (generally conflicting) outdoor temperature measurements for all houses and at the plant room (SPS 901) by taking the median of all valid values at each time step.

A typical energy density $U_{gas}$ = 10.5 kWh/m³ is assumed for gas[5].

[5] The CHPs are connected to the natural gas pipe, but only biomethane from the municipal utilities is bought and used on the site. Thus, the calorific value is the same as for natural gas. The calorific value of gas may be subject to variations. This choice of calorific value leads to calculated thermal and electrical efficiencies close to manufacturer data.

# ANNEX 2: MONITORING

## 1. MONITORING IN THE A2A DEMONSTRATION SITE

The monitoring concept for the A2A demonstrator is described in deliverable D4.2 (see [8]). As described there, delay in the realization of the mixing station resulted in a postponed installation of the monitoring equipment and to a delay in the monitoring of some parameters, as summarized in Table 3.

*Table 3: Data availability for the monitored parameters on the A2A demonstration site*

| Data | Available from | Remarks |
|---|---|---|
| Mixing station transferred weekly via FTP | 13.11.2019 | Some data gaps |
| Apartment building and single-family house: supply and return temperature | 13.11.2019 | Available over NODA EnergyView |
| Apartment building and single-family house: volume flow, power, energy | 15.01.2020 | Available over NODA EnergyView |
| Energy meter data for single-family houses of the branch: energy and volume at hourly intervals | 08.02.2021 | Extracted manually, transferred monthly |

## 2. DATA QUALITY IN THE A2A DEMONSTRATION SITE

The data have been checked for anomalies. Two "problem periods" (in December 2019 and May 2020) with unrealistic and/or missing values at the mixing station have been removed for subsequent analyses. Also, a few days for which the number of log intervals was inferior to 90% of the expected number of log intervals (5760 per day) were removed (see Figure 34).

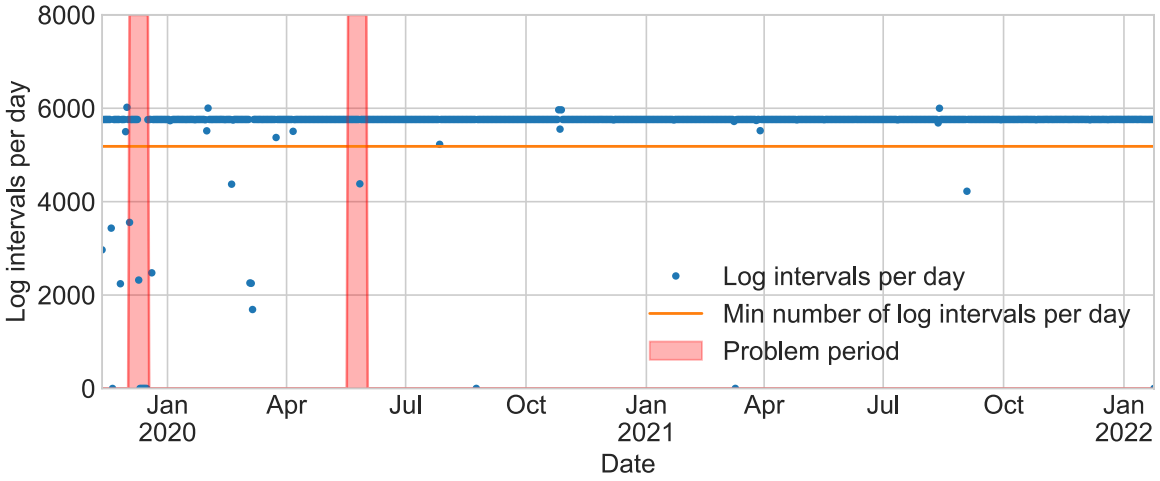


*Figure 34: Data quality for the A2A demonstrator: log intervals per days and problem periods.*

Since energy meter data for the single-family houses have only been extracted starting in February 2021. Also, 20 days with missing data in two or more houses were removed. This reduced the number of days in which distribution losses could be calculated from 313 to 293 days.

# 3.TEST SCHEDULES A2A

The test schedules for the A2A demonstrator are specified in the three tables below with one innovation per table, so as to reflect the structure of Chapter 3, whereby the baseline for the mixing station innovation (high-temperature operation, Table ) differs from the baseline for smart DH controller (low-temperature operation).

*Table 4: Test schedule for the comparison low-temperature vs high-temperature operation (**mixing station innovation**) in the A2A demonstrator: test (LT: low-temperature operation) and baseline (high-temperature operation) periods. Remark: this table contains the schedules for the comparison low-temperature vs high-temperature operation (Section 2.2), whereas smart controller tests are listed in Table  and Table .*

| start | end | Baseline or test | Test version | Remark, details |
|---|---|---|---|---|
| **2019-11-15** | 2020-01-13 | baseline | | |
| **2020-01-14** | 2020-05-03 | test | LT operation | Fixed constant temperature (95°C), set by A2A. Mixing: on. |
| **2020-05-04** | 2020-10-04 | baseline | | Normal setting during summer season (supply temp= 90°C, return=60°C) no mixing. |
| **2020-10-04** | 2020-11-26 | test | LT operation | Reduce supply T with local control (AIT/A2A). Some response tests at mixing station by NODA. |
| **2020-12-21** | 2021-01-10 | baseline | | |
| **2021-01-25** | 2021-01-31 | baseline | | |
| **2021-02-28** | 2021-03-01 | test | LT operation | |
| **2021-03-03** | 2021-03-03 | test | LT operation | |
| **2021-03-15** | 2021-03-18 | test | LT operation | |
| **2021-03-21** | 2021-04-04 | test | LT operation | |
| **2021-04-21** | 2021-07-31 | test | LT operation | Summer operation (not compared to high-temperature operation because of higher outdoor temperatures) |
| **2021-08-01** | 2021-10-03 | test | LT operation | |
| **2021-10-04** | 2021-10-24 | test | LT operation | |
| **2021-11-08** | 2021-11-14 | test | LT operation | |
| **2021-11-29** | 2021-11-30 | test | LT operation | |

| | | | | |
|---|---|---|---|---|
| **2021-12-01** | 2021-12-06 | fault | High-temperature operation | Mixing station failed to mix for unknown reasons |
| **2021-12-15** | 2021-12-16 | fault | High-temperature operation | Mixing station failed to mix for unknown reasons |
| **2021-12-22** | 2022-01-09 | baseline | | |
| **2022-01-13** | 2022-01-13 | fault | High-temperature operation | Mixing station failed to mix for unknown reasons |
| **2022-01-17** | 2022-01-18 | fault | High-temperature operation | Mixing station failed to mix (maintenance activities on the pump) |
| **2022-01-20** | 2022-01-23 | test | LT operation | |
| **2022-01-31** | 2022-02-07 | test | LT operation | |
| **2022-02-08** | 2022-02-21 | fault | | Mixing station failed to mix for unknown reasons |
| **2022-02-22** | 2022-02-28 | test | LT operation | |

*Table 5: Test schedule for testing of the smart district heating controller in the A2A demonstrator: test (**B1, B2**) and baseline (low-temperature operation) periods for the smart district heating controller (mixing station control for peak load reduction).*

| start | end | Baseline or test | Test version |
|---|---|---|---|
| **2021-08-01** | 2021-10-03 | baseline | |
| **2021-10-04** | 2021-10-24 | baseline | |
| **2021-11-08** | 2021-11-14 | baseline | |
| **2021-11-15** | 2021-11-28 | test | B1. Mixing station - peak shaving |
| **2021-11-29** | 2021-11-30 | baseline | |
| **2022-01-20** | 2022-01-23 | baseline | |
| **2022-01-24** | 2022-01-30 | test | B2. Mixing station - peak shaving |
| **2022-01-31** | 2022-02-07 | baseline | |
| **2022-02-08** | 2022-02-21 | fault | |
| **2022-02-22** | 2022-02-28 | baseline | |

*Table 6: Test schedule in the A2A demonstrator: test (**A1, A2**) and baseline (low-temperature operation) periods for the smart district heating controller (apartment building control for temperature reduction).*

| start | end | Baseline or test | Test version |
|---|---|---|---|
| **2021-08-01** | 2021-10-03 | baseline | |
| **2021-10-04** | 2021-10-24 | baseline | |
| **2021-10-25** | 2021-11-07 | test | A1. Temperature reduction |
| **2021-11-08** | 2021-11-14 | baseline | |
| **2021-11-29** | 2021-11-30 | baseline | |
| **2022-01-10** | 2022-01-12 | test | A2. Temperature reduction |
| **2022-01-13** | 2022-01-13 | fault | |
| **2022-01-15** | 2022-01-16 | test | A2. Temperature reduction |
| **2022-01-19** | 2022-01-23 | baseline | |
| **2022-01-31** | 2022-02-07 | baseline | |
| **2022-02-08** | 2022-02-21 | fault | |
| **2022-02-22** | 2022-02-28 | baseline | |

# 4. MONITORING IN THE ENERPIPE DEMONSTRATION SITE

Monitoring data at the plant room and at the house substation level are logged and obtained in several ways, as summarized in Table 7[6].

*Table 7: Numbers of buildings and substations per phase.*

| **Description phase 1** | **Number** | **Share** | **date: 31.03.2021** |
|---|---|---|---|
| Number of buildings in phase 1 | 57 | 100% | |
| CaldoTherm 250 l | 31 | | |
| Buffer unit 600 l | 6 | | |
| Standard Substation with buffer (mfh) | 1 | | |
| **Substations connected** | **38** | **67%** | |
| Standard Substation with buffer (mfh) | 2 | | |
| Vacant connections | 2 | | |
| **Max. possible connections** | **42** | **74%** | |

| **Description phase 2** | **Number** | **Share** | **date: 31.03.2021** |
|---|---|---|---|
| Number of buildings in phase 2 | 60 | 100% | |
| CaldoTherm 250 l | 31 | | |
| Buffer unit 600 l | 2 | | |
| **Substations connected** | **33** | **55%** | |
| Vacant connections | 18 | | |
| Max possible substations | 51 | 85% | |

| **Description phase 1+2** | **Number** | **Share** | **date: 31.03.2021** |
|---|---|---|---|
| Number of buildings phase 1+2 | 117 | 100% | |
| CaldoTherm 250 l | 62 | | |
| Buffer unit 600 l | 8 | | |
| Standard Substation with buffer (mfh) | 1 | | |
| **Substations connected** | **71** | **61%** | |
| Standard Substation with buffer (mfh) | 2 | | |
| Vacant connections | 20 | | |
| **Max. possible connections** | **93** | **79%** | |

[6] The monitoring concept for the ENERPIPE demonstrator is described in D3.2 (see [10]).

*Table 8: Data availability for the ENERPIPE demonstration site*

| **Data** | **Available from** | **Remarks** |
|---|---|---|
| Substation data transferred via FTP | 14.03.2019 | Newly connected substations are continuously added. This has to do with the gradual construction of the houses and installation of the substations. |
| Plant room heat meter data | 27.06.2018 | Transferred at intervals of 2 to 6 months |
| Manually logged gas and CHP consumption data | 02.01.2019 | Manually logged and transferred at irregular intervals |

As the scheme (Figure 35) represents, the heat network consists of two strings of which the heat consumption is measured by heat meters 1901 and 1902 (however the latter is not in operation yet). Heat is to be produced by two bio-CHP units, measured by heat meters 2901 and 3901. The second CHP was commissioned in the autumn 2021. Additionally, there is a natural gas boiler, represented by heat meter 4901, for peak and backup situations. Finally, heat can be transferred from and to a satellite heat network which is heated by the waste heat of a biogas installation. This heat is measured by heat meters 2903 (heat from the satellite to the network) and 3903 (heat from the network to the satellite). As can also be seen, the heat production plant comprises two hot water tanks (2x 20 $m^3$) as short-term thermal energy storage.

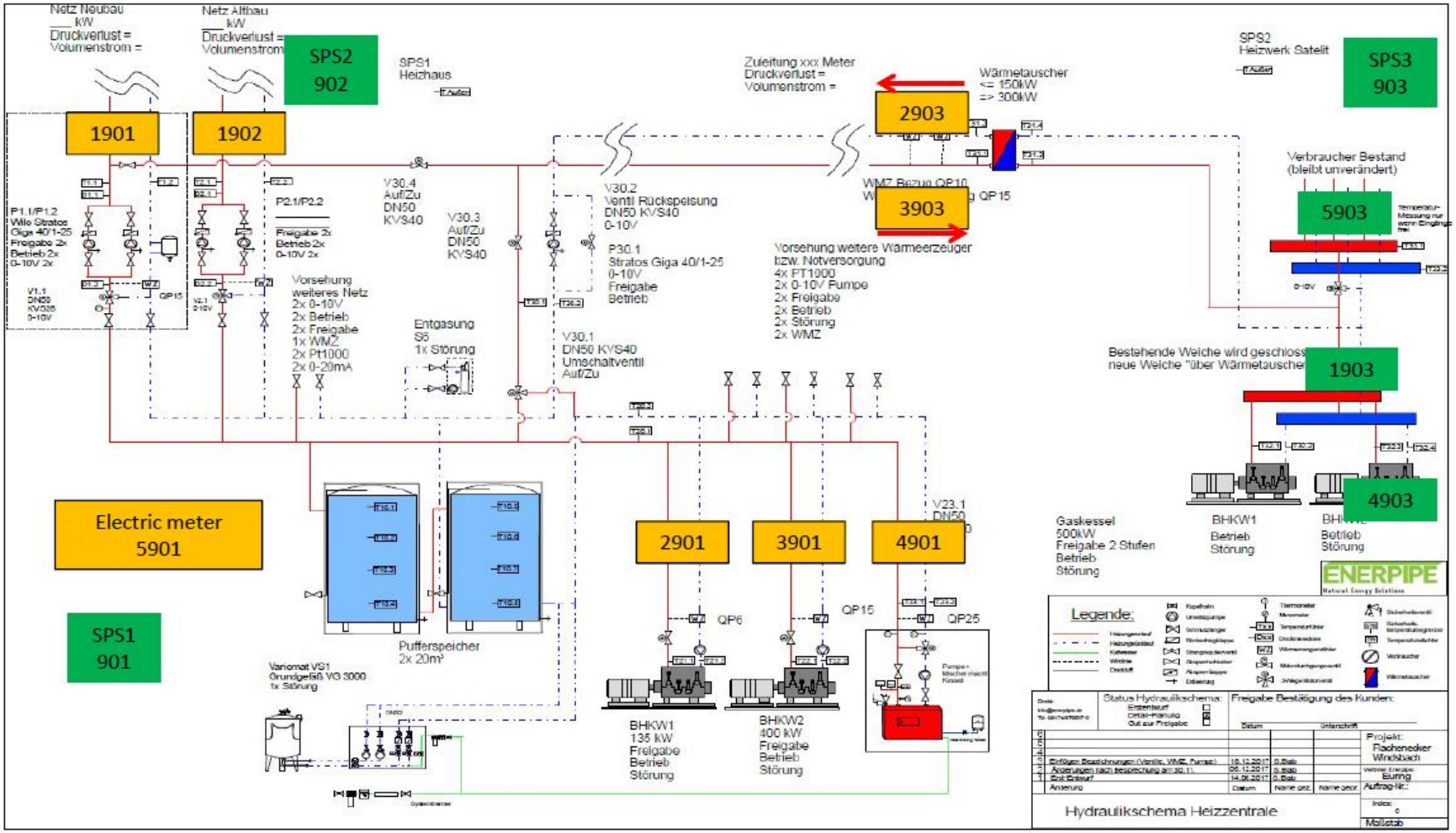


*Figure 35: Scheme of the plant room heat meter numbering*

# 5. DATA QUALITY IN THE ENERPIPE DEMONSTRATION SITE

The number of commissioned buffers at each point in time is calculated based on commissioning dates provided by Enerpipe. On the other hand, the number of connected units is determined for each day based on the available measurements. This results in a generally rising curve, with a few drops corresponding to temporary data losses. Days where the number of substations with data is inferior to 90% of the running max over 30 days are considered to be faulty in terms of data and thus not considered in the analyses. Interruptions in the data communication may for instance be caused by construction measures, new house connections or a cut off during groundworks.

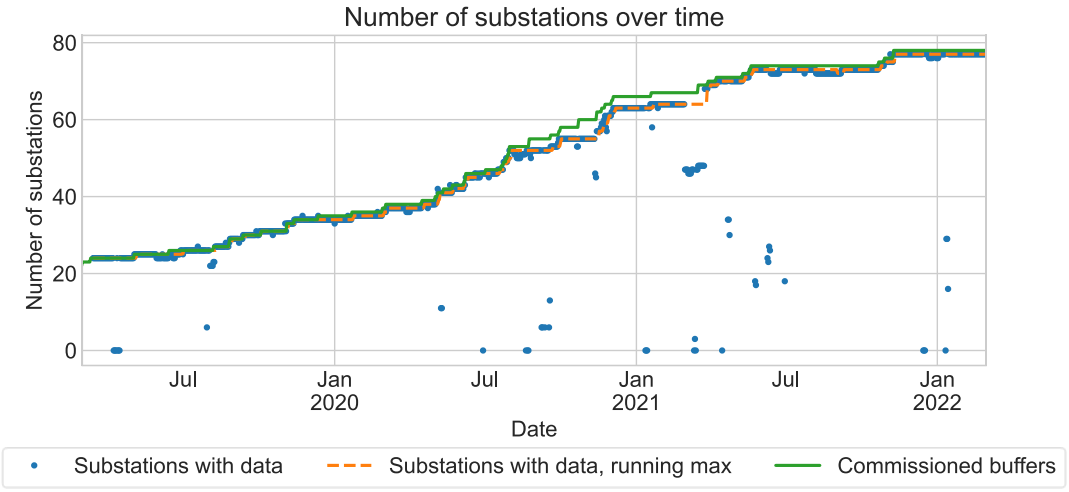


*Figure 36: Number of substations with available data across time (daily values)*

# 6.TEST SCHEDULE ENERPIPE

The test schedule for evaluation of coordinated buffer charging in the ENERPIPE demonstrator is specified in Table 9.

*Table 9: Test schedule in the ENERPIPE demonstrator*

| start | end | Baseline or test | Test version | Remark, details, exact test times |
|---|---|---|---|---|
| **2021-04-21** | 2021-07-18 | baseline | | |
| **2021-07-19** | 2021-08-22 | test | Coordinated buffer charging | Coordinated buffer charging on 20 buffers |
| **2021-08-23** | 2021-10-03 | test | Coordinated buffer charging | Coordinated buffer charging on 20 buffers |
| **2021-10-04** | 2021-11-14 | test | Coordinated buffer charging | |
| **2021-11-15** | 2021-11-18 | baseline | | |
| **2021-11-19** | 2021-11-24 | test | Coordinated buffer charging | 19/11/2021 11h00 CET – 24/11/2021 14h00 CET |
| **2021-11-25** | 2021-11-28 | baseline | | |
| **2021-11-29** | 2021-12-03 | test | Coordinated buffer charging | 29/11/2021 00h00 CET – 4/12/2021 11h30 CET |
| **2021-12-04** | 2021-12-05 | baseline | | |
| **2021-12-06** | 2021-12-13 | test | Coordinated buffer charging | 6/12/2021 10h00 CET - 14/12/2021 11h30 CET |
| **2021-12-14** | 2021-12-17 | baseline | | |
| **2021-12-18** | 2021-12-21 | test | Coordinated buffer charging | 18/12/2021 9h00 CET – 22/12/2021 5h00 CET |
| **2021-12-22** | 2021-12-23 | baseline | | |
| **2021-12-24** | 2021-12-26 | test | Coordinated buffer charging | 23/12/2021 14H00 CET – 27/12/2021 5h00 CET |
| **2021-12-27** | 2022-01-12 | baseline | | |
| **2022-01-13** | 2022-01-19 | test | Coordinated buffer charging | 12/01/2022 13h30 CET – 20/01/2022 00h30 CET |
| **2022-01-20** | 2022-01-26 | baseline | | |
| **2022-01-28** | 2022-02-08 | test | Coordinated buffer charging | 28/01/2022 11h00 CET – 8/2/2022 |
| **2022-02-09** | 2022-02-14 | baseline | | |
| **2022-02-15** | 2022-02-28 | test | Coordinated buffer charging | |

# ANNEX 3: DETAILED RESULTS

## 1. DETAILED RESULTS FOR THE A2A DEMONSTRATION SITE

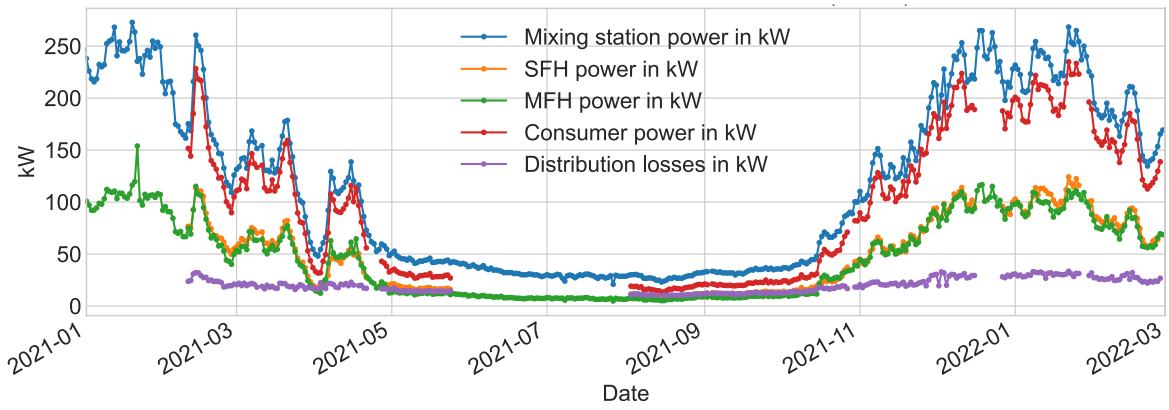


*Figure 37: Daily averages of thermal power at the mixing station, at the consumers and distribution losses (in kW)*

*Table 10: Performance by building and remarks on monitoring data and faults for the multi-family houses of the A2A "city demo" from September 2021 to February 2022; The contractual return temperature reference value is 60°C; * these buildings are above the contractual return temperature reference value*

| Building | Mean flow rate weighted return temperature in °C | Supplied energy in MWh | % fault prediction | Remarks |
|---|---|---|---|---|
| **06*** | 69.75 | 285.44 | 72.2 | This building has a high return temperature (mostly between 60 °C and 70 °C) in the heating season during daytime, increasing at lower outdoor temperatures. Night setback is clearly apparent from the data, with no heating between 23:00 and 6:00. Heat demand is already rather high at the beginning of the heating season (with high outdoor temperatures). The monitoring data point to a probable issue on the space heating side. |
| **22*** | 69.34 | 116.6 | 75.7 | This building has a constantly very high return temperature of around 70 °C in the heating season. Night setback does not appear to be implemented. Heat demand is already high at the beginning of the heating season (with high outdoor temperatures) and only slightly increases with lower outdoor temperatures. The monitoring data point to a probable issue in bypass or primary control valve not closing tightly. |
| **11*** | 61.8 | 370.48 | 96.1 | The return temperatures are rather constant outside of the heating season (between 55 and 57 °C) and tend to be higher (up to 60 to 65 °C) at times of high heat demand. The monitoring data point to a probable issue on the space heating side causing higher return temperatures at times of high heat demand. |
| **16** | 59.35 | 543.243 | 87.0 | This building has high return temperatures (60 °C and more) outside of the heating season and during the heating season during night temperature setback (with some improvement from November 7th, 2021). Return temperatures are at the lowest (around 45 °C) during the morning heating peak following night setback. The monitoring data point to a probable issue on the domestic hot water side. |
| **10** | 57.87 | 305.48 | 77.2 | Return temperatures are seen to increase significantly with lower temperatures, from daily average return temperatures around 50 °C for outdoor temperatures between 10 and 15 °C to 60 °C with outdoor temperatures around 5 °C. There is probably optimization potential on the space heating side. |
| **03** | 56.7 | 264.103 | 18.1 | Monitored temperatures are consistently between 50 °C and 60 °C during the heating period in the daytime, with higher values during the morning peak following night temperature setback. There may be some optimization potential on the space heating side. Despite rather high return temperatures, the fault detection algorithm tends not to predict any fault, perhaps because of the regularity of temperatures. |
| **14** | 56.24 | 254.443 | 46.1 | This substation provides heat for space heating and domestic hot water. The return temperatures of this building have significantly increased in December 2021, reaching temperatures above 70 °C. Communication with the technical personnel in charge of this building revealed that these high return temperatures were caused by a clogged domestic hot water heat exchanger. |
| **25** | 55.87 | 309.25 | 77.2 | The primary return temperatures in this building tend to increase with higher values of heat demand. There may be some optimization potential on the space heating side. |
| **04** | 55.15 | 289.23 | 85.0 | Return temperatures in this building are highest (up to 60 °C) at times of heat demand outside of the heating season and during the heating season after the morning peak, i.e. during domestic hot water loading. Night setback appears to be rather strong, with high heating peaks in the morning, which also corresponds to the times of lowest return temperature (down to |

| | | | | |
|---|---|---|---|---|
| | | | | 45 °C). The monitoring data point to a possible issue or suboptimal configuration on the domestic hot water side and/or on the space heating side. |
| **29** | 54.61 | 162.3 | 45.0 | This substation provides heat for space heating only. Return temperatures are higher at times of high space heating demand. There may be some optimization potential on the space heating side. |
| **23** | 53.87 | 197.843 | 0.0 | |
| **24** | 52.97 | 238.59 | 15.6 | |
| **31** | 52.72 | 240.253 | 22.6 | This building has unusually constant return temperatures across each day. Return temperatures were higher (around 55 °C) at the beginning of September 2021 and suddenly sank to around 52 °C on September 13, remaining quite constant since then. There may be some optimization potential on the domestic hot water side. |
| **19** | 52.52 | 499.92 | 76.3 | This building has a rather high return temperature (mostly between 55 and 60 °C) outside of the heating season and in the heating season during nighttime. Night setback is clearly apparent from the data, with low heat supply between 23:00 and 6:00. The monitoring data point to a probable issue on the domestic hot water side. Despite unremarkable average values of return temperature, automated fault detection often predicted faults for this building. A possible explanation is that return temperatures did often reach higher temperatures (above 60 °C and up to 67 °C), but mostly at times of low heat demand. |
| **05** | 52.19 | 262.117 | 43.3 | |
| **18** | 51.57 | 307.473 | 6.2 | |
| **17** | 51.26 | 245.473 | 8.9 | |
| **30** | 51.02 | 188.323 | 9.6 | There may be some optimization potential on the space heating side. |
| **12** | 49.27 | 261.62 | 36.2 | |
| **09** | 48.96 | 395.583 | 80.0 | The return temperatures in this building are highest (up to 55 °C) at times of domestic hot water production outside of the heating period, lowest at times of higher heat demand for space heating. There may be some optimization potential on the domestic hot water side. Despite rather good average values of return temperature, automated fault detection often predicted faults for this building. |
| **21** | 48.69 | 363.33 | 32.8 | |
| **28** | 48.66 | 314.58 | 3.3 | |
| **13** | 48.47 | 353.323 | 55.0 | |
| **20** | 48.47 | 76.94 | 3.9 | |
| **08** | 48.06 | 540.987 | 59.9 | The return temperatures in this building are low (mostly under 45 °C) at times of low heat demand and gradually increase with higher heat demands, reaching values up to 60 °C for higher heat demands (200 kW and above). |
| **02** | 47.72 | 234.707 | 5.0 | |
| **26** | 47.58 | 367.677 | 0.6 | The return temperatures in this building are always under 56 °C. |
| **01** | 47.36 | 188.637 | 27.1 | The return temperatures in this building are always under 59 °C. |
| **27** | 46.57 | 365.643 | 57.8 | The return temperatures in this building are low (mostly under 45 °C) at times of low heat demand and gradually increase with higher heat demands, reaching values up to 60 °C (max. 64.7 °C) for higher heat demands (150 kW and above). |
| **07** | 46.3 | 433.22 | 19.4 | The return temperatures in this building are always under 58 °C. |
| **15** | 43.86 | 387.78 | 10.2 | The return temperatures in this building are always under 58 °C. |

# 2. DETAILED RESULTS FOR THE ENERPIPE DEMONSTRATION SITE

Network behaviour with and without (baseline) coordinated buffer charging is compared in Figure 38, Figure 40 and Figure 39. The average power supplied to the network does not differ significantly between the two cases, except that is seems slightly lower during coordinated buffer charging at mild outdoor temperatures (10 to 18 °C). It can also be noticed that the power supplied to the network at low outdoor temperatures (below 0 °C) tends to be lower than predicted by the linear trendline, in both cases. The peak energy (defined as the energy supplied at powers over a notional threshold of 210 kW) follows a pattern similar to that of average power. While peak shaving could seem to have been achieved for the two days with lowest temperatures, this is not confirmed for temperatures between 0 and 5 °C.

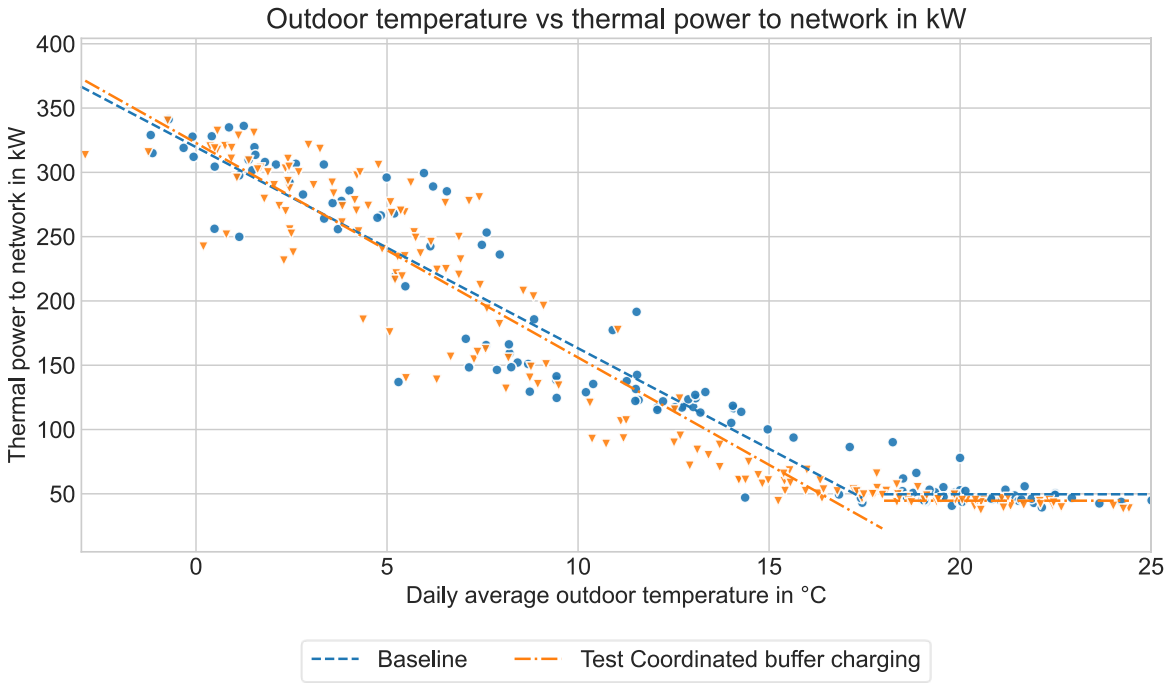


*Figure 38: Daily values of outdoor temperature vs daily averaged power supplied to network for the baseline vs coordinated buffer charging*

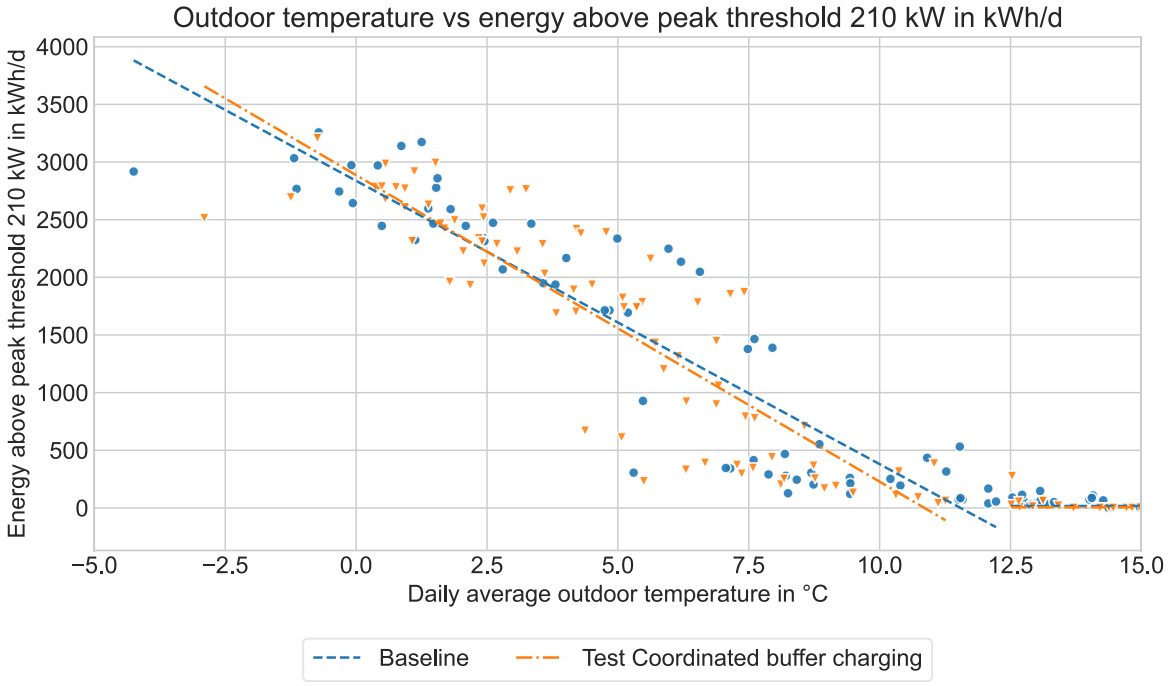


*Figure 39: Daily values of energy above peak power threshold of 210 kW vs outdoor temperature, for the coordinated buffer charging tests vs baseline (no coordinated buffer charging)*

The daily average-to-peak power ratio (Figure 40), on the other hand, which should be increased by peak shaving, tends to be lower during coordinated buffer charging when outdoor temperatures are mild, which indicates that coordinated buffer charging failed to reduce the maximum power in those cases.

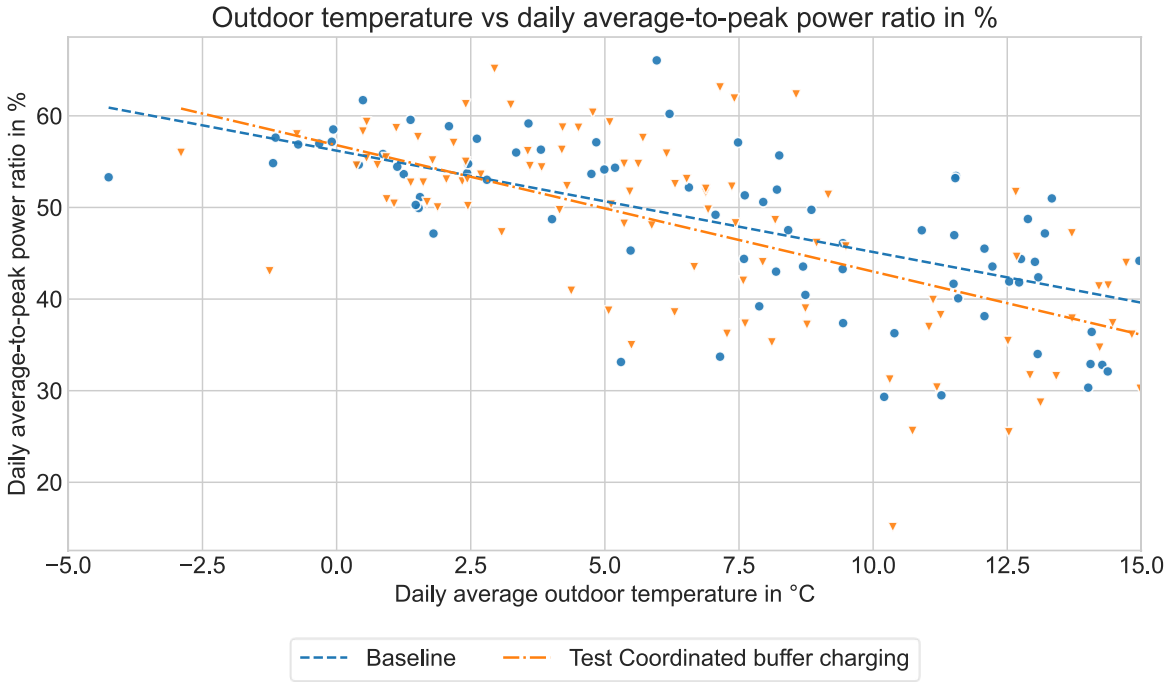


*Figure 40: Daily values of average-to-peak power ratio vs outdoor temperature, for the coordinated buffer charging tests vs baseline (no coordinated buffer charging)*

The breakdown of heat sources for the ENERPIPE demonstrator, illustrated in Figure 41, exhibits both seasonal variations (more energy from the satellite plant during summer) and historical changes, including the increasing energy demand due to new connections, which made peak gas boiler operation necessary during the winter season 2020-2021, but also the start of operation of the larger second CHP in October 2021, which reduced the need for peak gas boiler operation in the latest heating season.

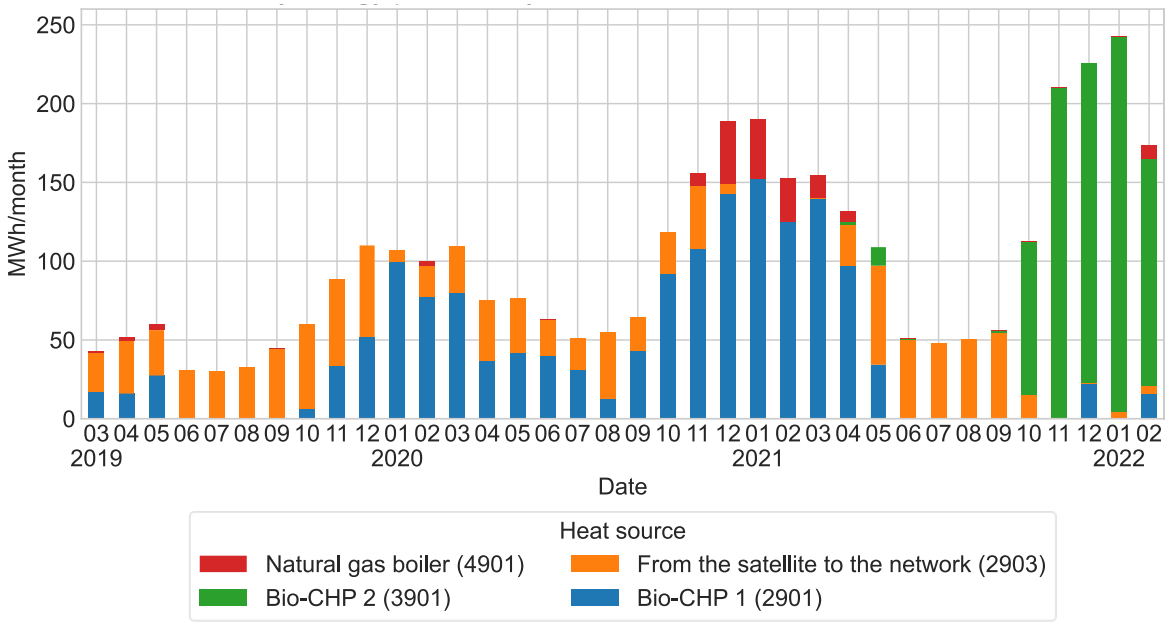


*Figure 41: Monthly energy provided by the various sources in the Enerpipe demonstration site, in MWh/month*

On the demand side, the central plant almost exclusively provides heat to the network, but also in very small amounts to the satellite plant.

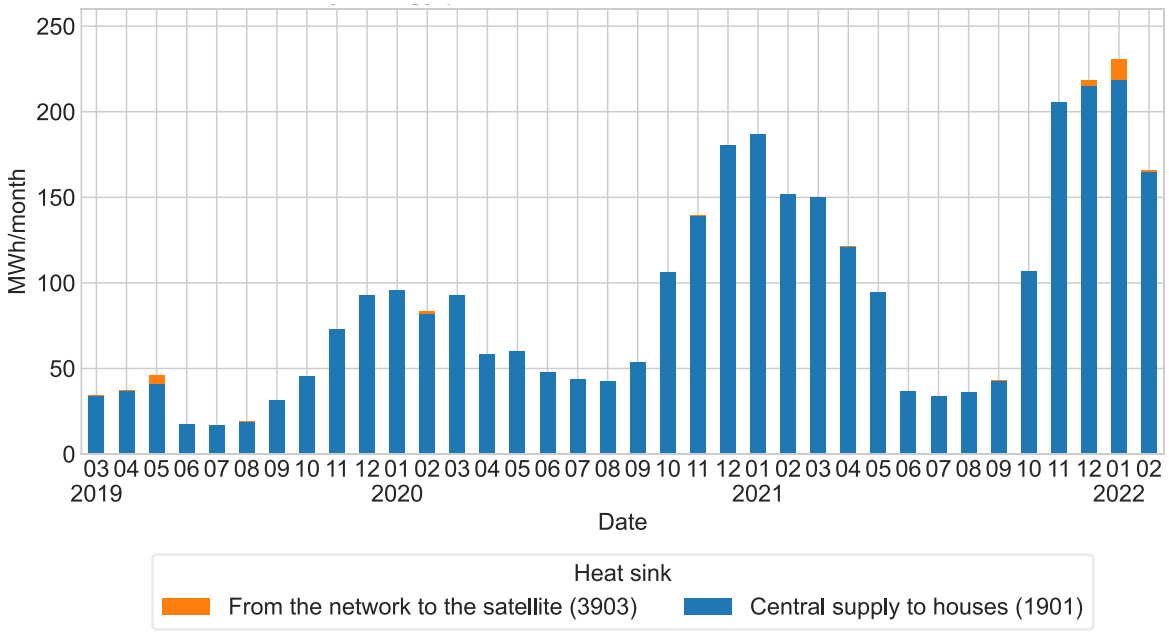


*Figure 42: Monthly energy provided to the various sinks in the Enerpipe demonstration site, in MWh/month*

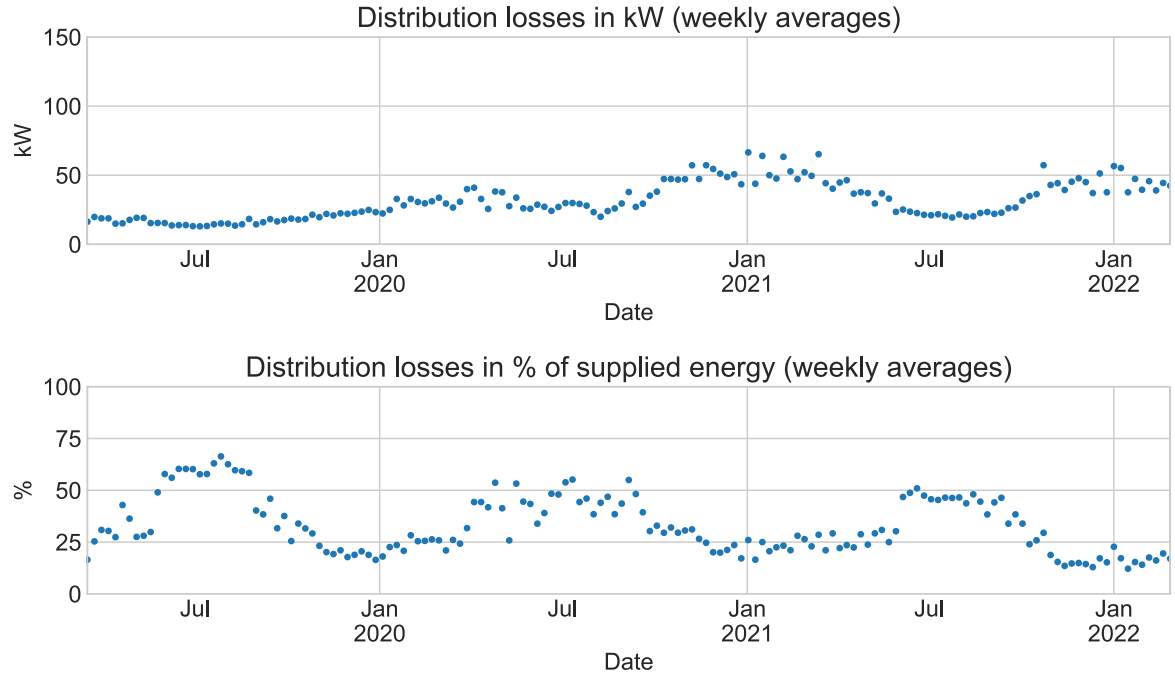


*Figure 43: Distribution losses in the ENERPIPE demo, weekly absolute and relative values*

Across the almost three years of monitoring, the distribution losses illustrated in Figure 43 tended to rise slightly in absolute terms and decrease in relative terms, as more consumers were connected.

*Table 11: Performance by building and remarks on monitoring data and faults for the single-family houses of the Enerpipe demo from September 2021 to February 2022*

| Mean flow rate weighted return temperature in °C | Supplied energy in MWh | % Predicted fault | Remarks |
|---|---|---|---|
| 64.85 | 4.984 | 74.8 | This unit has very high flowrate-weighted return temperatures, up to 70 °C. It is loading a high proportion of the day. There is a large (flowrate-weighted) temperature difference between primary return and buffer bottom temperature. The outdoor temperature sensor also gives unrealistic values (around 20 °C during the whole heating season). |
| 63.30 | 15.011 | 53.1 | This unit had very high flowrate-weighted return temperatures, up to 70 °C. There was a large (flowrate-weighted) temperature difference between primary return and buffer bottom temperature. |
| 59.79 | 10.589 | 43.5 | This unit had the highest flowrate-weighted return temperature for the period September-December 2021, and in average a significant difference (up to 20 °C) between buffer bottom temperature and primary return temperature. The fault was solved at the beginning of February 2022. |
| 54.27 | 8.689 | 26.6 | High return temperatures at low heat powers (highest around 5 to 10 kW). High mean flow rate weighted temperature difference primary return - buffer bottom temperature. Probable issue with return lance. |
| 52.67 | 7.829 | 26.5 | High return temperatures at low heat powers (highest around 2 kW) and rather high mean flow rate weighted temperature difference primary return - buffer bottom temperature. Probable (limited) issue with return lance. |
| 51.59 | 9.573 | 26.5 | High return temperatures at low heat powers (highest around 2 kW) and rather high mean flow rate weighted temperature difference primary return - buffer bottom temperature. Probable (limited) issue with return lance. |
| 51.01 | 7.028 | 11.2 | This unit showed average behaviour until November 2021. It started showing problematic behaviour in November and December 2021: high return temperatures, limited correlation between primary valve position and primary mass flow rate, high difference between primary return temperature and buffer bottom temperature during loading. In January and February 2022, the unit kept having days with problematic behaviour interspersed with days of apparently normal behaviour. |
| 49.37 | 5.052 | 15.3 | This unit had rather high return temperatures during charging and some difference between primary return temperature and buffer bottom temperature, as well as frequent short charging cycles. Behaviour improved in February 2022. |
| 49.18 | 6.456 | 40 | This unit had rather high return temperatures during charging and some difference between primary return temperature and buffer bottom temperature, as well as frequent short charging cycles. Behaviour improved in February 2022. |
| 48.85 | 9.381 | 42.9 | |
| 48.12 | 3.9 | 10 | |
| 48.02 | 7.863 | 17.6 | |
| 47.96 | 4.633 | 5.3 | |
| 47.4 | 7.081 | 21.8 | |

| | | | |
|---|---|---|---|
| 47.29 | 14.097 | 45.9 | High rate of predicted faults despite moderate return temperatures. The unit is characterized by high heat consumption and a weaker correlation between valve position and flow rate than in other units. |
| 47.11 | 8.46 | 15.4 | Irregular performance: daily average return temperatures between 43 °C and 61 °C in February 2022. The average difference between buffer bottom and top temperature is much lower than average and often less than 10 °C. |
| 46.61 | 4.428 | 18.4 | |
| 46.40 | 12.435 | 9.9 | |
| 46.26 | 21.427 | 58.3 | High rate of predicted faults despite moderate return temperatures. The unit is characterized by high heat consumption and a weaker correlation between valve position and flow rate than in other units. |
| 45.92 | 6.353 | 0 | |
| 45.84 | 12.783 | 9.9 | |
| 44.85 | 7.696 | 1.8 | |
| 44.72 | 4.719 | 4.1 | |
| 44.46 | 9.632 | 4.1 | |
| 44.32 | 4.799 | 17.5 | |
| 43.73 | 5.652 | 0 | |
| 43.72 | 7.726 | 0 | |
| 43.61 | 3.803 | 0 | |
| 43.58 | 11.59 | 0.6 | |
| 43.51 | 7.3 | 1.2 | |
| 43.29 | 7.697 | 9.4 | |
| 43.27 | 6.629 | 0.6 | |
| 43.20 | 6.838 | 1.2 | |
| 43.18 | 7.547 | 0 | |
| 42.66 | 8.997 | 24.1 | This unit exhibited a high number of starts (more than 20 starts per day) in December. |
| 42.45 | 6.319 | 0.6 | |
| 42.42 | 6.634 | 3.7 | |
| 42.37 | 5.008 | 17.1 | |
| 42.37 | 6.568 | 10.5 | |
| 42.25 | 6.665 | 5.3 | |

| | | | |
|---|---|---|---|
| 42.09 | 6.904 | 8.8 | |
| 41.73 | 5.69 | 9.9 | |
| 41.66 | 3.64 | 0 | |
| 41.38 | 6.45 | 1.2 | |
| 41.32 | 11.885 | 5.9 | |
| 41.31 | 10.17 | 1.8 | |
| 41.02 | 5.672 | 1.8 | |
| 41.01 | 5.234 | 1.2 | |
| 40.92 | 9.238 | 0.6 | |
| 40.66 | 7.111 | 2.3 | |
| 40.60 | 7.975 | 11.8 | |
| 40.38 | 10.338 | 3.5 | |
| 40.34 | 7.68 | 5.3 | |
| 40.33 | 7.449 | 3.1 | |
| 40.27 | 12.327 | 6.4 | |
| 40.09 | 5.834 | 2.4 | |
| 40.07 | 11.235 | 0.6 | |
| 39.75 | 7.016 | 24 | |
| 39.62 | 6.296 | 8.2 | |
| 39.58 | 7.45 | 8.2 | |
| 39.46 | 12.904 | 1.2 | |
| 39.32 | 10.406 | 6.5 | |
| 39.15 | 10.145 | 6.4 | |
| 38.88 | 8.479 | 14.6 | |
| 38.69 | 6.714 | 4.1 | |
| 38.44 | 5.594 | 8.2 | |
| 38.42 | 8.447 | 21.2 | |
| 38.07 | 15.259 | 33.7 | High energy consumption and high proportion of loading time (often >50%) but good return temperatures. |

| | | | |
|---|---|---|---|
| 37.75 | 7.916 | 7 | |
| 37.18 | 17.146 | 37.1 | High energy consumption and high proportion of loading time (sometimes >50%) but good return temperatures. |
| 35.63 | 8.657 | 2.9 | |

# ANNEX 4: SIMULATION STUDY FOR THE TECHNICAL AND ECONOMICAL OPTIMISATION OF THE DECENTRALISED BUFFER TANK CONCEPT

# ANNEX 5: EVALUATION OF THE PRIMARY ENERGY FACTORS FOR THE OPTIMIZED CHP OPERATION AT THE ENERPIPE DEMO

Grant Agreement: 768936

TEMPO

# D5.3: ANNEX 4
# SIMULATION STUDY FOR THE TECHNICAL AND ECONOMICAL OPTIMISATION OF THE DECENTRALISED BUFFER TANK CONCEPT

This project has received funding from the European Union's Horizon 2020 research and innovation programme under grant agreement No 768936.

# TABLE OF CONTENTS

# 1 INTRODUCTION

A simulation study was conducted to elaborate the technical and economical optimisation potential of the decentralised buffer tank concept. It comprises the decentralised buffer tank approach in the consumer buildings and the district heating (DH) network supplying the consumer buildings. Aim of the simulation study is a supply concept optimisation, which allows improvements in the design of future projects.

Buffer tanks installed in the consumer buildings reduce the peak load demand of the consumers and thus also the peak load demand of the entire DH network. This allows for smaller DH network pipe dimensions which can lead to lower investment costs for the piping as well as reduced thermal losses in the DH network. On the other hand, the concept leads to increased investment costs and thermal losses in the house stations compared to standard heat transfer substations. The simulation study considers those effects and results thus allow to quantify the advantages of the buffer tank concept compared to standard solutions.

The design of the Windsbach DH network was done based on the experience of Enerpipe who has realised comparable projects before, with the assumptions described in deliverable D3.1. The simulation study investigates the relationship of consumer peak load reduction by various buffer tank volumes and the potential reduction of DH network pipe dimensions. This also considers dynamic effects in the DH network.

Due to the high complexity of a DH network with a large number of consumers the applied simulation model is simplified while preserving all the essential effects described above. This simplification focuses on a representative DH network branch with only a limited number of consumers. In this branch the mutual dependency of buffer tank volumes and DH network pipe dimensions is investigated in detail. Both the consumer substation part of the simulation model as well as the DH network branch model are verified with monitoring data to ensure high quality simulation results.

# 2 METHODOLOGY

For the study presented here the following general methodology was applied. In a first step available monitoring data was selected and evaluated to allow for a verification of simulation models. For this a special focus was given to consumer heat demands and house supply capacity rates, buffer tank charging characteristics as well as supply and return temperatures.

Simulation models were developed on two levels. A first model represents the Enerpipe CaldoTHERM house station with primary buffer tank. This model was verified in a first step with laboratory data from Enerpipe and in a second step with data from the Windsbach plant. The house station model was used for first investigations on buffer tank charging characteristics and house connection flow rate reduction potential. The second model considers a selected DH network branch with, at the time of consideration, ten connected single-family houses. This model was again verified with measurement data from Windsbach and applied for detailed investigations on heat balances, DH pipe dimensioning and simultaneity factors for different buffer tank sizes and house connection flow rates.

With the results from the detailed simulations generalised results were derived that can also be used for investigations on full-size DH networks. Based on these, additional analysis for the entire Windsbach DH network, e.g., on improved DH network design for various buffer tank volumes and charging capacity rates as well as economical and technical investigations were performed.

# 3 HOUSE STATIONS WITH BUFFER STORAGE TANK

## 3.1 MODEL SETUP

A TRaNsient SYstem Simulation (TRNSYS) [TRNSYS, 2020] model reproducing the Enerpipe CaldoTHERM V4 unit shown in Figure 1 is established and verified. The house station comprises a 250 l buffer tank with direct charging. The domestic hot water (DHW) fresh water station can be supplied either by discharging the buffer storage tank or directly by the house connection line. A DHW circulation lance is an optional unit which is installed only in some buildings. For covering the space heating (SH) demand the storage tank is indirectly discharged with an internal heat exchanger.

Figure 2 shows the simulation model where the buffer storage tank is simulated with the so-called multiport store model (TRNSYS type 340). Individual components are connected specifying the input and output temperatures and flow rates. The green lines symbolize the house connection pipes of the heat distribution network. The blue lines represent the connection between the buffer storage tank and the freshwater station. The heat exchanger used for hydraulic decoupling of the DHW cycle is modelled with heat exchanger TRNSYS type 5. A further storage port is used for the DHW circulation where the set point temperature is obtained with a bypass flow modelled with the controlled flow diverter TRNSYS type 11. Brown lines represent the SH supply with bypass. The model allows a detailed investigation of the effects of different buffer tank sizes and house connection capacity rates in one-minute time steps considering the fast dynamics and inertia.

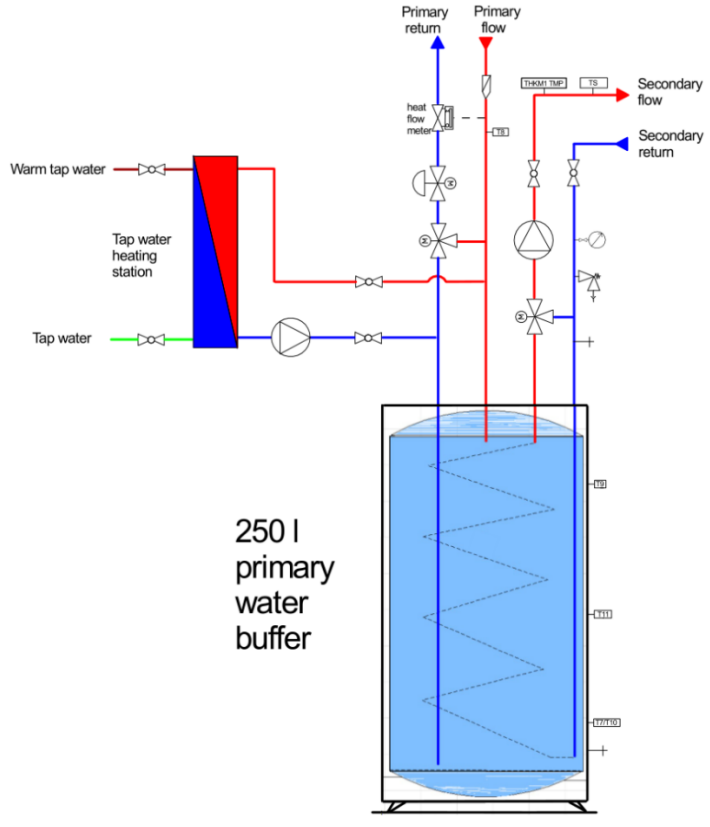


*Figure 1: Hydraulic sketch for the Enerpipe CaldoTHERM unit (V4)*

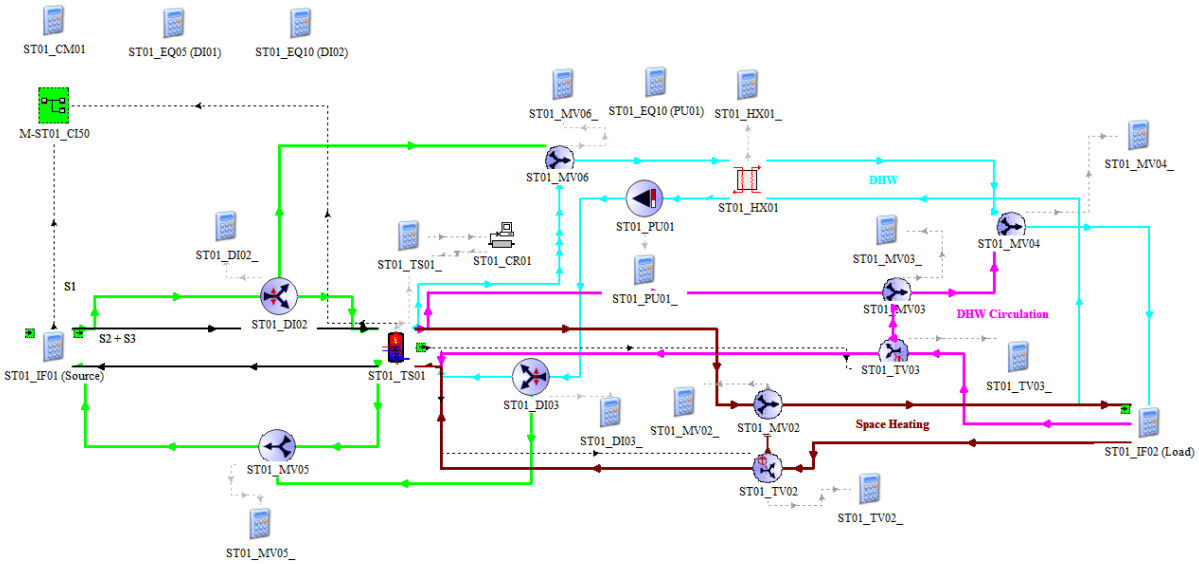

Figure 2: Simulation model for the Enerpipe CaldoTHERM unit (V4)

## 3.2 INPUT DATA

The house supply temperature is set to 77 °C in winter with a constant house connection flow rate of 425 l/h which is the design value for standard single-family buildings in Windsbach.

The SH set point temperature equals 50 °C which is a typical value for standard low-temperature heating systems. The supply temperature for DHW is set to 45 °C. To account for an increasing cold-water temperature with higher ambient temperatures, a periodic equation is applied with a yearly maximum of 15 °C on summer days and a minimum of 10 °C on winter days.

Measurement data for SH and DHW load is not included in the monitoring concept applied for the Windsbach network. The required simulation input of characteristic load profiles are therefore obtained by applying VDI 4655 guideline [VDI 4655, 2021]. For single-family buildings the standard provides normalized load profiles as one-minute average values for typical day categories. A total of ten typical day categories exists with differentiation between seasons (summer, winter or transition period), weekday types (workday or weekend) and the cloud conditions (clear or cloudy sky). The absolute load profile of a typical day corresponds to the normalized load profile multiplied by the energy factor of the typical day category and the annual heat demand. The annual DHW heat demand is set to 2 000 kWh, the annual SH heat demand to 10 000 kWh. Figure 3 shows the resulting daily load profile and load duration curve for a typical workday in winter with cloudy sky and a daily total heat load of 62 kWh.

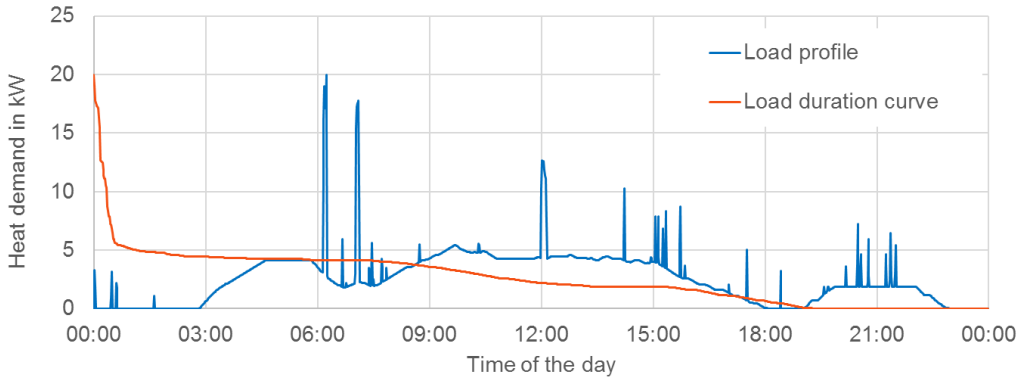


*Figure 3: Daily load profile and load duration curve for a typical work day in winter with cloudy sky based on [VDI 4655, 2021]*

## 3.3 VERIFICATION

The simulation model is verified in a three steps procedure. In a first step the model is verified with measurement data from Enerpipe laboratory tests. Subsequently, the heat demand and maximum heat capacity rate determined by simulations with the inputs described in 3.2 is compared with Windsbach monitoring data to verify that the VDI 4655 load profiles correctly represent the consumption behaviour of the single-family houses in Windsbach. Finally, the charging duration and number of charging cycles is evaluated to verify the control strategy.

### 3.3.1 VERIFICATION OF HOUSE STATION MODEL

The simulation model is verified by means of laboratory measurements. The CaldoTHERM V4 unit is tested by Enerpipe with a constant SH load of 6 kW over a period of 3.5 hours including one DHW drawing for a unit without DHW circulation. For verification, the measured primary flow temperature and the measured SH and DHW return temperatures are given as inputs into the model. Figure 4 shows the buffer tank temperature, accumulated amounts of heat and heat capacity rates. The temperature at the buffer tank top is underestimated by the simulation while it is overestimated for the middle and bottom parts. The deviations between simulated and measured temperatures are nearly constant after a time of 0.5 hours. The reason for deviations in simulation is a simplified initialisation method with initial temperatures for each of the 30 tank layers determined by linear interpolation based on measured temperatures from only 3 different heights. The simulated heat capacity rates and accumulated heat amounts are rather accurate. Small deviations between the simulated and measured heat transfer at the house connection are observed resulting from higher primary return temperature in simulation. The higher primary return temperature is explained by a higher temperature in the buffer tank bottom.

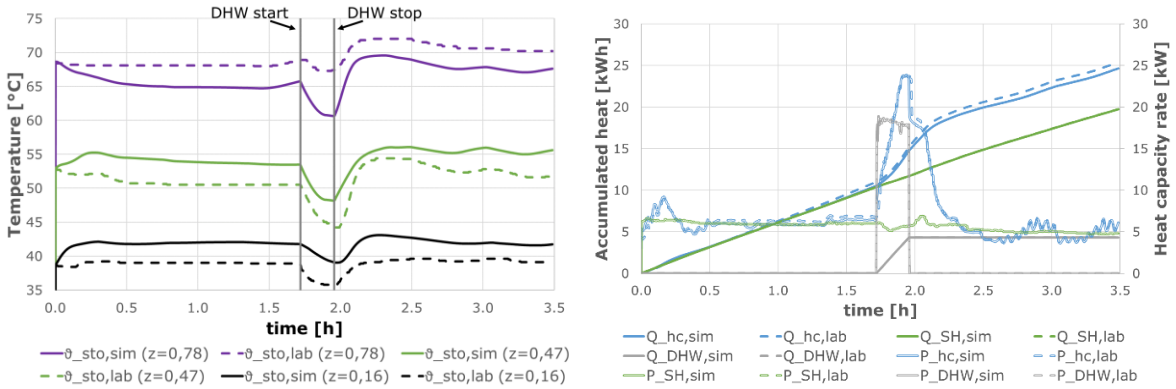


*Figure 4: Simulation results and laboratory data for buffer tank temperatures (left) and heat (right) for a laboratory test of the CaldoTHERM V4 unit with 6 kW SH load and DHW drawing (sto: storage, sim: simulation data, lab: laboratory data, z: relative height of temperature sensor in the tank; hc: house connection, P: heat capacity rate, Q: accumulated heat)*

### 3.3.2 HEAT CONSUMPTION OF SINGLE-FAMILY BUILDINGS

The DH network in Windsbach is monitored with a volume flow meter and sensors for the supply and return temperature as well as heat meters for the consumptions of the house stations. The simulation results for typical days are compared to measurement data to verify the control strategy and the assumptions concerning the load profile. The house stations included in the comparison is a selection of stations fulfilling all of the following criteria:

- Stations with Enerpipe V4 CaldoTHERM unit
- Single-family buildings with SH capacity rate of 6 kW (Enerpipe categorisation)
- Monitoring data available for at least one summer, winter and transition period
- Well-working stations according to fault detection method introduced by AIT (http://tempo-dhc.ait.ac.at/building-guide/)

The fault detection method includes several criteria to identify problems in house stations. Four criteria are evaluated to identify well-working stations used for the verification procedure. High difference between the return temperature and the buffer tank bottom temperature are caused by a suboptimal height of the outlet or a too short return lance of the DHW circulation system. This can also be detected by a high mean flow-weighted return temperature. Suboptimal charging control causes a high charging duration per supplied energy amount. A low correlation coefficient between the valve position and the volume flow results from primary control valve issues. Following the procedure with eliminating house stations with at least one fault, ten out of 18 stations are classified to be without problems concerning the technical equipment and charging control.

The mean heat consumption and maximum heat capacity rate from simulation is compared with Windsbach data to verify the assumptions regarding the heat demand and peak load of single-family buildings described in 3.2.

The heat demand mainly depends on the ambient temperature so that one typical day of each season is included in the verification. Figure 5 shows the simulated buffer tank charging heat demand as average of 20 simulated days with identical load profile and the maximum charging heat capacity rate. The measured heat demand corresponds to the average of all days belonging to the respective typical day according to the VDI 4655

criteria. The measured maximum heat capacity rate corresponds to the 99th percentile of all measurements for a typical day to eliminate measurement errors.

Especially the charging heat demand differs between the 10 regarded house stations caused by different consumption behaviour, different position in the heat distribution network and different start of operation between the house stations. For a cloudy winter workday (WWB) the house station with the highest heat demand (116) has a 2.4 times higher heat demand than the one with the lowest (64). The simulated value is 20 % above the average over all stations but in the range of the measurements. The latter is also the case for a summer workday (SWX) and a cloudy workday in transition period (ÜWB). While for the winter day the heat demand is above the measured average, it is below for the summer day and the day in transition period. In summer, the charging heat demand is the sum of thermal buffer tank losses and the DHW heat demand while in winter the SH heat demand is dominant. Therefore, the SH heat demand is slightly overestimated by simulation while the DHW heat demand is slightly underestimated.

The simulated maximum charging heat capacity rate is in the range of measurements and higher than the measurement average for all three typical days. Therefore, the peak load is slightly overestimated by simulation. The maximum heat capacity rate tends to be lower in summer caused by a lower supply temperature which is the case both for simulation and measurements.

With the simulated values in range of the measurements it is demonstrated that the load profiles used for the simulation study are appropriate for modern single-family houses.

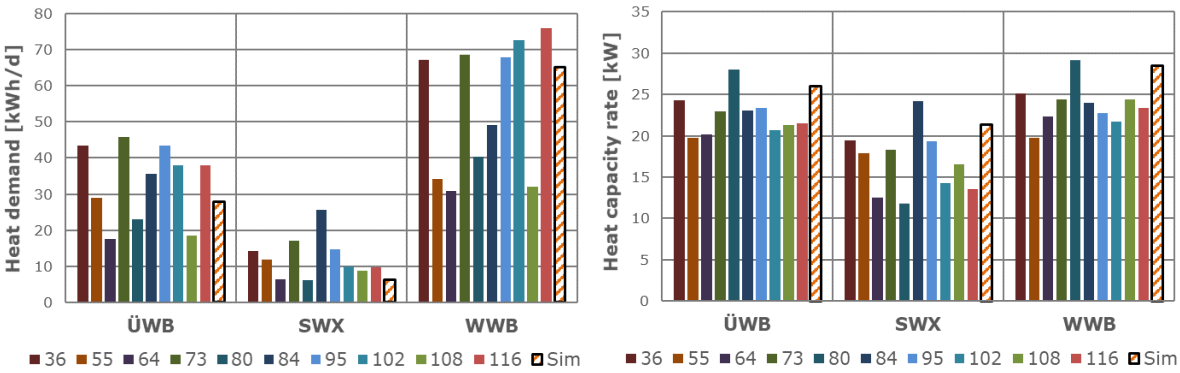


*Figure 5: Comparison between measured and simulated charging heat demand (left) and maximum charging heat capacity rate (right) for a day in transition period (ÜWB), summer (SWX) and winter (WWB)*

### 3.3.2.1 VERIFICATION OF CHARGING CONTROL

Metrics are evaluated to verify that the simulation model represents the charging control of house stations in the Windsbach DH network. The mean daily charging duration depends on both the charging control and the charging heat demand, as the charging duration is higher in case of higher heat demand given an equal heat capacity rate. As the simulated charging heat demand is comparable with the measurements (Figure 5), this metric is therefore appropriate to verify both that the house connection flow rate and return and supply temperatures match with the Windsbach network. The number of charging cycles per day depends on the settings for stopping the charging process as it increases if the charging stops earlier. Therefore, the number of charging cycles is a second important metric to evaluate.

As demonstrated in Figure 6, the charging duration tends to be higher for stations with higher heat demand meaning that the stations are charged with a comparable heat capacity rate. With a simulated charging duration per day in the range of measurements it is verified that the constant house connection flow rate of 425 l/h assumed in the simulation model is appropriate for approximating the house connection flow rate which can vary with values up to 500 l/h for a standard single-family house station depending on the valve position.

The buffer tank temperature criteria for starting and stopping the charging procedure can be set for each individual house station. For setting the respective values in the simulation model, the monitoring data is analysed to evaluate the criteria used in most of the ten well-working stations. The charging starts with a temperature below 51 °C at the buffer tank top (upper temperature sensor) and stops with a temperature above 50 °C at the buffer tank bottom (lower temperature sensor). Those values are appropriately set verified with a number of daily charging cycles in the range of measurements for the winter and transition day. The relatively low simulation value for the charging duration and number of daily charging cycles for the summer day can be explained by a heat demand in the lower range of measurements (Figure 5).

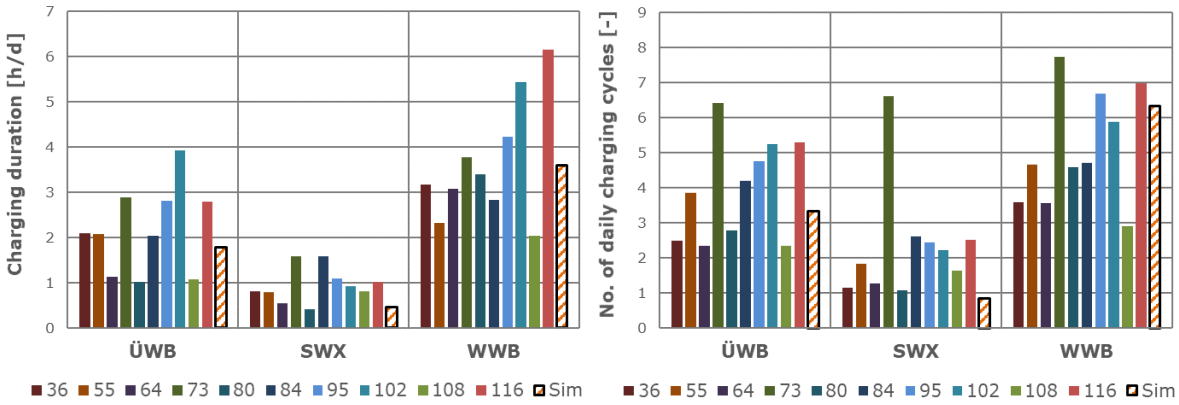


*Figure 6: Comparison between measured and simulated charging duration per day (left) and number of daily charging cycles (right) for days in the transition period (ÜWB), summer (SWX) and winter (WWB)*

By evaluating the average duration per charging cycle a metric more independent of the heat demand is regarded. It equals the quotient of the charging duration per day and the number of daily charging cycles. The simulated value is in the range of measurements (Figure 7) for all typical days. While the duration per charging cycle evaluated from measurements are considerably lower for summer days compared to winter days, in simulation it is less dependent on the season. The reason is that for simplicity the charging control parameters are constant in the simulation model for the entire year whereas in Windsbach network they are adapted to seasonal characteristics.

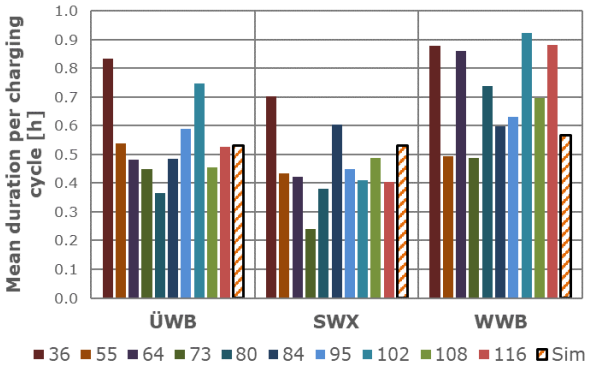


*Figure 7: Comparison between measured and simulated average duration per charging cycle for a day in transition period (ÜWB), summer (SWX) and winter (WWB)*

## 3.4 PARAMETER STUDY FOR HOUSE STATIONS

The verified simulation model is applied for a parameter study aiming to analyse the effects of a modified buffer tank volume and a modified house connection flow rate on the charging characteristics, thermal losses and the maximum heat capacity rate. The simulation study is conducted for a typical winter day (WWB) and the results are evaluated as average over a period of 20 simulated days after one initialisation day.

### 3.4.1 PARAMETER VARIATIONS

The main parameters included in the study are the buffer tank volume $V_{sto}$ and house connection flow rate $\dot{V}_{hc}$. Several other parameters are adapted respectively as described in this section.

The relative heights of the buffer tank inlet and outlet positions ($z_{hx,in}$ and $z_{hx,out}$; 0: tank bottom, 1: tank top) for the SH circuit heat exchanger ports, the heat exchanger area $A_{hx}$ and the heat exchanger water volume $V_{hx}$ vary for different buffer tank volumes. Correlations are calculated from Enerpipe catalogue data for buffer tanks with 250 l, 600 l and 1000 l. This results in the following correlations used for the simulation study with the buffer tank volume $V_{sto}$ in m³:

$$z_{hx,in} = 0.14 \bullet {V_{sto}}^2 + 0.31 \bullet V_{sto} + 0.28$$
$$z_{hx,out} = \max(-0.2 \bullet V_{sto} + 0.95, 0.83)$$
$$A_{hx} = -4.38 \bullet {V_{sto}}^2 + 10.01 \bullet V_{sto} + 1.07$$
$$V_{hx} = -15.95 \bullet {V_{sto}}^2 + 41.27 \bullet V_{sto} + 10.98$$

The stand-by volume $V_{sb}$ for house connection volume flows above 200 l/h is set to the stand-by volume of the reference configuration (250 l buffer), corresponding to 33 l. To show the potential of peak load reduction, parameter configurations with charging capacities less than the peak load demand are considered. The maximum stand-by volume is determined as a function of the lower limit for the heat exchanger outlet set to 0.4:

$$V_{sb,max} = (z_{hx,out} - 0.4) \bullet V_{sto}$$

The stand-by volume is linearly interpolated for $\dot{V}_{hc}$ between 50 l/h and 200 l/h. The height of the temperature sensor T9, which determines the start of a charging cycle, is calculated from:

$$z_{T9} = z_{hx,out} - \frac{V_{sb}}{V_{sto}}$$

### 3.4.2 BUFFER TANK TEMPERATURES

Figure 8 shows the temperatures for a 250 l buffer tank for two different house connection flow rates on a typical winter day (WWB). Stratification exists observed by a temperature increase with the buffer tank height. Buffer tank charging starts with a temperature at z = 0.77 below 51 °C and stops with a bottom temperature of 50 °C. Between 4 am and 4 pm, when the SH load is highest, the charging and discharging of the buffer tank is cyclic. The shape of the heat capacity rate during charging is rather uniform with a decreasing load at the end of each cycle resulting from higher return temperatures. In times with simultaneous charging and SH load (e.g. at 6 am in left figure), the return temperature is below the bottom storage temperature caused by a mixing of the buffer tank return and DHW preparation return flow. This corresponds to the periods with the highest house connection heat capacity rates.

The heat capacity rate during charging is reduced with a lowered house connection flow rate (right figure) causing a higher duration per charging cycle and slower increase of buffer tank temperatures. The number of charging cycles decreases with a lowered flow rate. The buffer tank temperature change is slower with a butter tank volume greater than 250 l (Figure 9). With a 1000 l buffer tank, a single charging cycle per day is sufficient to cover the sum of SH and DHW load.

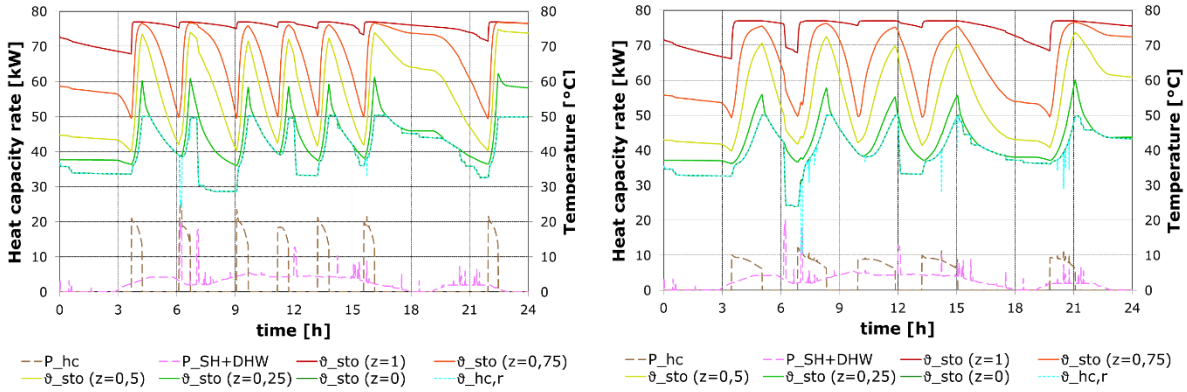


*Figure 8: Simulated buffer tank temperatures and heat capacity rate for a 250 l buffer tank with a house connection flow rate of 425 l/h (left) and 200 l/h (left) (P: heat capacity rate, sto: storage, hc: house connection, z: relative height of temperature sensor (0: bottom, 1: top))*

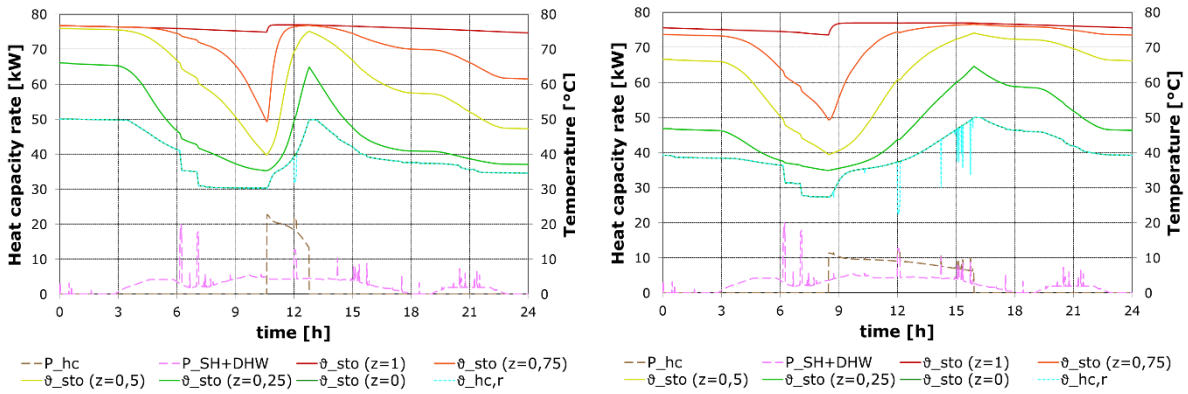


*Figure 9: Simulated buffer tank temperatures and heat capacity rate for a 1000 l buffer tank with a house connection flow rate of 425 l/h (left) and 200 l/h (left) (P: heat capacity rate, sto: storage, hc: house connection, z: relative height of temperature sensor (0: bottom, 1: top))*

### 3.4.3 HEAT CAPACITY RATE

Figure 10 shows the maximum house connection heat capacity rate which increases with the applied flow rate. The behaviour is almost linear for all buffer tank volumes. The heat capacity rate depends on the flow rate and flow temperature (which are constant during charging) and on the return temperature which varies according to the temperature level in the buffer tank and the mixture ratio between buffer tank outlet flow and DHW freshwater station return flow. It therefore depends on the magnitude of DHW load peaks during charging which can be different between variants. Thus, deviations from the linear increase are observed. The deviations from linear behaviour are significant especially in the range from 250 l/h to 500 l/h. There is no dependence between maximum heat capacity rate and buffer tank volume.

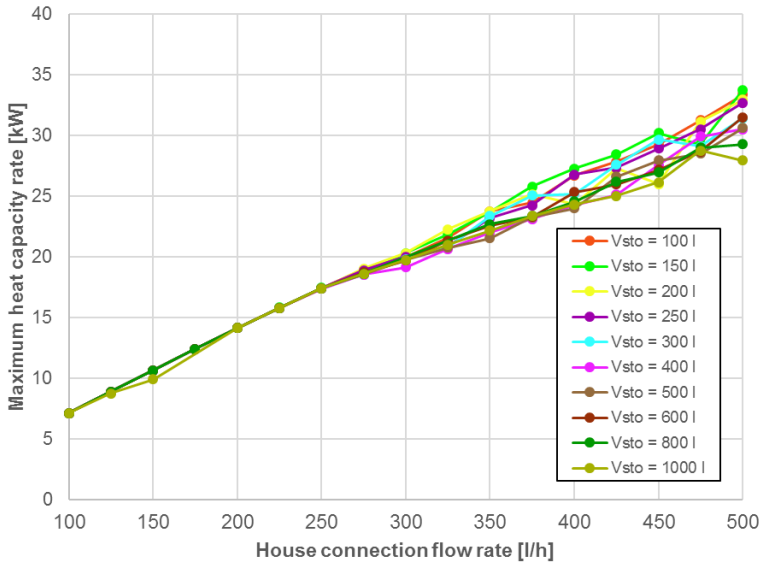


*Figure 10: Simulated maximum charging heat capacity rate for different buffer tank volumes and house connection flow rates*

### 3.4.4 BUFFER TANK CHARGING CHARACTERISTICS

The absolute charging duration reduces with increasing house connection flow rate caused by higher heat capacity rates (Figure 11). The charging duration tends to decrease with a higher buffer tank volume which becomes most clear comparing the 50 l buffer tank with other volumes. This is explained by a higher return temperature for small buffer tank volumes resulting in lower heat capacity rates. Figure 11 verifies the dependency described in section 3.4.2 of an increasing required no. of daily charging cycles with larger buffer tank volumes and with lower house connection flow rates. This can be explained by a higher total amount of energy transferred to the buffer tank during one charging cycle for larger buffer tank volumes.

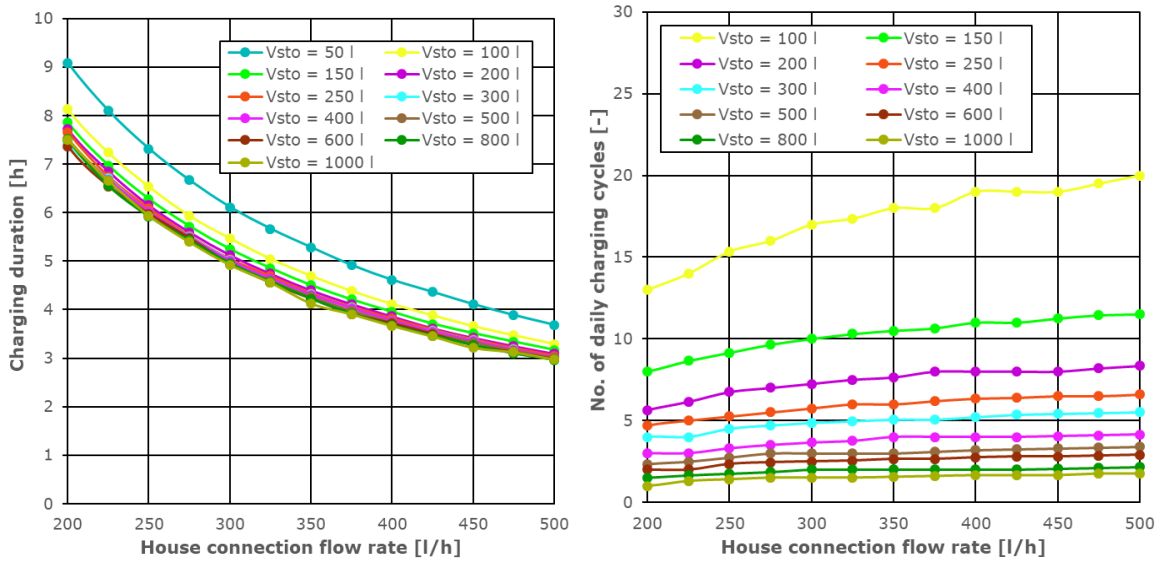


*Figure 11: Simulated charging duration per day (left) and number of daily charging cycles (right) for different buffer tank volumes and house connection flow rates*

Figure 12 shows a lower duration per charging cycle with higher house connection flow rates explained by an increasing heat capacity rate. With higher buffer tank volumes more thermal energy is transferred to the buffer tank during one charging cycle causing longer charging durations.

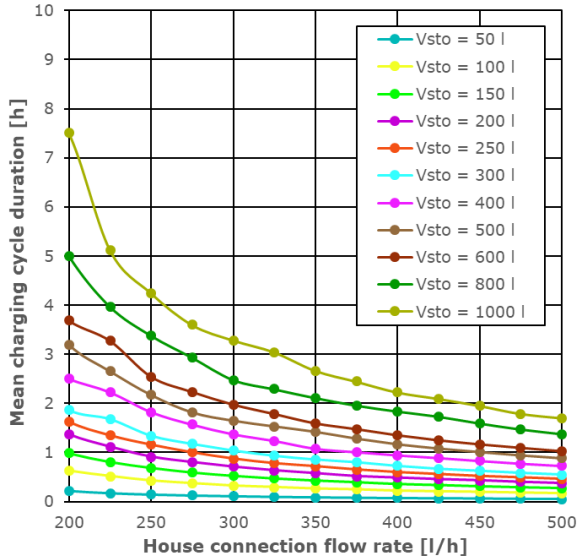


*Figure 12: Simulated average duration per charging cycle for different buffer tank volumes and house connection flow rates*

### 3.4.5 BUFFER TANK THERMAL LOSSES

Thermal losses increase with the buffer tank surface so that they are usually higher for buffer tanks with a larger volume, which is also the case for the simulation results as shown in Figure 13. The thermal losses slightly vary with the house connection flow rate resulting from differing buffer tank temperature levels.

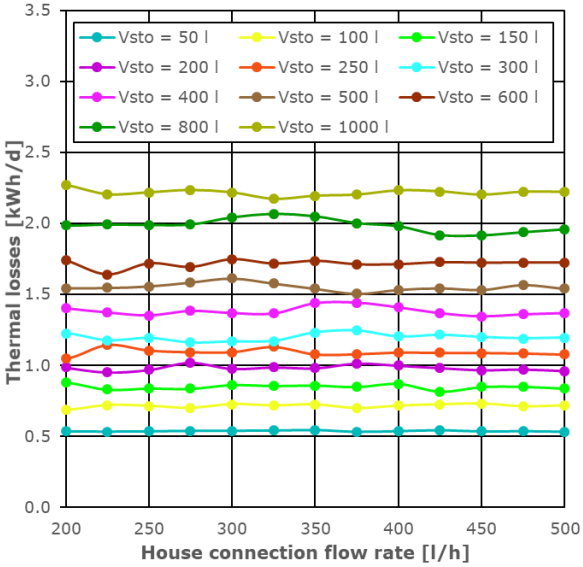


*Figure 13: Simulated buffer tank thermal losses for different buffer tank volumes and house connection flow rates*

### 3.4.6 SHORTAGE IN HEAT SUPPLY

The minimum theoretical house connection flow rate for covering the required amount of heat for a typical winter day corresponds to 60 l/h, which is sufficient for a supply without shortage if an 800 l or a 1000 l buffer tank is installed. With a buffer tank volume above 100 l, a flow rate of 100 l/h is always sufficient to supply the heat demand of a standard VDI 4655 typical winter day without shortage.

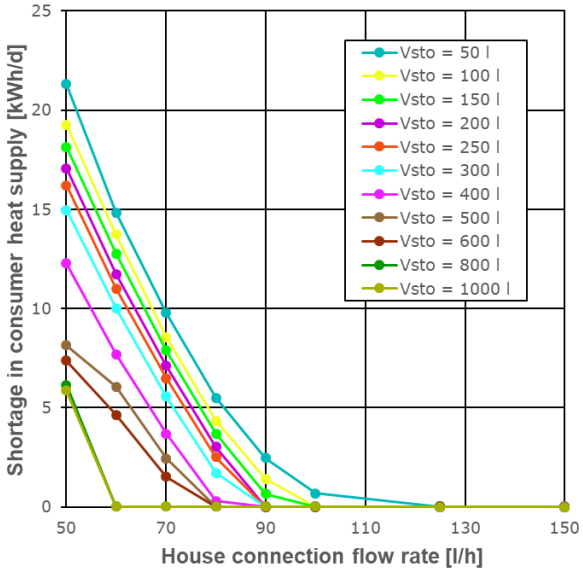


*Figure 14: Simulated shortage in consumer heat supply for different buffer tank volumes and house connection flow rates*

# 4 DH NETWORK WITH DECENTRALISED BUFFER TANKS

For the detailed simulations on DH network level one specific branch of the Windsbach DH network is selected and investigated in detail, see Figure 15. For the branch 17 consumers are foreseen, until end of 2021 ten consumer buildings were connected (consumer nos. 66, 67, 69, 70, 71, 73, 75, 79, 80, 81). To allow a comparison of simulation results with monitoring data only the ten connected consumers are considered in the simulations.

Relevant findings from the detailed simulations are used to investigate an up-scaled full-size DH network with the total heat load of the Windsbach DH network. Results for the full-size network can be seen in section 4.4.

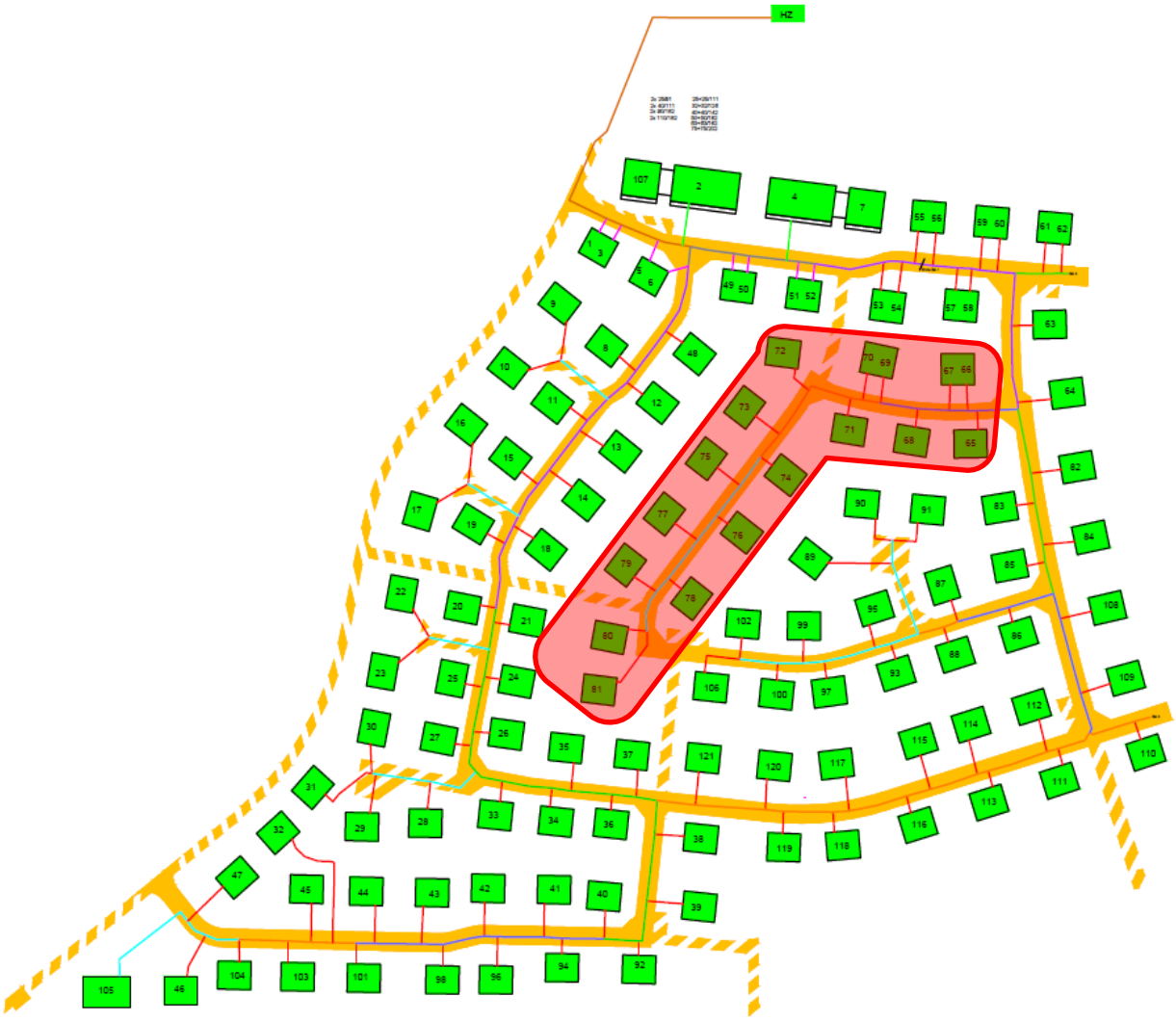


*Figure 15: District heating scheme of the Windsbach project (phases 1 and 2), branch for detailed simulations marked in red*

## 4.1 DH NETWORK BRANCH SIMULATION MODEL

The DH network branch simulation model reproduces an exemplary branch from the Windsbach DH network shown in Figure 15. Until end of 2021 ten single-family houses were connected to this branch. For each of these houses a house station model (see section 3) is used as a sub-module in the branch simulation model. The DH network branch simulation model is also created in the simulation software TRNSYS [TRNSYS, 2020]. For the DH pipes a component model (Type 952) from TESS libraries [TESS, 2018] is used. Pipe configuration parameters are taken from Windsbach design data provided by Enerpipe. Pipe diameters for the considered configurations of the parameter study (see 4.2) are determined iteratively. As initial values design diameters from Windsbach design are used. With the initial values maximum flow rates are determined for each pipe section. In a second step updated pipe diameters are re-calculated for each pipe section with the corresponding maximum flow rates and a design flow speed of 1.25 m/s.

Pipe heat loss coefficients are taken from Enerpipe catalogue data for CaldoPEX series for various diameters, pipe types (single or double) and insulation types (standard or improved insulation (PLUS series)). The analysed DH network branch is realised with double pipes with standard insulation for diameters up to DN 65, for larger pipes single pipes are installed. In the parameter study in addition other pipe types and insulation standards are considered.

### 4.1.1 INPUT DATA

#### *Domestic hot water draw-off profiles*

For multiple consumers the stochastic variation of DHW draw-offs from multiple houses and inhabitants has to be considered in the simulations. For this, 'DHWcalc for districts' [DHWcalc, 2021], a tool to generate DHW draw-off profiles for districts based on distribution functions and random number generators, is used to create yearly DHW draw-off profiles in one-minute time steps for the ten considered houses with parameters according to section 3.2 but with a stochastic draw-off variation. To account for different consumption behaviour and unequal numbers of persons in the houses the volume flow obtained by DHWcalc is multiplied with scaling-factors referencing the total heat demand for DHW of the considered buildings to the reference value from the underlying VDI 4655 profile.

As no separate measurement data on DHW heat demand is available, the DHW heat demand of the considered houses is determined from the difference of measured total heat demand on an average summer day and buffer tank thermal losses from simulations. DHW circulation is implemented in building 71 only. For the other buildings DHW circulation is switched off.

#### *Space heating demand*

The demand profile for space heating is obtained from the VDI profiles described in section 3.2. A stochastic variation between different houses is neglected. The demand profiles are scaled for the considered houses according to Windsbach monitoring data. Space heating demand of the considered houses is determined by subtracting the DHW demand and the buffer tank thermal losses from the measured total house heat demand on an average winter day (WWB). It is assumed that the DHW heat demand in winter is equal to the determined value for typical summer days.

Each day of the year is referenced to a typical day category in VDI 4655, depending on the outside temperature, cloudiness and weekday. To obtain a yearly profile, the daily space heating load profiles are lined up according to the typical day category of a given day using 2020 weather data for Nuremberg provided by DWD (Deutscher Wetterdienst).

### 4.1.2 VERIFICATION

For the verification of the DH network simulation model monitoring data from 54 typical single-family house stations with the Enerpipe CaldoTHERM station with 250 l buffer tank volume in the time period December 2020 to June 2021 is used. Maximum house supply capacity rate and simultaneity factor is calculated from the data as a function of the number of houses by the following procedure:

- For a given number of houses, a random subset of houses is selected from monitoring and simulation data
- For the selected houses the simultaneous total supply capacity rate is calculated in five-minute time steps, then the absolute maximum value in the evaluation period is determined for each house in the subset
- The simultaneity factor is calculated as the ratio of the determined absolute maximum value of the total supply capacity rate referred to the sum of the maximum supply capacity rates of the considered single houses
- The procedure is repeated 50 times and the average value of the 50 runs is calculated

Figure 16 shows the results of the calculations. Both the maximum supply capacity rates as well as the simultaneity factors according to measurements and simulations show good agreements. The simulation results slightly overestimate both the maximum supply capacity rates and the simultaneity factors but with only minor deviations.

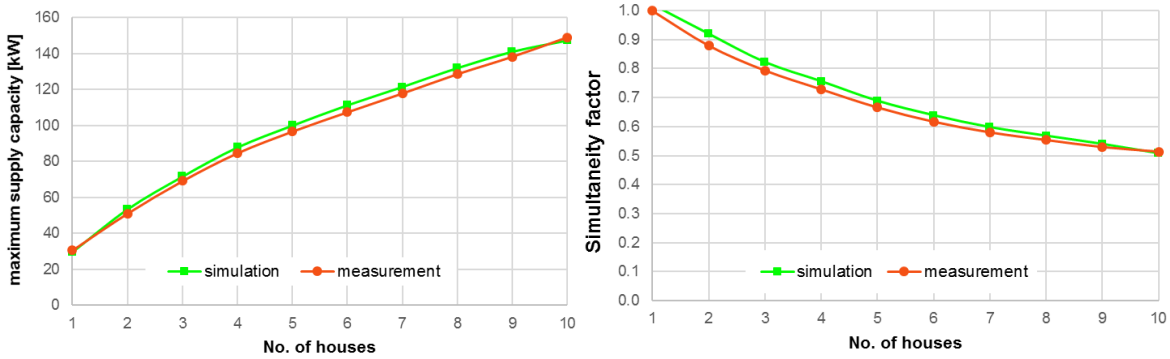


*Figure 16: Maximum supply capacity rate (left) and simultaneity factor (right) as a function of the no. of houses according to measurement data and simulation results*

In Figure 17 thermal losses of the DH network are illustrated according to simulation results and measurement data. Simulation results are only available for the exemplary branch shown in Figure 15. As these results only represent one part of the entire DH network the results from the branch simulations are up-scaled to be able to calculate corresponding results for the full-size network. For this length-related heat loss numbers are evaluated from the yearly simulation results separately for house connection pipes and for main pipes and also for different pipe diameters. For pipe diameters not available in the simulated branch correction factors are introduced to account for higher thermal losses for larger pipes. The correction factors are calculated from heat loss data for different pipe diameters

available in the Enerpipe product catalogue. The length-related heat loss numbers are used to calculate the heat loss of the entire Windsbach DH network as a sum of the single pipe sections. By applying the described methodology, the deviating usage of the DH pipes in the single configurations in terms of usage hours is considered in the DH network heat loss calculation.

When comparing the two full DH network data series in Figure 17 months with rather good agreement can be observed (e.g. April and May) as well as months with larger deviations. When looking at Figure 17 it has to be considered that the measured values of the Windsbach plant represent a rather non-uniform DH network operation, as e.g. a number of new houses were connected in the measurement period 2021. Newly connected houses show a very different heat load characteristic that is not induced by residential usage of the houses but by construction heating for several weeks and months before people move in. Additionally, the measurement data evaluations showed that a number of house stations did not work properly for certain periods what caused both higher heat loads and higher return temperatures compared to standard operation. At last monitoring data is missing for several stations for considerable time periods. As the measured thermal losses are calculated as difference of the heat supplied to the DH network and the sum of heat consumed by the houses, missing heat measurements are automatically added to the thermal losses. This causes an overestimation of thermal losses. In the simulations on the other hand no technical malfunctions occur, so simulation results reflect an optimal behaviour of the entire DH network.

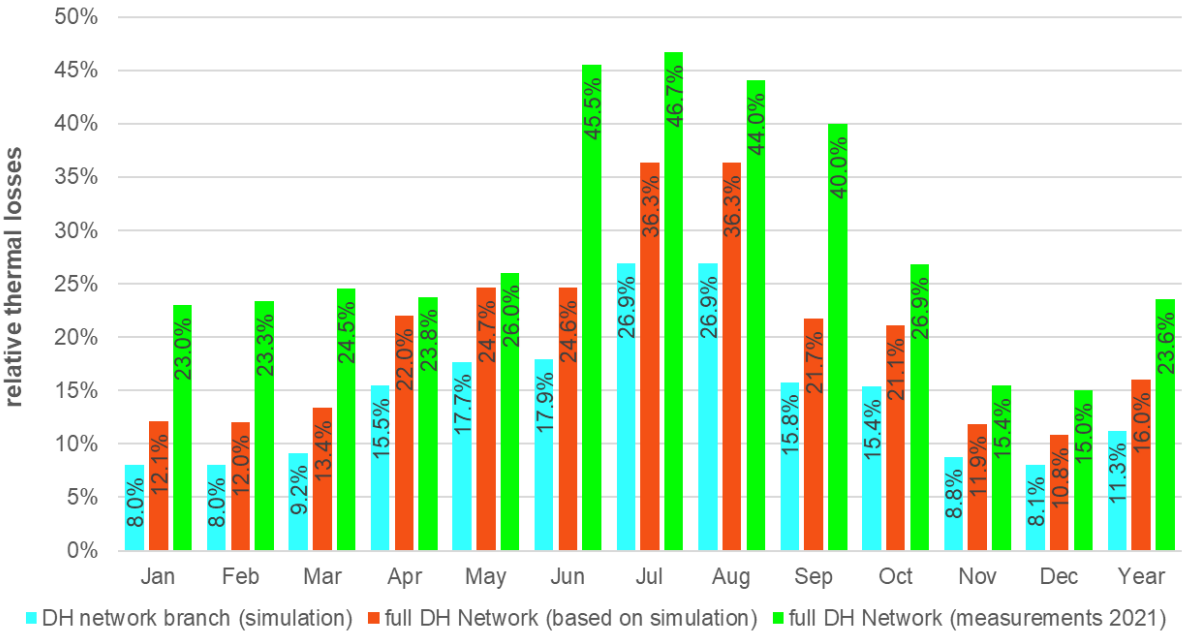


*Figure 17: Thermal losses of DH network branch pipes according to simulation results (250 l buffer tank and 500 l/h house connection flow rate) and measurements*

Figure 18 shows the branch supply and return temperatures resulting from the simulations. In Figure 19 the simulated supply and return temperatures are compared to measured values from the consumers connected to the branch as well as supply and return temperatures measured at the central heating plant for the entire DH network. The supply temperature development considered for the simulations corresponds well to the supply temperature of the DH network. Simulated return temperatures are lower than measured values, especially in summer. Measured return temperatures however show a rather large deviation between single consumer houses.

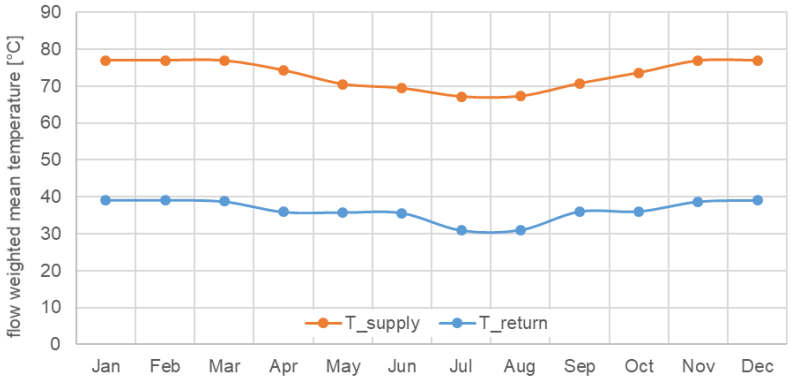


*Figure 18: Yearly development of supply and return temperatures in the DH network branch according to the simulations (250 l buffer tank and 500 l/h house connection flow rate)*

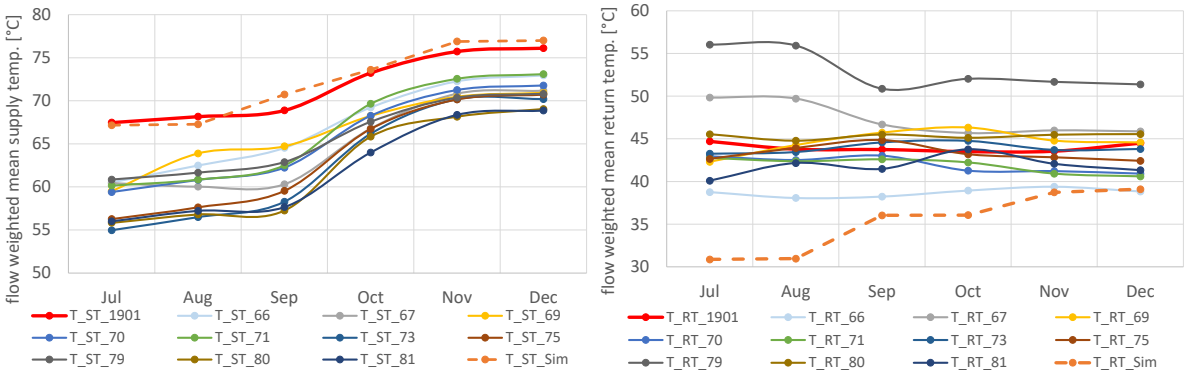


*Figure 19: Yearly development of supply (left) and return (right) temperatures in the DH network branch according to simulations (T_(RT)/(ST)_Sim), measurement data for houses connected to the branch (T__(RT)/(ST)_number) and central heating plant (T _(RT)/(ST)_1901)*

## 4.2 DH PIPE DIMENSIONING

With the verified simulation model a parameter study for the two parameters buffer tank volume and house connection flow rate is conducted. The parameters were varied as follows[1]:

- buffer tank volumes: 100 l – 250 l – 500 l – 1000 l
- house connection flow rates: 100 l/h – 200 l/h - 500 l/h
- pipe types: DP I0 - double pipe with standard insulation
  DP I+ - double pipe with improved insulation (PLUS series)
  SP I0 - single pipe with standard insulation
  SP I+ - single pipe with improved insulation (PLUS series)

In a first step a 3-week winter period (repeated WWB profile, see Figure 3) is simulated to determine the required maximum flow rates for each pipe section. This is done for all the possible parameter combinations of buffer tank volumes and house connection flow rates. With the evaluated maximum flow rates a re-dimensioning of the DH pipes is possible for each of the configurations. A design maximum flow speed in the pipes of 1.25 m/s is considered for the pipe dimensioning.

Figure 20 shows the pipe dimensions of the pipe sections in the considered branch as a function of the house connection flow rate for various buffer tank volumes. The orange line shows the corresponding pipe dimensions according to the design that was realised in Windsbach. The realised piping is somewhat larger compared to the simulation results as the design is done for 17 houses whereas in the simulations only the ten so far connected houses are considered. The four charts show very little dependency of the pipe dimensions from the buffer tank volume but a clear dependency of the house connection flow rate. If the design house connection flow rate for the houses is reduced from 500 l/h to 200 l/h or even 100 l/h the nominal diameters of the main pipe sections can be reduced by 1 or even 2 dimensions.

[1] In the Windsbach plant the new CaldoTHERM house stations with 250 l buffer tanks is installed; design house connection flow rate is 425 l/h; DP I0 pipes are installed for pipe dimensions up to DN 65, SP I0 for larger diameters.

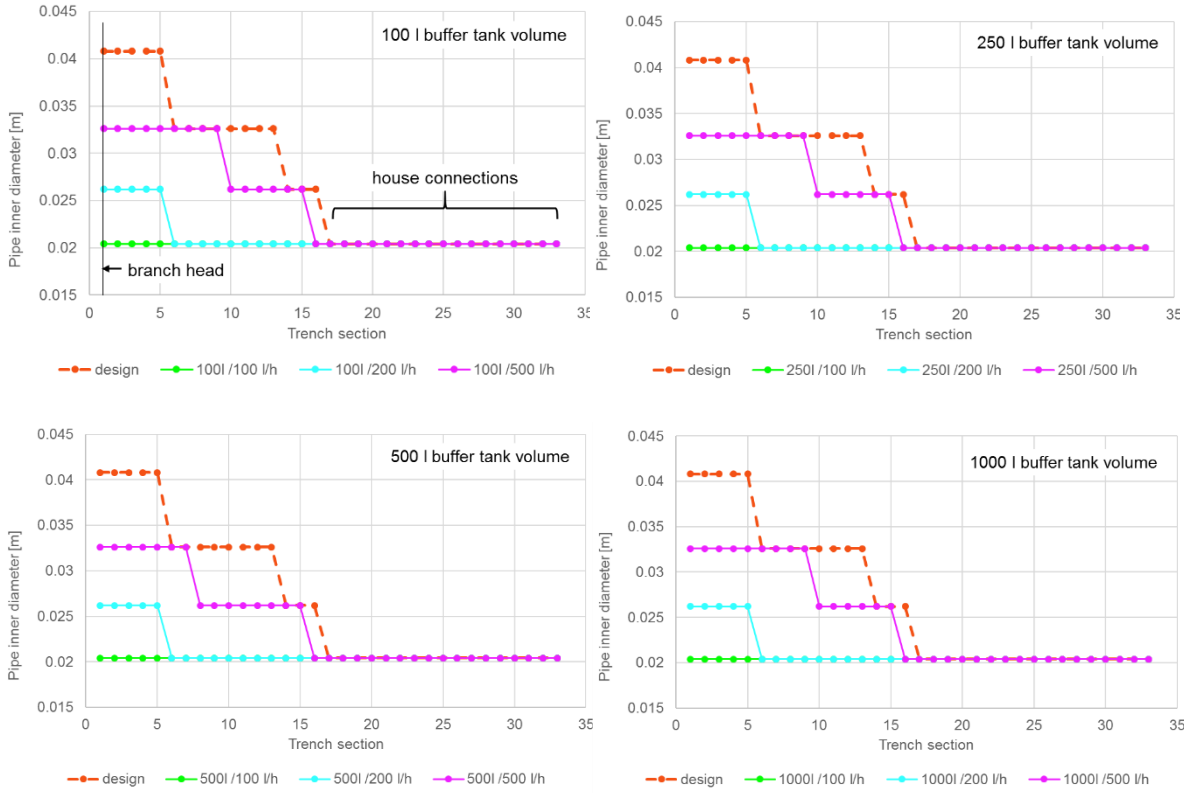


*Figure 20: Pipe dimensions as a function of the house connection flow rate for various buffer tank volumes (design: configuration realised in Windsbach)*

Even if the buffer tank volume is not a significant parameter for the pipe dimensioning the existence of buffer tanks in the houses is still a mandatory prerequisite for house connection flow rates below values necessary to cover peak loads from consumption directly.

## 4.3 SIMULTANEITY

Simultaneity factors are an important aspect for the design of DH network pipe dimensions as they are applied to determine the design heat loads for single DH network sections and the entire DH network. From the parameter study simulations described above simultaneity factors for DH networks with decentralised buffer tanks can be calculated, see Figure 21. No relevant correlation of the simultaneity factors with the buffer tank volume was identified, the given numbers are calculated as mean values for buffer tank volumes of 250 l and 500 l.

For comparison selected literature values are also shown in Figure 21. Simultaneity according to [Winter et.al., 2001] is valid for DH networks with existing single-family houses and traditional heat transfer substations for both DHW preparation and space heating. Simultaneity factors according to TUD [AGFW, 2004] and DIN 4708 [AGFW, 2004] are valid for DHW preparation only.

The simultaneity factors for DH networks with decentralised buffer tanks are partly calculated from the simulations and Windsbach monitoring data (solid lines) and partly extrapolated from the calculated values (dashed lines). For the extrapolations an approach according to [Winter et.al., 2001] is applied:

$$GLF(n) = a + \frac{b}{1 + \left(\frac{n}{c}\right)^{d}}$$

n: number of consumers

GLF: simultaneity factor

For the three considered house connection flow rates and the Windsbach monitoring data the following sets of coefficients were identified:

| | 100 l/h | 200 l/h | 500 l/h | Windsbach data (425 l/h) |
|---|---|---|---|---|
| a | -88.236710 | -0.343790 | 0.285503 | 0.2487 |
| b | 90.375886 | 3.981482 | 0.855871 | 0.9960 |
| c | $4.32555*10^{24}$ | 0.018732 | 4.757875 | 3.0117 |
| d | 0.076685 | 0.170180 | 1.042957 | 0.9917 |

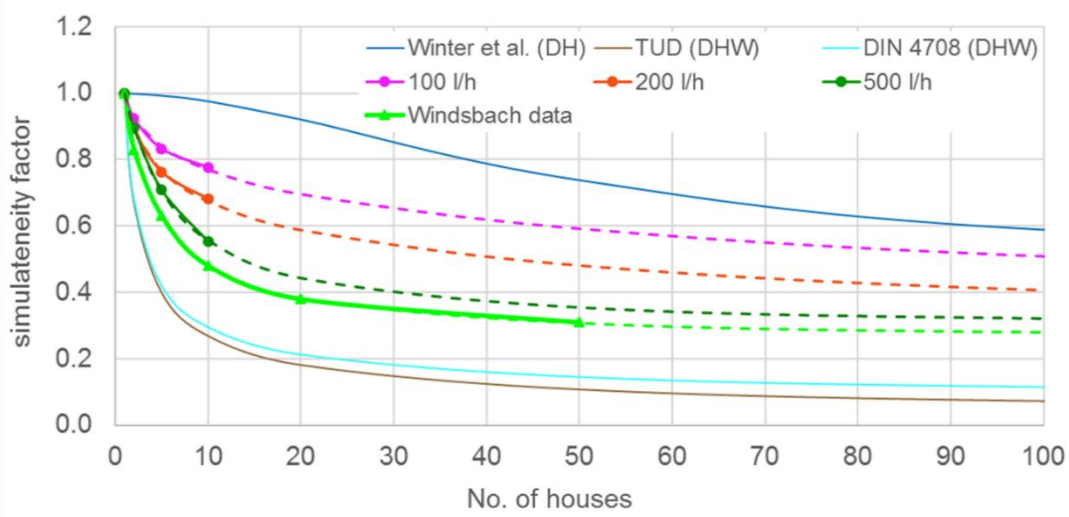


*Figure 21: Identified simultaneity factors for decentralised buffers and different house connection flow rates in comparison to selected literature values.*

## 4.4 RESULTS FOR WINDSBACH FULL SIZE DH NETWORK

With the findings from the detailed simulations for the exemplary branch further investigations on Windsbach DH network size are made. For this a full-size DH network with the total heat load of the Windsbach DH network (phases 1 and 2 with consideration of additional heat load from phase 3) is considered. In the real Windsbach plant the network design considers 116 single family houses and 3 multifamily houses in phases 1 and 2 as well as a 3rd future extension phase with additional 20 single family houses. For the up-scaling of simulation results to a full-size DH network it is assumed that all consumers are single-family houses with the characteristics described in section 3. A total equivalent number of single-family houses of 154 is assumed for this.

The design heat load for all pipe sections in the DH network is calculated for each of the considered design house connection flow rates based on the respective consumer nominal heat load according to Figure 10 and the simultaneity factors given in Figure 21. The design values given in Table 1 are determined for the three considered design house connection flow rates.

*Table 1: Design heat loads and simultaneity factors for the full-size DH network*

| Design house connection flow rate [l/h] | Resulting design heat load for DH network [kW] | Simultaneity factor for DH network [-] |
|---|---|---|
| 100 | 470 | 0.47 |
| 200 | 750 | 0.37 |
| 500 | 1450 | 0.31 |
| Windsbach design (425) | 1050 | - |

Annual heat losses for the buffer tanks are assumed equal to the average heat loss per buffer tank determined by the simulations for each parameter constellation. Annual heat losses from pipes per meter are assumed equal to the average heat loss determined by simulations for each parameter constellation with differentiation between house connection and main pipe, see also explanations in section 4.1.2.

### 4.4.1 DH NETWORK PIPE DIMENSIONING

The new findings on design house connection capacity rates (Figure 10) and simultaneity factors (Figure 21) are applied to re-design the Windsbach DH network for the considered design house connection flow rates and a design flow speed in the DH pipes of 1.25 m/s. Pipe data (diameters, heat loss coefficients etc.) is taken from Enerpipes CaldoPEX pipe series.

Figure 22 shows the distribution of the pipe dimensions for the re-designed DH network configurations in comparison to the Windsbach design. Smaller house connection flow rates mean smaller design heat loads and thus allow the installation of smaller pipe diameters in wider areas of the DH network. Note that the Windsbach DH network is designed based on Enerpipe experience while for the re-design a different method based on the new simultaneity factors is applied.

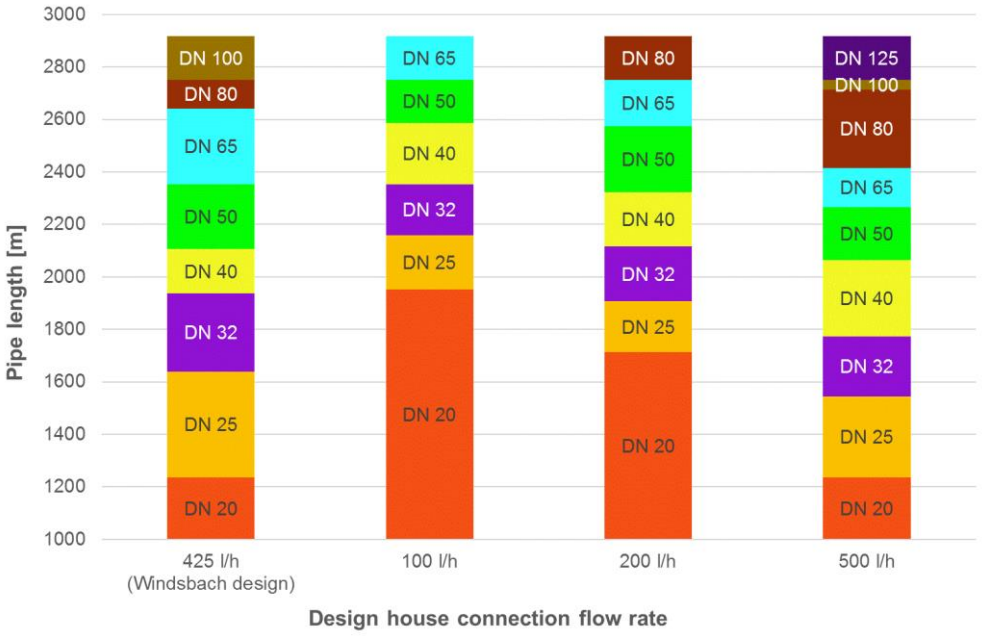


*Figure 22: Distribution of pipe dimensions for the Windsbach DH network for different house connection flow rates*

### 4.4.2 HEAT BALANCE AND THERMAL LOSSES

Figure 23 shows the DH network heat balances of the investigated configurations. For configurations with larger buffer tanks the total thermal losses of the buffer tanks increase. At the same time the total thermal losses of the DH network pipes decrease. The sum of the thermal losses varies between 9% and 14% of the total heat delivery to the DH network for the different configurations.

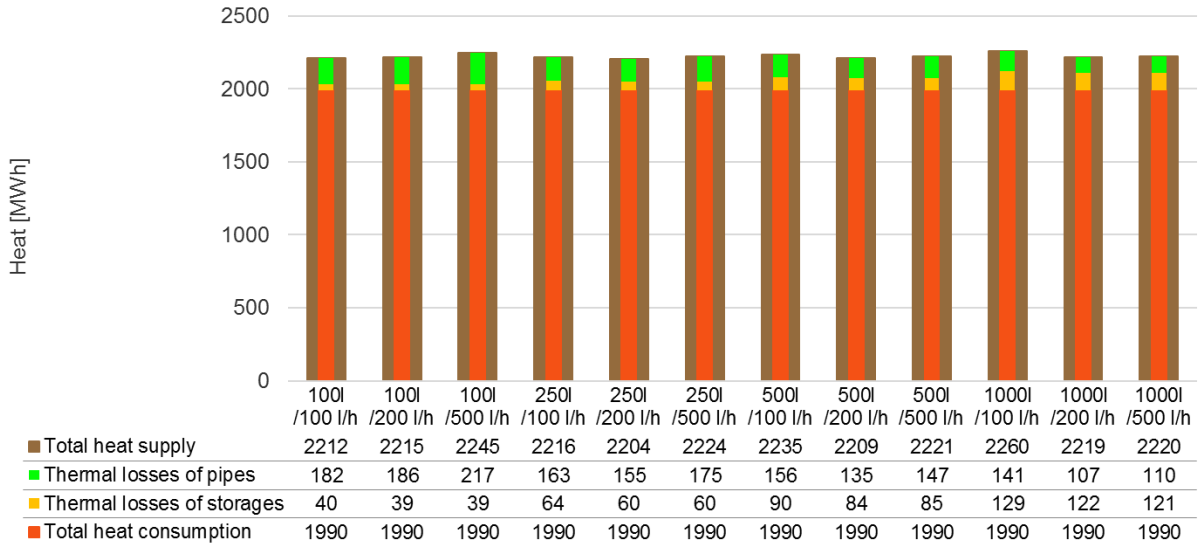


*Figure 23: Heat balances of the DH network in different configurations*

A more detailed consideration of thermal losses is shown in Figure 24, Figure 25 and Figure 26 for different types of pipes. The buffer tank thermal losses are independent from the house connection flow rate and the type of DH pipes and increase with increasing buffer tank volumes. DH pipe thermal losses depend on the pipe type and nameable decrease with increasing buffer tank volumes for house connection flow rates of 500 and 200 l/h,

but only slightly for 100 l/h. In total the thermal losses stay rather constant for buffer tank volumes above 250 l for house connection flow rates of 500 and 200 l/h. They however increase for a small house connection flow rate of 100 l/h. The reasons for the differences in the development of DH pipe thermal losses, that also strongly influences the total thermal losses, are caused by both different pipe diameters and different usage hours. Figure 27 shows that in general the usage of the DH pipe sections decreases with increasing house connection flow rates. This is illustrated in Figure 27 in terms of usage hours with flow rates > 0 l/h for the single pipe sections of the detailed branch simulation model. It can be seen that especially the house connection pipes are used less when using larger house connection flow rates as the total daily buffer tank charging duration decreases compared to smaller house connection flow rates, see also Figure 11. The lower usage hours for a flow rate of 500 l/h compared to 200 l/h is the reason for a similar development of pipe thermal losses even though the pipe diameters are larger for 500 l/h. For a house connection flow rate of 100 l/h the reduction in pipe usage from branch head to branch end is much fewer what results in a smaller reduction of pipe thermal losses.

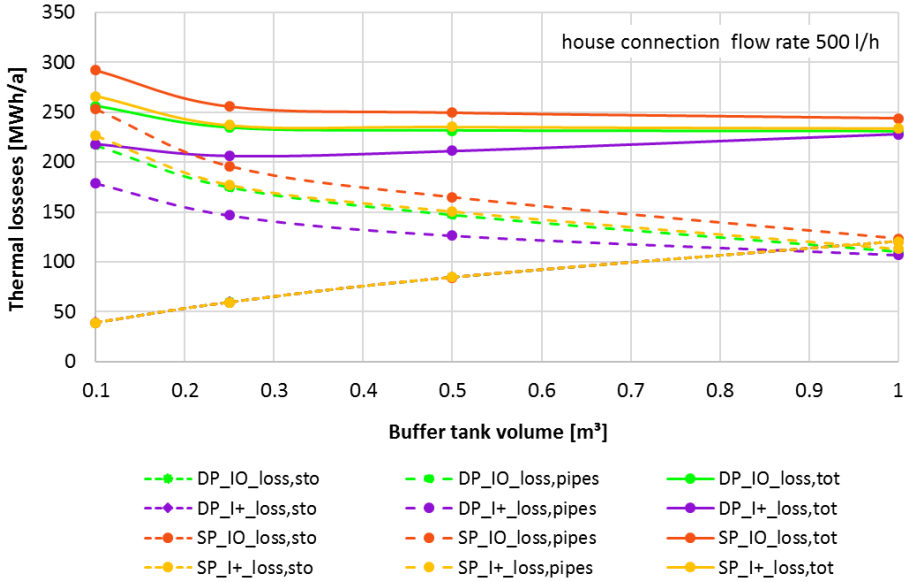


*Figure 24: Thermal losses as a function of buffer tank volume for different pipe types and a house connection flow rate of 500 l/h (DP: single pipe, DP: double pipe, I0: standard insulation, I+: improved insulation, sto: storage, tot: total)*

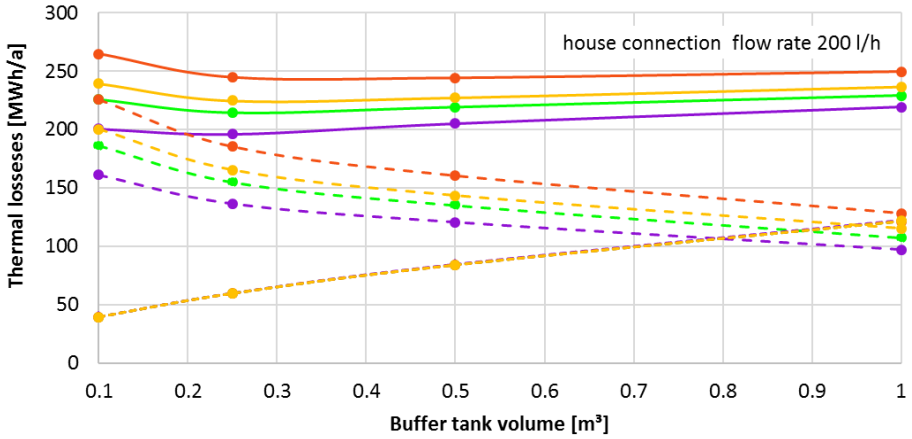


*Figure 25: Thermal losses as a function of buffer tank volume for different pipe types and a house connection flow rate of 200 l/h (legend see Figure 24)*

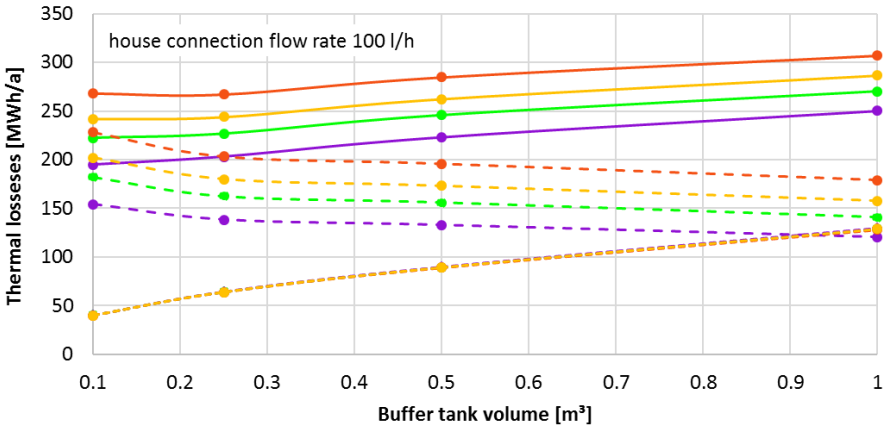


*Figure 26: Thermal losses as a function of buffer tank volume for different pipe types and a house connection flow rate of 100 l/h (legend see Figure 24)*

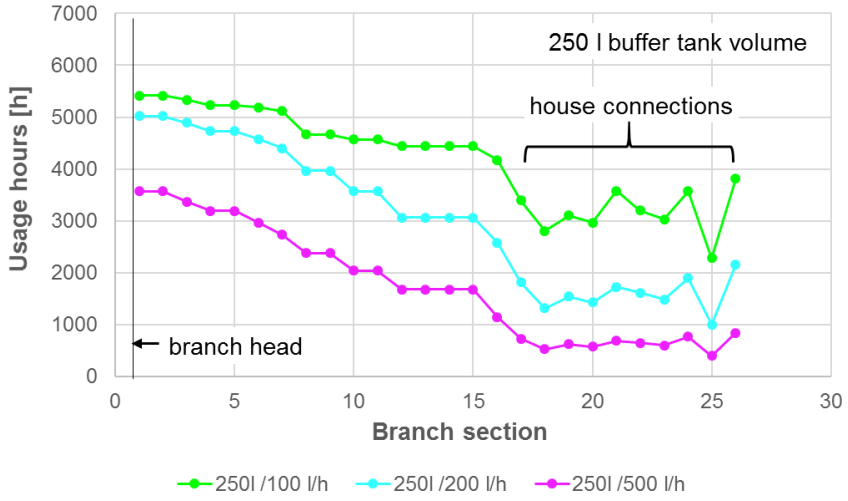


*Figure 27: Usage of pipe sections for different house connection flow rates according to branch simulations*

### 4.4.3 COST & ECONOMY

For the cost estimations investment cost for the DH network and the house stations are considered. Corresponding unit cost is provided by Enerpipe. For the DH network separate cost for materials (pipes, joints), installation and ground works are taken into account, separately for each nominal pipe diameter. Furthermore, unit prices for house stations with different buffer tank sizes and installation cost are considered.

For the economic calculation a period of 20 years is assumed with a service life of the DH piping of 40 years and an interest rate of 4%. Maintenance cost of 1% per year for the DH network piping and 2% per year for the house stations is applied. For the consideration of thermal losses, a mean heat price of 7 ct/kWh is assumed.

Figure 28 to Figure 31 show the results of the economic calculation for the investigated configurations and the four considered pipe types. For comparison, Figure 28 also includes a cost estimation of the latest Windsbach design. To be able to consider also the cost of thermal losses from DH pipes and buffer tanks yearly annuities are presented.

Total yearly annuities vary by 11% for the configurations with double pipes (Figure 28 and Figure 29) and 6% for the configurations with single pipes (Figure 30 and Figure 31). Single pipe configurations are between 11% and 17% more expensive than the corresponding double pipe configurations. According to Figure 28 a reduction of the house connection flow rate from 500 l/h to 200 l/h reduces the yearly cost between 5% and 7%, a reduction from 200 l/h to 100 l/h reduces the yearly cost by another 1.5% to 3.5%. For house connection flow rates of 200 l/h and 500 l/h, annuities for configurations with larger buffer tanks but the same house connection flow rate only slightly increase, as part of the extra cost for the larger buffer tanks can be compensated by reduced thermal losses.

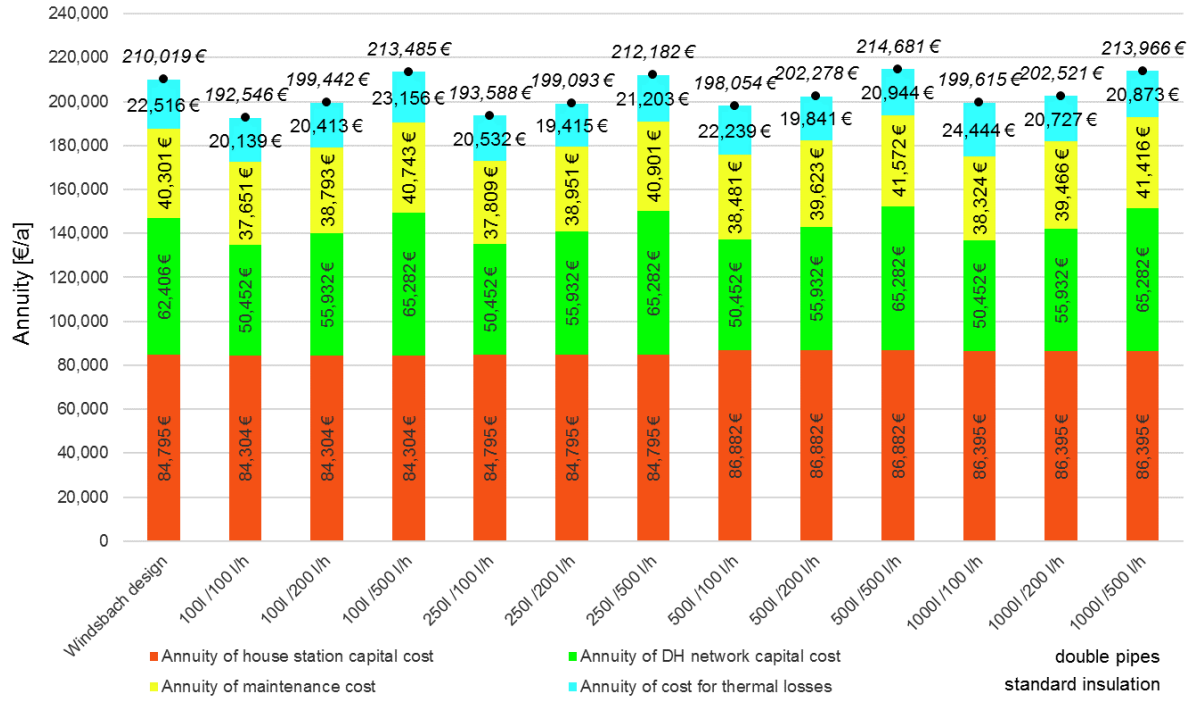


*Figure 28: Yearly cost for different configurations (double pipes with standard insulation)*

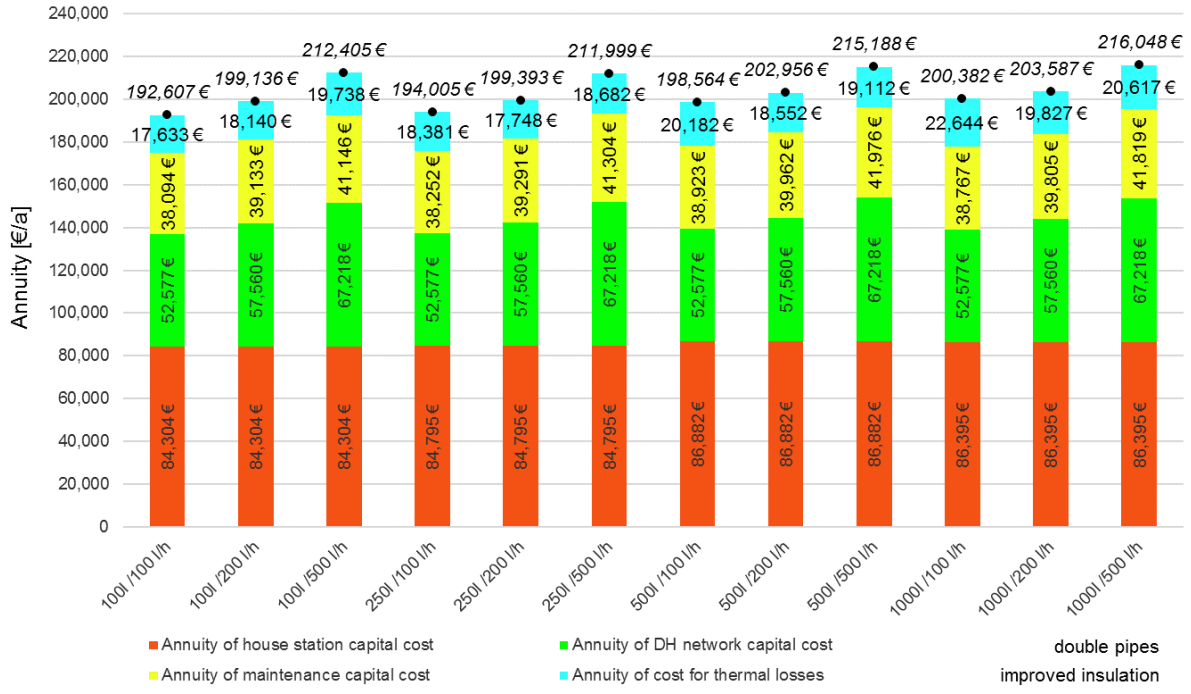


*Figure 29: Yearly cost for different configurations (double pipes with improved insulation)*

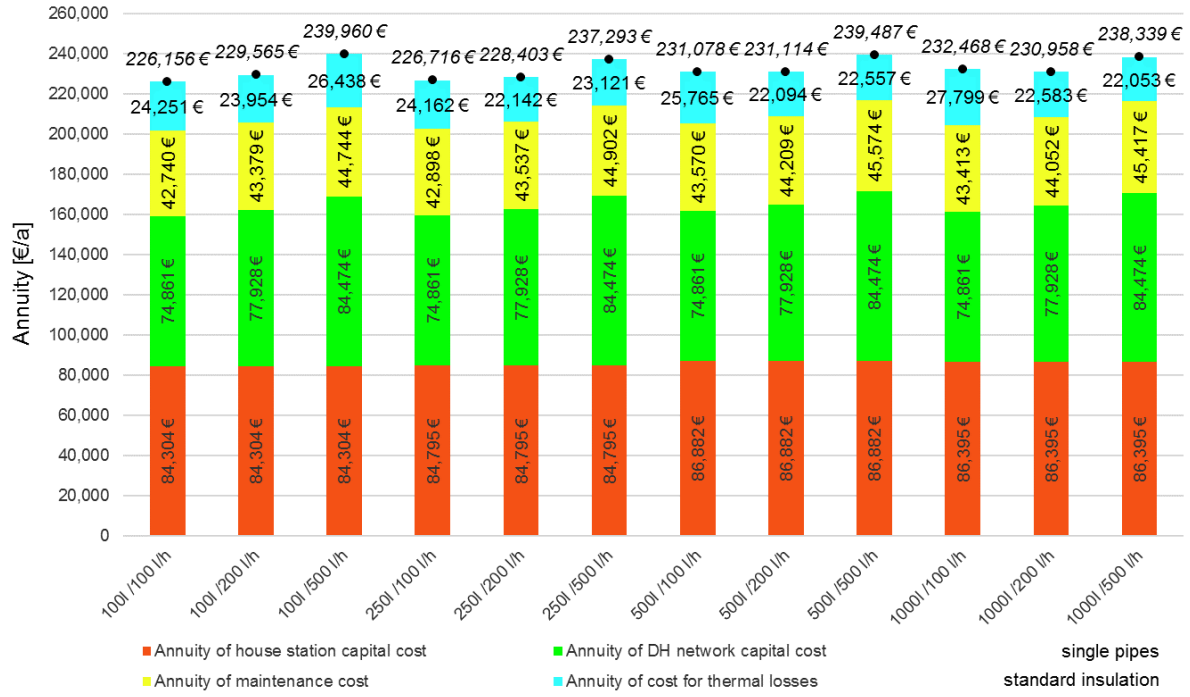


*Figure 30: Yearly cost for different configurations (single pipes with standard insulation)*

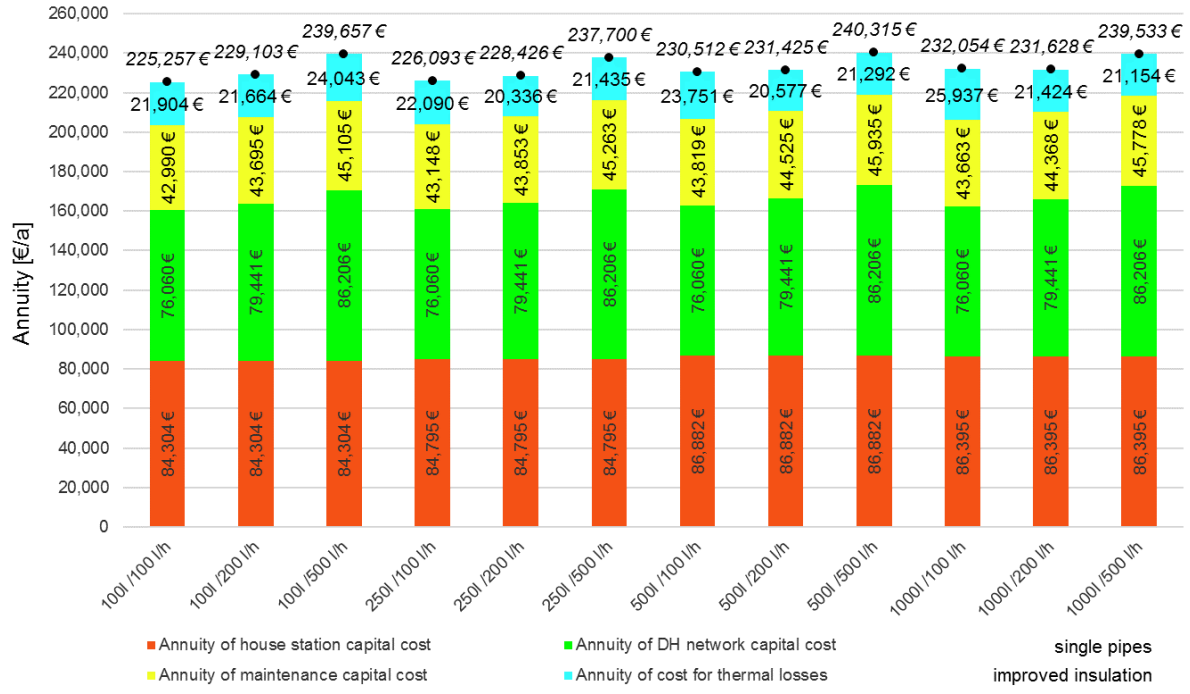


*Figure 31: Yearly cost for different configurations (single pipes with improved insulation)*

# 5 RISK CONSIDERATION

As demonstrated above, a reduction of the design house connection flow rate shows technical and economical optimisation potential for the overall system consisting of DH network and house stations with buffer tanks. On the other hand, a reduction of design values for the house connection flow rate also reduces the technical capability of the system to overcome exceptional larger heat demands of single or multiple consumers. Figure 32 and Figure 33 allow for an assessment of some kinds of extra loads compared to the assumed standard demand (see 3.2).

Figure 32 shows the theoretical possible load coverage duration for a continuous and constant 15 kW DHW heat load as a function of the house connection flow rate for different buffer tank volumes. 15 kW is the short term DHW peak load according to the standard profile presented in 1.2.2. In the calculations a parallel discharging of the buffer tank and heat supply from the DH network is taken into account. For the example of a 250 l buffer tank and a 200 l/h house connection flow rate a constant 15 kW heat load can be covered for approximately 1 hour. Figure 32 furthermore illustrates that for house connection flow rates somewhat above 250 l/h the 15 kW continuous heat load can be covered continuously without restrictions.

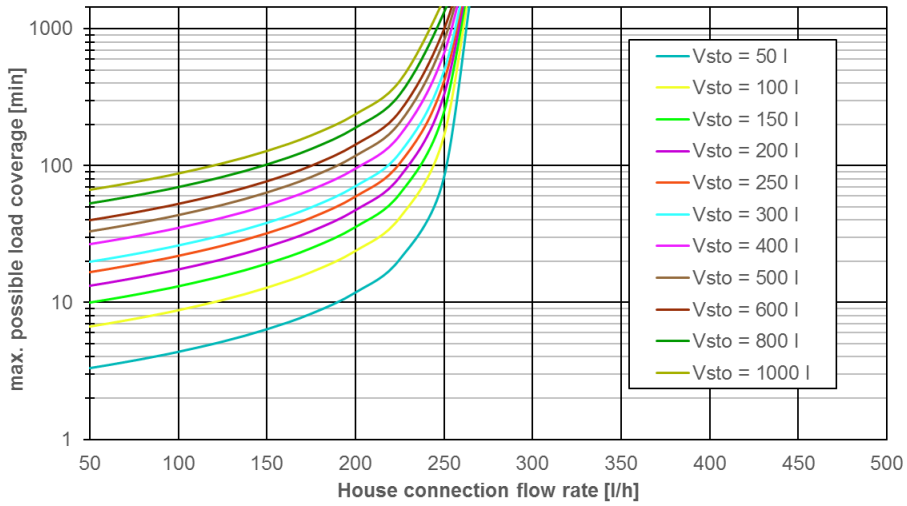


*Figure 32: Possible continuous 15 kW DHW load coverage as a function of house connection flow rate for different buffer tank sizes (Vsto: buffer tank volume)*

In Figure 33 the same considerations are presented for a constant and continuous DHW heat load of 30 kW. This represents the maximum heat capacity rate transferable by the actual CaldoTHERM house station. In this case the example configuration from above (250 l and 200 l/h) is only able to cover the load for 11 minutes. This period could e.g. be doubled by either increasing the flow rate to 350 l/h or by increasing the buffer tank volume to 400 l.

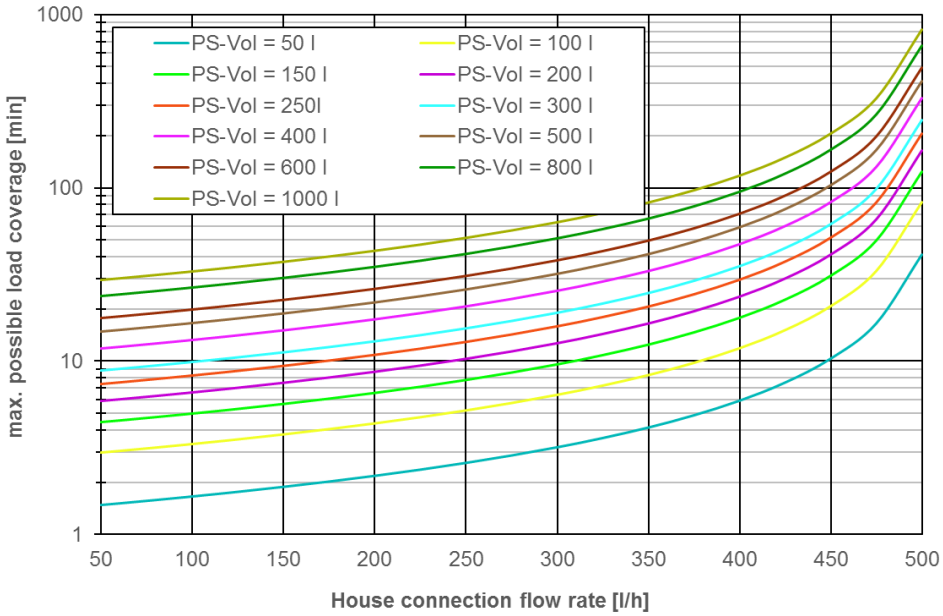


*Figure 33: possible continuous 30 kW DHW load coverage as a function of house connection flow rate for different buffer tank sizes (Vsto: buffer tank volume)*

# 6 CONCLUSIONS

DH network house stations with buffer tanks offer the technical potential for a reduction of house connection capacity rates as peak load from consumption can be covered from the buffer tanks and do not directly affect the DH network. If all or most of the consumers connected to a DH network are equipped with decentralised buffer tanks this can be considered in the design of the DH piping network. Because of reduced peak heat demand from consumers also the design heat load for the DH network can be reduced. Two main effects can be distinguished in this respect. **At first, the design house connection capacity rate of the single consumer buildings can be lower compared to standard substations without buffer tanks, if not designed for covering peak loads from consumption. Secondly, also the consumption profile of a house station with decentralised buffer tanks changes compared to standard substations. This has an influence also on the simultaneity behaviour of multiple consumers.**

Investigations conducted here are based on the Windsbach demonstrator with almost exclusively new single-family houses. For this application case, detailed simulation models were created for house stations with buffer tanks and for one selected DH network branch with, at the time of consideration, ten connected single-family houses. Investigations show **a reduction potential of design house connection capacity rates for new standard single-family houses from today's 30 kW down to theoretically 7.5 kW**.

**New simultaneity factors** could be derived for DH networks with single family houses and house stations equipped with buffer tanks and for different design house connection capacity rates or house connection flow rates, respectively. The new simultaneity factors allow DH network pipe designs taking into account the decentral buffer tank approach and reduced house connection capacity rates compared to standard designs.

Larger buffer tank volumes in house stations enable lower house connection capacity rates, smaller DH network pipe dimensions and reduced DH network thermal losses. At the same time, on the other hand, the reduction of DH network thermal losses is compensated to a nameable extend by increased thermal losses of the larger buffer tanks in the houses. In total, **a variation of 26% of yearly heat demand necessary to cover total thermal losses was found for the investigated configurations with double pipes in standard insulation**.

A similar development as for the thermal losses can be observed for the investment cost. Smaller DH pipe dimensions enable cost savings for the DH network, but larger buffer tank volumes generate higher cost in the house stations. Besides, yearly total cost figures are influenced by the varying thermal losses for different configurations. In sum the **variation in total yearly cost for the investigated configurations with double pipes in standard insulation was calculated to 11%.**

As demonstrated, **a reduction of design house connection capacity rates offers technical and economical optimisation potential**. On the other hand, it goes along with an increased risk of reduced comfort for the consumers or temporal shortages in heat supply, if heat demands differ too much from design conditions. Presented analysis allow an assessment of these effects based on maximum load coverage periods for two excess demand scenarios and different technical configurations.

# 7 REFERENCES

[AGFW, 2004] FW 520 Part 2, Information sheet on basic design of apartment stations for heating water networks, AGFW, Frankfurt, Germany

[DHWcalc, 2020] Braas, H., Jordan, U., Best, I., Orozaliev, J. Vajen, K., District heating load profiles for domestic hot water preparation with realistic simultaneity using DHWcalc and TRNSYS, https://doi.org/10.1016/j.energy.2020.117552, Energy 201 (2020), Elsevier Ltd.

[TESS, 2018] TESSLibs 17 – Component Libraries for the TRNSYS Simulation Environment, TESS – Thermal Energy Systems Specialists, Madison, USA

[TRNSYS, 2020] TRNSYS - A TRaNsient SYstems Simulation Programme, Version 18, Solar Energy Laboratory, University of Wisconsin, Madison, USA und Transsolar, Stuttgart, 2021

[VDI 4655, 2021] VDI 4655:2021-07. Reference load profiles of residential buildings for power, heat and domestic hot water as well as reference generation profiles for photovoltaic plants, VDI – The Association of German Engineers and Beuth Publisher, Düsseldorf and Berlin, Germany

[Winter et.at., 2001]Winter, W., Haslauer, T., Obernberger, I. (2001). Untersuchung der Gleichzeitigkeit in kleinen und mittleren Nahwärmenetzen. Part I in Euroheat & Power Volume 09/2001, p. 53-57, Part II in Euroheat & Power Volume 10/2001, p. 42-47

Grant Agreement: 768936

# D5.3: ANNEX 5
# EVALUATION OF THE PRIMARY ENERGY FACTORS FOR THE OPTIMIZED CHP OPERATION AT THE ENERPIPE DEMO

This project has received funding from the European Union's Horizon 2020 research and innovation programme under grant agreement No 768936.

# TABLE OF CONTENTS

# 1 INTRODUCTION

In this report, the impact of a given optimized hourly operating mode for a biogas CHP plant in the ENERPIPE demo on the fossil primary energy it displaces in the electricity grid is investigated. The operating mode was developed within the TEMPO project, based on forecast of heat demand and day-ahead electricity prices. The period between 15.10.2021 9:00 and 28.02.2022 23:00 was considered[1].

[1] Due to missing data the periods between 19.11.2021 00:00 to 24.11.2021 23:00 and between 27.12.2021 00:00 and 03.01.2022 23:00 had to be removed from the evaluation

# 2 ASSUMPTIONS

A constant electrical efficiency $\eta_{el}$ of 34% and a constant thermal efficiency $\eta_{th}$ of 53% were assumed for this evaluation. The optimized operation mode is compared to a non-optimized operation mode, which corresponds to the current heat demand. Whereby this was adjusted accordingly in percent to have the same energy consumption for both operating modes in the entire period to ensure comparability. The thermal output is converted into electrical output and the knowledge of the current energy mix in the German power grid is used to determine how much fossil primary energy would be required to provide the respective amount of electricity produced by the power plant.

# 3 ELECTRIITY SUPPLY DATA PREPARATION

The operating mode for the hourly operation of the biogas CHP plant was supplied by VITO based on simulation data. The optimized thermal output $Q_{in,1,o}$ is constant at 530 kW, or it is turned off. From this, the electrical output $P_{el,1,o}$ was determined using the efficiencies.

$$P_{el,1,o} = Q_{in,1,o} \cdot \frac{\eta_{el}}{\eta_{th}} \quad (1)$$

For the non-optimized operation, it was assumed that the operating mode of the power plant is following the current heat demand $Q_{in,2,no}$. However, since the sums of the respective energy supplied in the period are different between optimized and non-optimized operation, the non-optimized operation was adjusted by a factor f. This factor is composed of the two sums over the period of the energy quantities. The electrical power $P_{el,2,no}$ was determined in the same way as in formula (1).

$$f = \frac{\sum Q_{in,1,o}}{\sum Q_{in,2,no}} \quad (2)$$

# 4 ENTSO-E DATA PREPARATION

ENTSO-E, the association of European transmission system operators, provides hourly data for the electricity mix in Europe. For this purpose, the data for the electricity mix in Germany was used, as well as that of the respective neighboring countries, to take electricity imports and exports into account. The neighboring countries include the Netherlands, Luxembourg (no data available), the Czech Republic, Austria, Denmark, Norway, Sweden, Belgium, Poland, France, and Switzerland. Table 1 shows the components of the electricity mix. [1]

*Table 1: Electricity mix [1]*

| Components of the electricity mix |
|---|
| Biomass - Actual Aggregated [MW] |
| Fossil Brown coal/Lignite - Actual Aggregated [MW] |
| Fossil Coal-derived gas - Actual Aggregated [MW] |
| Fossil Gas - Actual Aggregated [MW] |
| Fossil Hard coal - Actual Aggregated [MW] |
| Fossil Oil - Actual Aggregated [MW] |
| Fossil Oil shale - Actual Aggregated [MW] |
| Fossil Peat - Actual Aggregated [MW] |
| Geothermal - Actual Aggregated [MW] |
| Hydro Pumped Storage - Actual Aggregated [MW] |
| Hydro Pumped Storage - Actual Consumption [MW] |
| Hydro Run-of-river and poundage - Actual Aggregated [MW] |
| Hydro Water Reservoir - Actual Aggregated [MW] |
| Marine - Actual Aggregated [MW] |
| Nuclear - Actual Aggregated [MW] |
| Other - Actual Aggregated [MW] |
| Other renewable - Actual Aggregated [MW] |
| Solar - Actual Aggregated [MW] |
| Waste - Actual Aggregated [MW] |
| Wind Offshore - Actual Aggregated [MW] |
| Wind Onshore - Actual Aggregated [MW] |

## 4.1 HYDRO PUMPED STORAGE

"Hydro Pumped Storage - Actual Aggregated" is the electricity used in the respective country from pumped storage power plants. To distribute this among the individual energy sources, the percentage share of the energy sources in the total period was used. In this way, the electricity was distributed accordingly at each hour.

"Hydro Pumped Storage - Actual Consumption" is the electricity injected into pumped storage power plants in the respective country. In this report, this electricity is considered as electricity export. It is therefore no longer included in the electricity mix of neighboring countries. The electricity stored in Germany's pumped storage power plants is subtracted from the respective energy sources according to the percentage distribution of the energy sources in the period under consideration.

## 4.2 DOMESTIC ELECTRICITY GENERATION

For Germany's neighboring countries, the percentage domestic electricity generation is now determined, whereby here the electricity from the pumped storage power plants has already been distributed among the other energy sources. Thus, the electricity mix of the countries can be determined for each hour.

## 4.3 CROSS BORDER

ENTSO-e provides the respective electricity import and export data of the countries. According to the respective hourly electricity mix in Germany, the electricity export is divided among the individual energy carriers and subtracted from the existing values. Electricity imports to Germany from neighboring countries are allocated to the energy sources in Germany according to the electricity mix in the respective country.

## 4.4 PRIMARY ENERGY FACTORS

In this report, the primary energy factors according to DIN V 18599-1: 2011-12 were used. [2]

*Table 1: Primary energy factors according DIN V 18599-1*

| Energy Carrier | Fossil Primary Energy Factor |
|---|---|
| Fossil Brown coal/Lignite - Actual Aggregated [MW] | 1.2 |
| Fossil Coal-derived gas - Actual Aggregated [MW] | 1.2 |
| Fossil Gas - Actual Aggregated [MW] | 1.1 |
| Fossil Hard coal - Actual Aggregated [MW] | 1.1 |
| Fossil Oil - Actual Aggregated [MW] | 1.1 |
| Fossil Oil shale - Actual Aggregated [MW] | not used |
| Fossil Peat - Actual Aggregated [MW] | not used |

| | |
|---|---|
| Nuclear - Actual Aggregated [MW] | 1.1 |
| Other - Actual Aggregated [MW] | 1.1 |
| Biomass - Actual Aggregated [MW] | 0.2 |
| Waste - Actual Aggregated [MW] | 0.1 [2] |

## 4.5 EFFICIENCIES

In Table 3 the used efficiencies of the fossil fuel power plants are displayed. As biomass has a small fossil share, it is also displayed on the list.

*Table 2: Efficiencies per energy carrier*

| Energy Carrier | Efficiency |
|---|---|
| Fossil Brown coal/Lignite - Actual Aggregated [MW] | 0.389 [3] |
| Fossil Coal-derived gas - Actual Aggregated [MW] | 0.467 [3] |
| Fossil Gas - Actual Aggregated [MW] | 0.467 [3] |
| Fossil Hard coal - Actual Aggregated [MW] | 0.35 [3] |
| Fossil Oil - Actual Aggregated [MW] | 0.4 [4] |
| Fossil Oil shale - Actual Aggregated [MW] | Not used |
| Fossil Peat - Actual Aggregated [MW] | Not used |
| Nuclear - Actual Aggregated [MW] | 0.37 [5] |
| Other - Actual Aggregated [MW] | 0.4* |
| Biomass - Actual Aggregated [MW] | 0.4 [6] |
| Waste - Actual Aggregated [MW] | 0.25 [7] |

*…. Average of the available efficiencies

# 5 RESULTS

With the help of the primary energy factors PEF from table 2 and the efficiencies η from table 3, the primary energy could be determined with the hourly electricity generation. The hourly electricity generation comes from the domestic production, the import and the export, provided by ENTSO-e. [1]

$$Primary\ Energy = Electricity\ Generation \cdot \frac{PEF}{\eta} \tag{3}$$

With the known percentage distribution of the electricity mix in Germany, the required primary energy can now be determined. For the respective hour, the fossil primary energy is now calculated which would have to be provided by the grid in order to generate the electrical output $P_{el,1,o}$ or $P_{el,2,no}$ provided by the power plant.

Figure 1 shows the comparison between the cumulated displaced fossil primary energy by the optimized and the not optimized operating mode. Even though differences can be seen over the course of the period, the overall difference in the end is neglectable at <1%.

At the beginning of the project, it was assumed that more fossil primary energy would be displaced from the grid with the help of the optimized operating mode. Since the power plant would be in operation especially at times of expensive electricity and thus high fossil content.

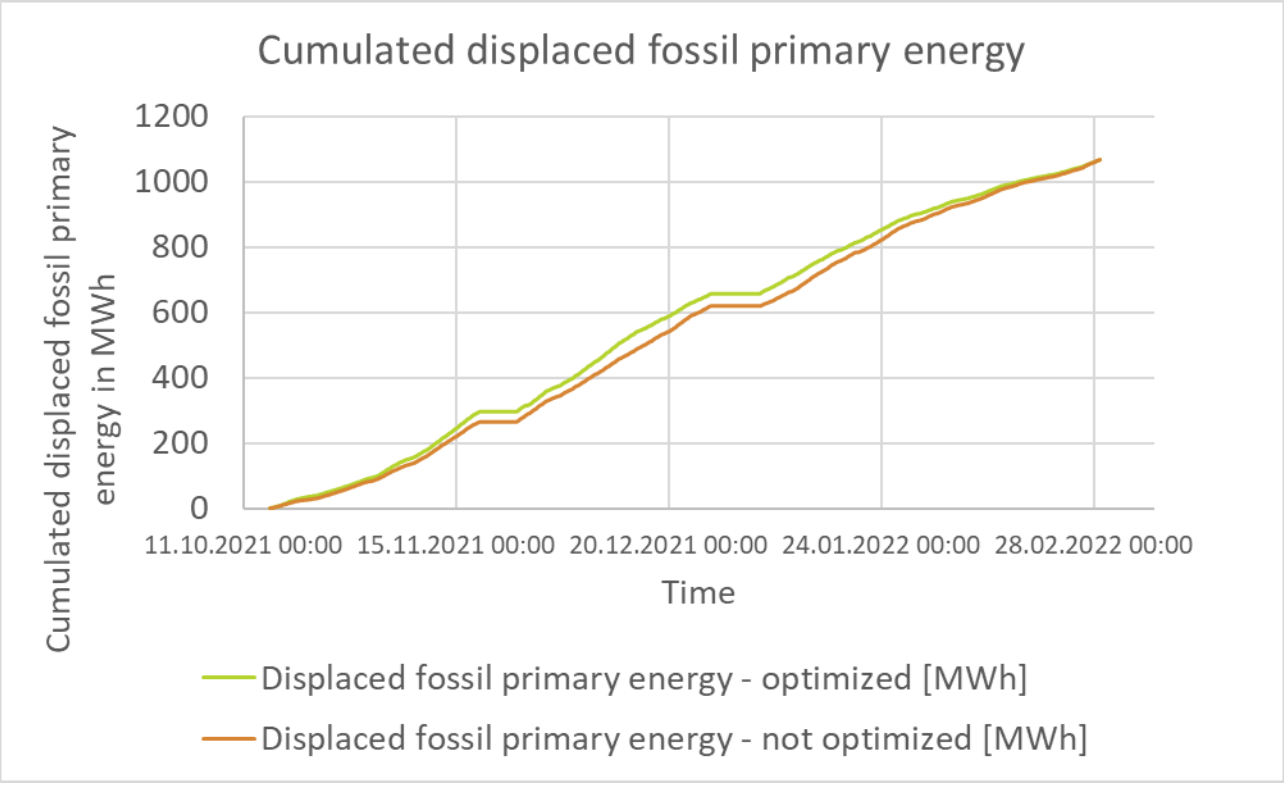


*Figure 1: Total Primary Energy in Period*

Figure 2 shows the displaced fossil primary energy at different day ahead prices for electricity. The majority of the optimized values (green) is above the not optimized values (red), which could lead to the conclusion, that, when in operation, more fossil primary energy is displaced in the optimized mode.

However, there are many occasions, where the CHP is turned off in the optimized mode, so no fossil primary energy is displaced. This is an advantage for the non-optimized mode, sine it is running more often and this is displacing fossil primary energy.

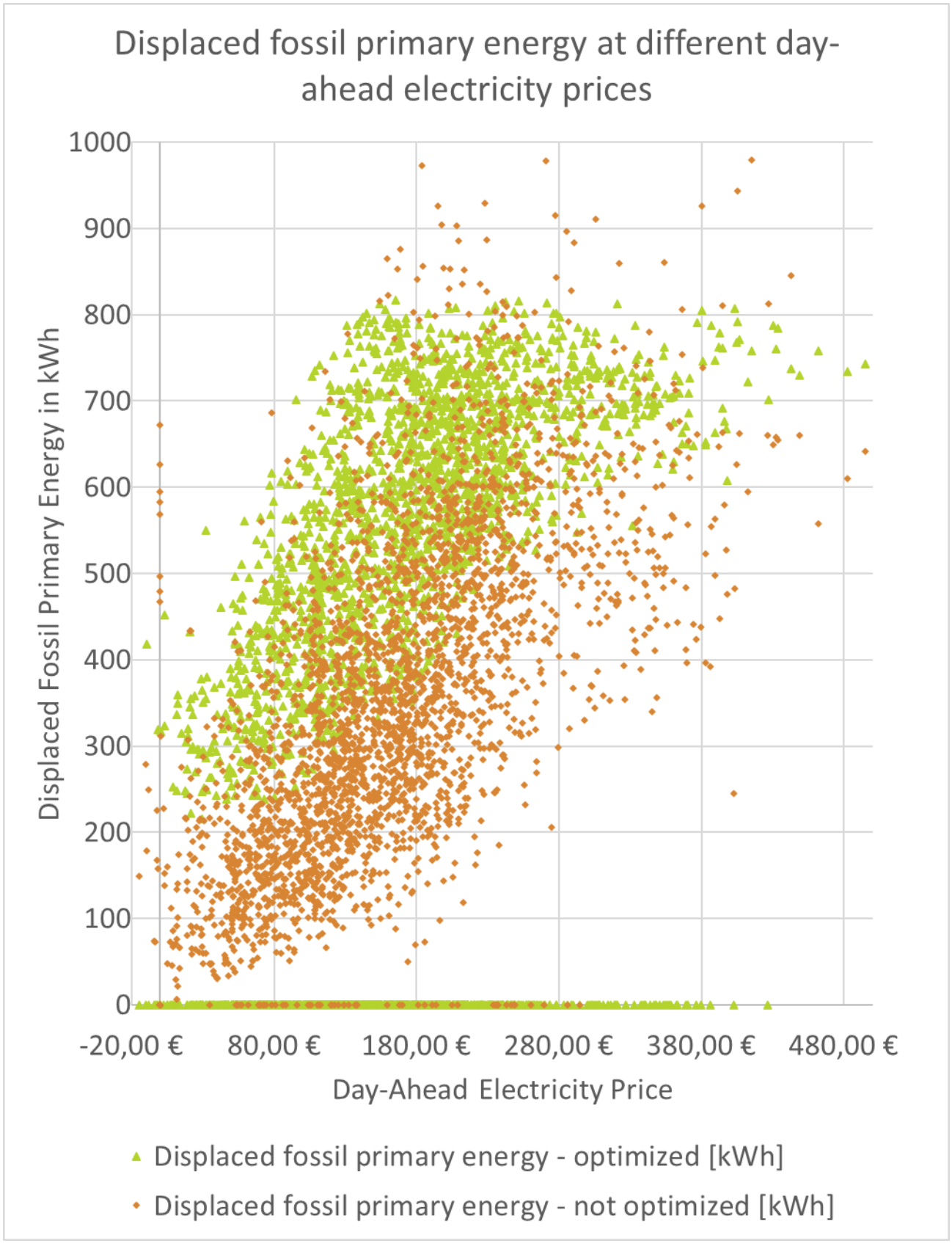


*Figure 2: Primary energy at different day-ahead prices*

## 5.1 DAILY RESULTS

Figure 3 below shows the percentage difference between the optimized and the not optimized operation mode for the daily displaced fossil power from the electricity grid. Positive values indicate that the optimized operation mode displaces more, while negative values indicate, that the not optimized operation mode will displace more.

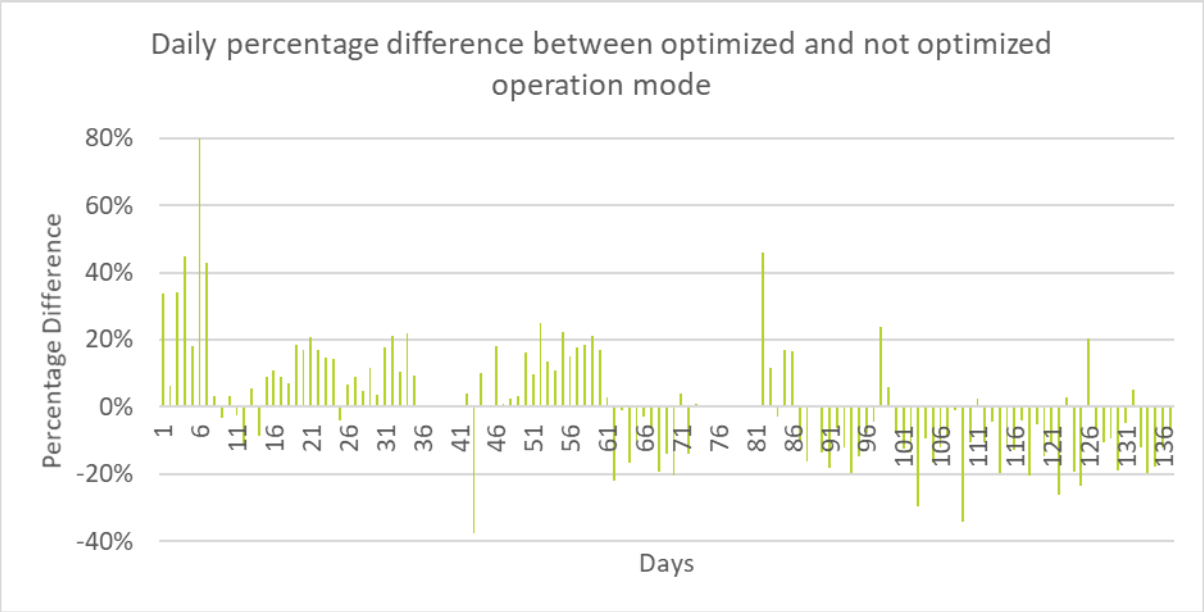


*Figure 3: Daily percentage difference between optimized and not optimized operation mode (displaced fossil power from the electricity grid)*

Figures 4 and 5 show a typical day where more fossil primary energy is displaced by the optimized operating mode compared to the not optimized mode. Figure 4 shows the fossil primary energy and the day-ahead electricity prices. As the day-ahead prices increase, the fossil primary energy will increase, as well as the displaced primary energy.

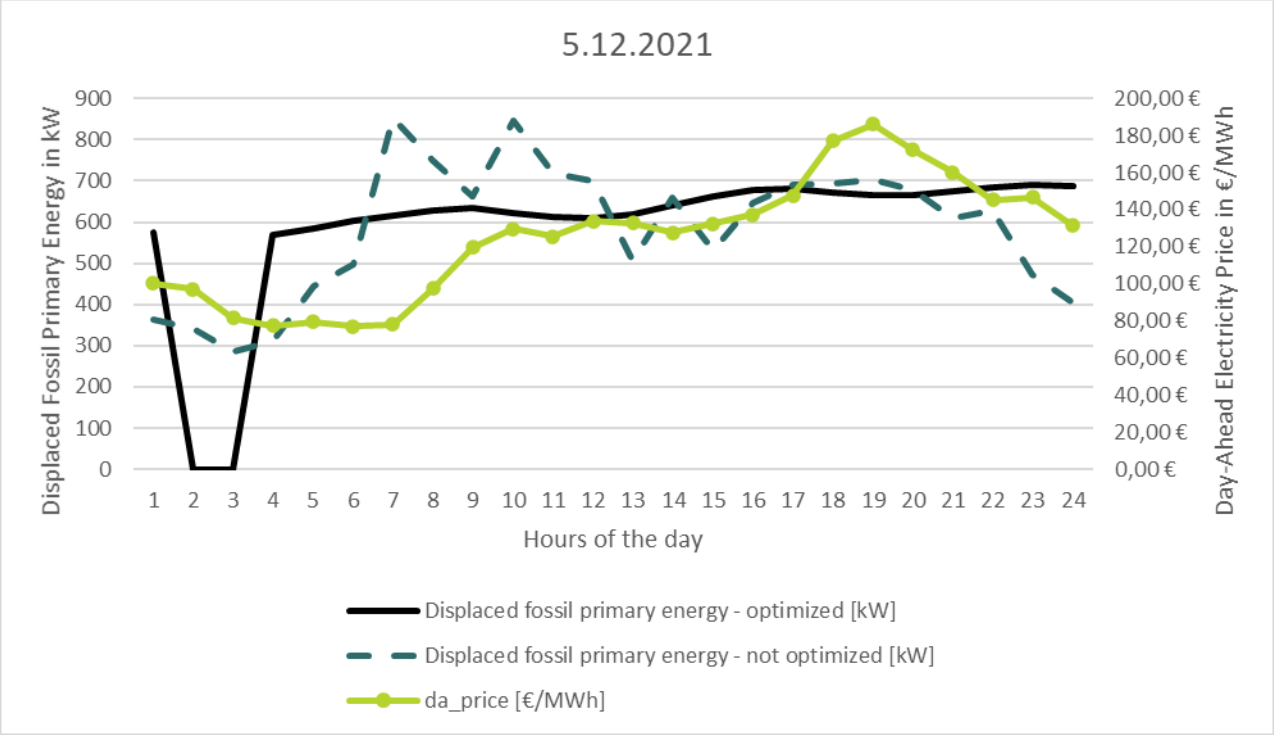


*Figure 4: 5.12.2021: Displaced fossil primary energy template umbauen*

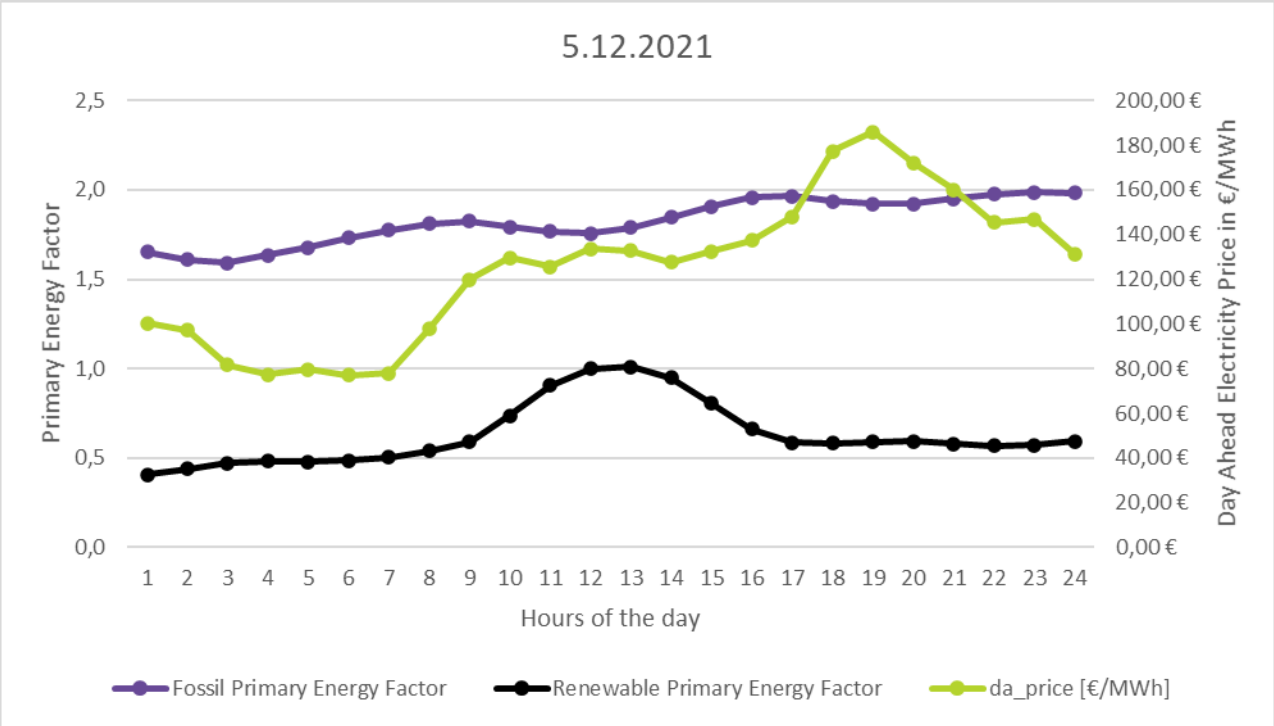


*Figure 5: 5.12.2021: Primary energy factors*

Figures 6 and 7 show a typical day where more fossil primary energy is displaced by the not optimized operating mode compared to the optimized mode. Figure 6 shows the fossil primary energy and the day-ahead electricity prices. As the day-ahead prices increase, the fossil primary energy will increase, as well as the displaced primary energy.

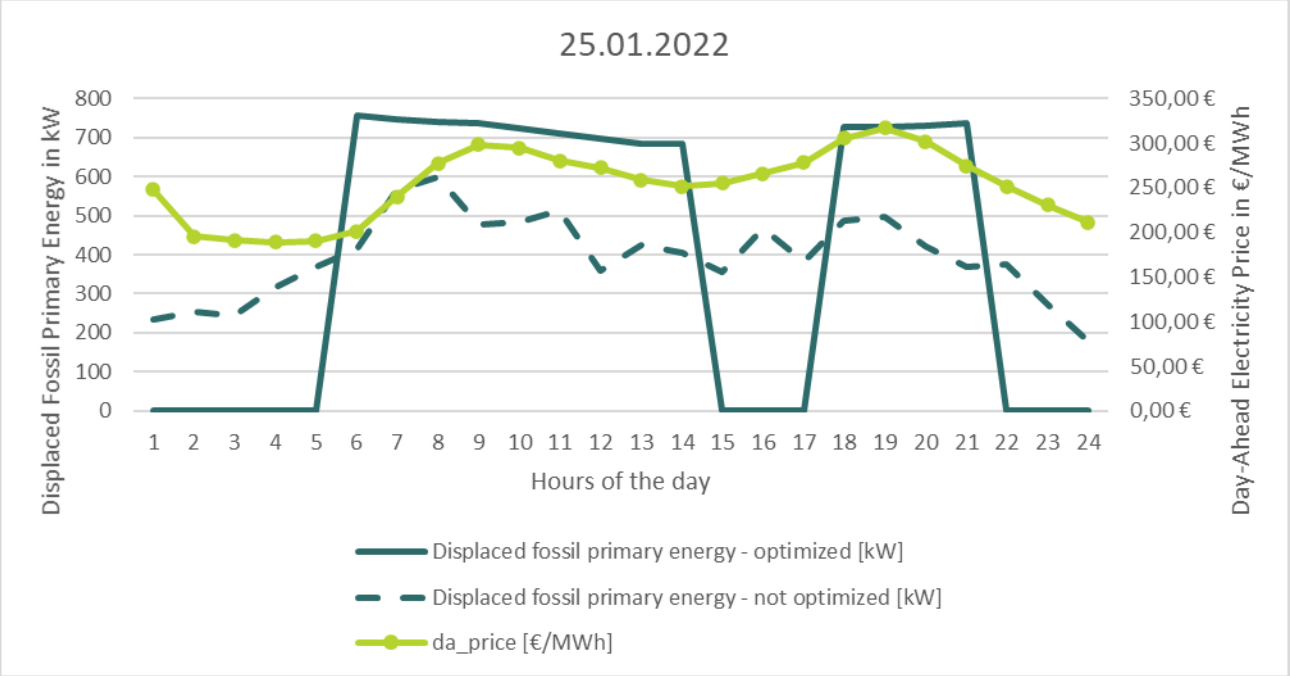


*Figure 6: 25.01.2022: Displaced fossil primary energy*

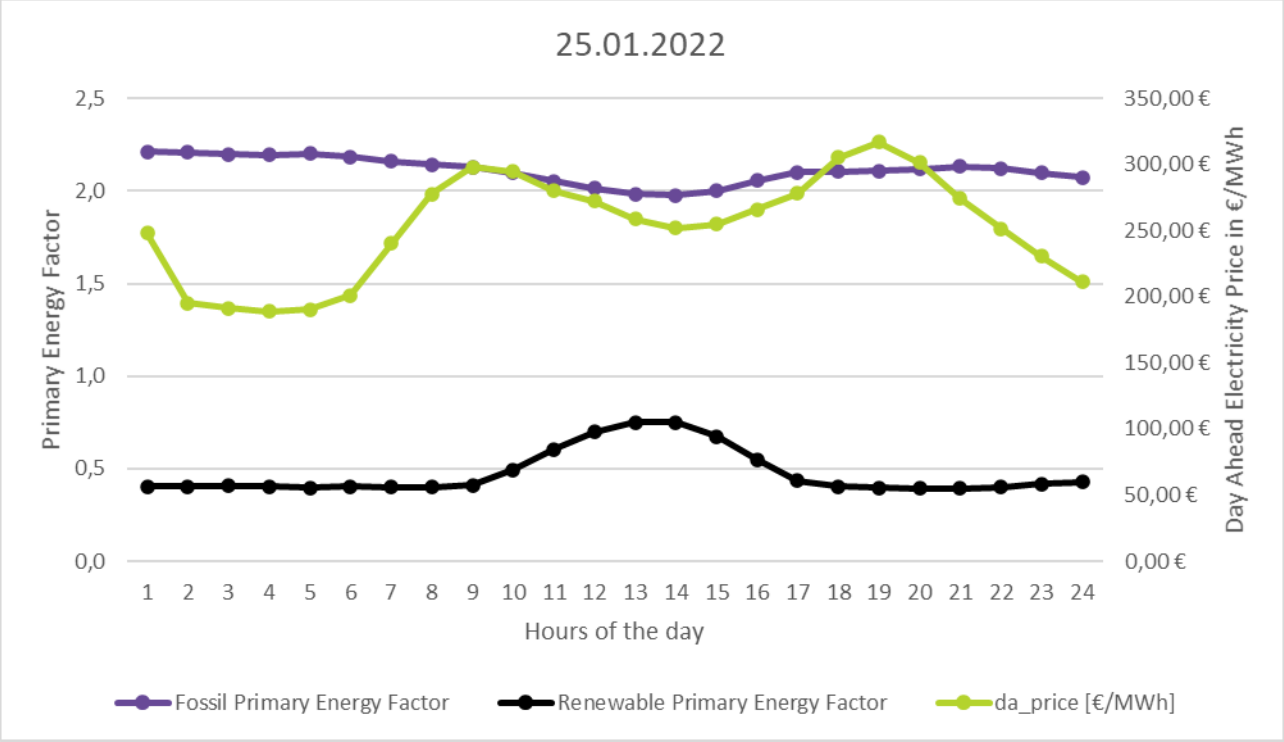


*Figure 7: 25.01.2022: Primary energy factors*

# 6 REFERENCES

[1] „ENTSO-E Transparency Platform“. https://transparency.entsoe.eu/ (zugegriffen 24. März 2022).

[2] „20150422_Grundlagenpapier-Primaerenergiefaktoren.pdf“. Zugegriffen: 24. März 2022. [Online]. Verfügbar unter: https://www.bdew.de/media/documents/20150422_Grundlagenpapier-Primaerenergiefaktoren.pdf

[3] S. Wilke, „Kraftwerke: konventionelle und erneuerbare Energieträger“, *Umweltbundesamt*, 18. Juli 2013. https://www.umweltbundesamt.de/daten/energie/kraftwerke-konventionelle-erneuerbare (zugegriffen 24. März 2022).

[4] D. R. Paschotta, „Ölkraftwerk“. https://www.energie-lexikon.info/oelkraftwerk.html (zugegriffen 24. März 2022).

[5] K. Leibstadt, „Funktion des Kernkraftwerks“. https://www.kkl.ch/kernenergie/unser-kraftwerk/funktion-des-kernkraftwerks (zugegriffen 24. März 2022).

[6] „Biomassekraftwerke“. https://www.vde.com/de/etg/arbeitsgebiete/informationen/biomassekraftwerke (zugegriffen 24. März 2022).

[7] „Incineration - The Heating Power of Refuse“, *Planète Énergies*. https://www.planete-energies.com/en/medias/close/incineration-heating-power-refuse (zugegriffen 25. März 2022).